Universidad Nacional Autónoma de México

Facultad de Ciencias

Slow relaxation and jamming transition in non-Brownian systems

(Relajación lenta y transición de atoramiento en sistemas no Brownianos)

Tesis

Que para obtener el grado de:

Doctor en Ciencias (Física)

presenta:

Gabriel Arturo Caballero Robledo

Director de tesis: **Dr. Eric Clément**

Enero 2006

Acknowledgments

I want to thank Eric Clément for having allowed me to share with him for some years this passionating exercise that is the scientific research. After all this time I'm still impressed by his creativity, his profound knowledge and his passion for physics.

Without the incredible creativity and 'savoir faire' of José Lanuza, the experimental set up would have never worked that good. Thank you also for your friendship.

Also in a special way, I want to thank Ramón Peralta for having interested me on granular matter, for having encouraged me to do the PhD, and for his friendship.

I specially thank Anke Lindner, Evelyne Kolb, Víctor Romero, Raúl Rechtman and Carlos Ruiz for their interest in my work and their advice all along the evolution of this project.

Thanks to Eric Clément, Ramón Peralta, Gerardo García, Roberto Zenit, Raúl Rechtman, Carlos Málaga and Catalina Stern for carefully reading and correcting the whole manuscript. I learned a lot with all this process.

Thanks to Yanalté and Rocío Jáuregui for their support.

Thanks to the people of the PMMH at the ESPCI in Paris for receiving me. It was a great place to work and learn, and to taste the beauty of physics and friendship.

I also want to thank the institutions. La Maison du Mexique and the University of Paris 6 for receiving me in Paris. The UNAM and the Faculty of Sciences for still being my home. Thanks to CONACYT and DGEP for the financial support. This thesis was part of the Project ECOS-Nord M03P01, which successfully increased the collaboration between laboratories of Mexico and France.

To all the people of the granular group: Albens, Anke, Berengere, Bruno, Christophe, Eric, Evelyne, Florent, Hischam, Jacques, José, Philippe and Thierry. You made me to pass a great time in Paris. Thanks.

Florent, it was great to share all this process with you. Thanks a lot.

The Mexican community in Paris: Víctor, Maika, Juan Carlos, Paola, Fabio and Yasmín. It was like being at home. Thanks.

The friends of all my life, it's been a long time, but you are also part of this work.

Again, like some years ago, thanks to my parents and my brother, who know that this work is theirs to some extent.

The most beautiful result of this project was the finding of Yasmín. Thanks for all your support and love.

Contents

Abstract

A granular system can flow like a liquid under the action of an external force, but it can also auto organize and jam, becoming able to support shear stress to some extent, like a solid. Thermal systems can also present jamming, like the glassy state of a fluid. Some amazing analogies in the dynamics of very different systems near jamming, like colloids, foams and grains, gave rise to several proposals about describing in a unified and general way all the systems that jam.

With the idea of testing experimentally these proposals, we studied the mechanical properties of a dense granular material under weak random vibration. By putting in direct contact millimetric glass beads with piezoelectric transducers, we managed to inject energy to the system in a disordered manner with accelerations much smaller than gravity, resulting in a slow compaction dynamics and no convection.

The weak vibration and the fact that the container was not shaken, allowed to perform in the system very precise measurements at the same time of the vibration. The design of the set up made possible to measure the agitation induced in the grains by using an accelerometer buried in the bulk, to measure the packing fraction, to directly see boundary particles and follow their trajectories, to measure the drag force on an intruder grain dragged at constant velocity and, finally, to make Diffusing Wave Spectroscopy experiments.

In chapter 1 it is presented a general introduction of the state of the art concerning granular materials and jamming, together with a brief description of some experimental works by other groups that show analogies between dense granular materials and thermal jammed systems. Also from other groups, there are presented two experiments that study the drag force on granular systems under conditions that are close to our own rheology experiments.

The experimental set up is described in chapter 2 and it is shown how we managed to create a weak and disordered vibration without convective flux. There are also presented systematic measurements of the acceleration and kinetic energy induced on the granular medium by the piezoelectric transducers as a function of frequency and voltage of the input signal. The measurements were done with an accelerometer buried in the grains.

Chapter 3 includes the study of the relaxation of the packing fraction of the weakly vibrated granular material. The density showed to logarithmically increase with time. A central result of these experiments was that the relevant parameter that controls the rate of compaction is the mean kinetic energy and not the r.m.s. acceleration, as is usually considered. It was also studied the response of the density to abrupt changes on the intensity of vibration, finding interesting analogies with the response of thermal systems to changes in temperature.

Direct observation of boundary particles allowed to follow and study their trajectories during long time compaction experiments. The results of these experiments are the subject of chapter 4. The diffusion properties of these particles suggest that their dynamics is similar to the cage dynamics found in glasses, and it was even possible to get a rough estimation of the cage size. An astonishing finding here was that, despite the continuous compaction of the system, the dynamics of the particles was homogeneous in time, which suggests that compaction is governed by collective modes.

Chapter 5 shows rheology experiments where a thread and an intruder grain were dragged quasi statically through the granular material at constant velocity and the resulting drag force was measured. The objects could be dragged while vibrating the system. An exhaustive study of the drag force as a function of velocity, intruder size and vibration intensity is presented. It was possible to separate the contributions to the drag force that came from the thread and those that came from the intruder grain. Interestingly, the rheology of the intruders dragged through the vibrated phase shared features with solid - solid friction, which suggests that models of thermal activated processes could be used to describe granular drag force. It was even measured the 'direct effect' parameter of friction models.

An analysis of the fluctuations of the drag force is also included in chapter 5, where it is shown that the size of the fluctuations were independent of the size of the intruder. The power spectra of the force fluctuations showed to be Lorentzian, with a characteristic length that coincides with the mean diameter of the grains of the medium. Finally, it is developed a simple model based on an Ornstein-Uhlenbeck process which recovers the principal features of the fluctuations of the drag force.

The general conclusions and perspectives of the work are discussed in chapter 6.

Chapter 1

General Introduction

1.1 Granular materials

Systems of many particles that interact mainly by contact forces is what is understood by *granular matter*. It is conventionally accepted that the minimum size that can have the constituent particles to be considered a granular material is of $d = 100\mu m$ [1], where the criteria are that the thermal energy is much smaller than gravitational energy and that the Van der Walls interactions can be neglected. The non-thermal character of a granular material becomes clear when one sees that the potential energy of a glass sphere of diameter $d = 100\mu m$ at a height d at room temperature $T = 27°C$ is of the order of $10^8 k_B T$.

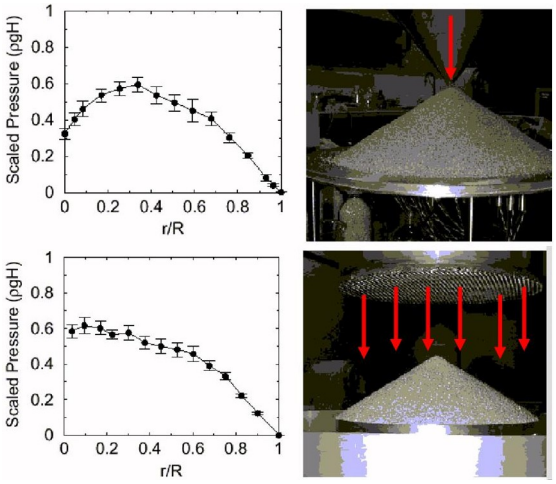

Figure 1.1: *The pressure at the bottom of two granular piles. The stress distribution at the bottom of the pile is different for a pile prepared by point source deposition and for one prepared by rain deposition. Figure taken from reference [2].*

When the surrounding fluid in a granular medium is not highly viscous, and the constituent particles are big enough so that the capillary forces and viscous interactions can be neglected, the mechanical properties of the material are governed by inelastic collisions and frictional contacts between grains. Even in this simple case, the disorder of the medium and the complexity inherent to dissipative and frictional interactions make such mechanical properties very complex. An impressive phenomenon that illustrates this fact is the stress distribution at the bottom of a granular pile. Figure 1.1 shows measurements of the pressure at the bottom of two granular piles by Vanel et al. [2]. The difference between the two piles was the preparation: the pile on the top of the figure was prepared by point source deposition and it showed a pressure dip below the peak of the pile. Such a dip was not present in the other pile which was prepared by rain deposition. Therefore, two macroscopic identical piles, with identical volume and shape, present different stress distributions depending on their preparation history.

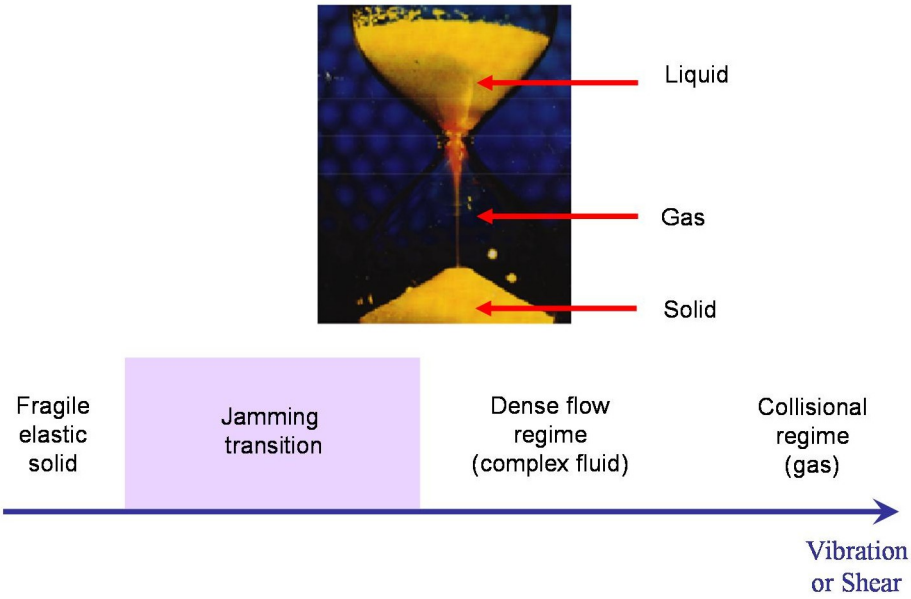

Figure 1.2: *A sand clock is an example of a system where the solid, liquid and gas phases of granular matter coexist. Depending on external actions, granular matter can behave in very different ways.*

Depending on the external forcing, granular matter can behave like a solid able to support compression and to some extent shear, but it can also flow like a fluid when sheared stronger or vibrated (see figure 1.2). However, the behavior of a granular material is always peculiar due to the highly dissipative frictional and collisional interactions between grains and, consequently, a perfect analogy with a common solid, liquid or gas is not usually possible. As a result, up to now it has not been possible to develop a complete theoretical framework to describe the physics of granular matter.

Specially interesting is the transition between the static elastic-like and the dense flow regimes: the jamming transition. Dynamics and mechanical properties of a granular material near this jamming/unjamming transition are not quite well understood and they present surprising analogies with very different systems like foams and even with thermal systems like colloids and glasses.

The motivation of the present work was to investigate the rheology, relaxation processes and grain dynamics of a granular material near the jamming transition.

1.2 Jamming, force chains and fragile matter

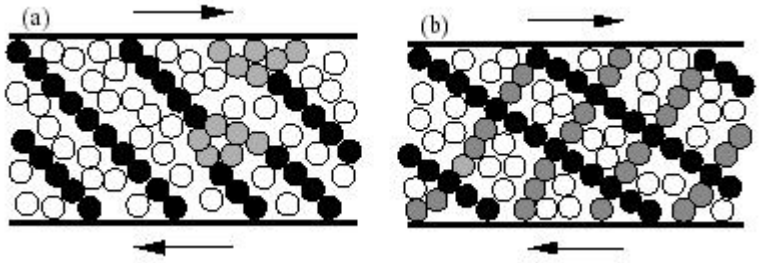

Figure 1.3: *(a) A jammed colloid (schematic). Black: force chains; grey: other force-bearing particles; white: spectators. (b) Idealized rectangular network of force chains. Picture taken from reference [3]*

A jammed granular assembly like a pile is what is called by Cates et al. [3] *fragile matter*. It is a rigid system that can support stresses elastically but whose rigidity comes precisely from the applied stresses. In other words, under stress, the system self organizes to support the load and becomes rigid. However, it is fragile because it can only support stresses in the directions determined by the stresses that rigidified it; stresses in any other direction, even if infinitesimal, cause irreversible reorganizations in the medium. Moreover, when there is no stress, it is not jammed. Thus, the authors considered as fragile the jammed systems with no tensile forces.

Cates et al. modeled a jammed colloid by an assembly of force chains that supported the external load and that were immersed in a sea of 'spectator' particles (figure 1.3). With this work Cates et al. introduced a precise definition of fragility. They also talked about jamming as a general phenomenon that could be present in systems as different as colloids and grains, and they pointed out the importance of force chains in jammed systems.

Inspired in the work by Cates et al. [3], Liu and Nagel [4] proposed that all jammed systems present common properties even if they were jammed not because of external loads

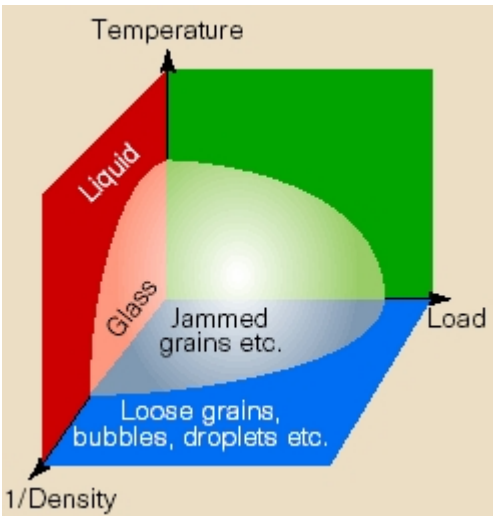

Figure 1.4: *Jamming phase diagram. Picture taken from reference [4]*

but as a result of internal attractive forces between particles. They argued that a glass was a disordered jammed liquid, that has come to rest due to a lowering of temperature and that could be unjammed by rising the temperature again. This took Liu and Nagel to suggest that if temperature and stress played a similar role in jamming and unjamming systems, there should be a universal way to describe jammed thermal and non thermal systems. They sketched a speculative jamming phase diagram that would unify the description of all systems that jam: grains, bubbles, droplets, liquids (see figure 1.4). In this scenario, jamming would be controlled by temperature, external load and the inverse of density.

From the equivalent role of temperature and load in the jamming phase diagram, Liu and Nagel pose the question of how similar is the dynamics of thermal and non thermal systems when approaching the jamming transition. They also talk about the pertinence of defining an effective temperature and the possibility of applying concepts of statistical mechanics to describe non thermal systems.

We will see in section 1.4 experimental evidence of analogies in the dynamics of thermal and non thermal systems that support the jamming phase diagram proposed by Liu and Nagel, but first we will see that these authors were not the first ones to apply statistical mechanics to granular media.

1.3 Statistical physics approach

One of the reasons why granular materials are so difficult to describe is that they are composed of many interacting particles. This took S. F. Edwards [5] to try to apply the tools of statistical mechanics to granular matter.

The ergodic hypothesis proposed by Edwards [5] consists in considering equally probable to occur all the particular configurations of N grains with a given volume V that are blocked, and that result from any macroscopic mechanical action on the system. Then it is possible to define the configurational entropy as:

$$S_{Edw}(V, N) = ln\Omega_{Edw}(V, N), \tag{1.1}$$

where $\Omega_{Edw}(V, N)$ is the number of blocked configurations compatible with a macroscopic state defined by the volume V. From here, the compactivity of Edwards $X_{Edw} = \partial V/\partial S_{Edw}$ can be defined, which is the analog to temperature in thermodynamics.

Another attempt to use statistical physics concepts to describe granular matter was done by Makse and Kurchan [6]. They made numerical simulations that suggest that an effective temperature T_{eff} can be defined in granular systems in the same way that it is done in glassy systems. In these thermal out of equilibrium blocked systems, a well defined temperature appears when fluctuation-dissipation relations are used[1]. It is called effective temperature and is defined as $T_{eff} = D/\chi$, where D is the diffusivity of the molecules and χ the mobility. It turns out that T_{eff} is different from the bath temperature but it governs the heat flow and the slow components of the fluctuations and responses of all observables [6]. Makse and Kurchan suggest the existence of an effective temperature that can be defined and measured in granular systems by using fluctuation-dissipation relations.

[1]The fluctuation-dissipation theorem relates the viscous dissipation with the random collisions of a Brownian particle in a fluid in thermodynamic equilibrium. If the particle follows the Langevin equation:

$$m\frac{d^2x}{dt^2} = -m\gamma\frac{dx}{dt} + A(t),$$

where $A(t)$ is a random force, the fluctuation-dissipation theorem states that:

$$\gamma = \frac{1}{mk_BT}\int_0^\infty \langle A(t)A(t+\tau)\rangle\, d\tau,$$

where k_B is Boltzman's constant and T is the temperature. This is equivalent to Einstein's relation:

$$\frac{D}{\chi} = k_BT,$$

where D is the diffusion coefficient and $\chi = v/F$ is the mobility, with v the velocity and F an external force applied to the particle.

The validity of these ideas are still subject of an intense debate, and they have motivated a great number of theoretical, numerical and experimental investigations.

1.4 Analogies between thermal and granular systems

1.4.1 Glass transition

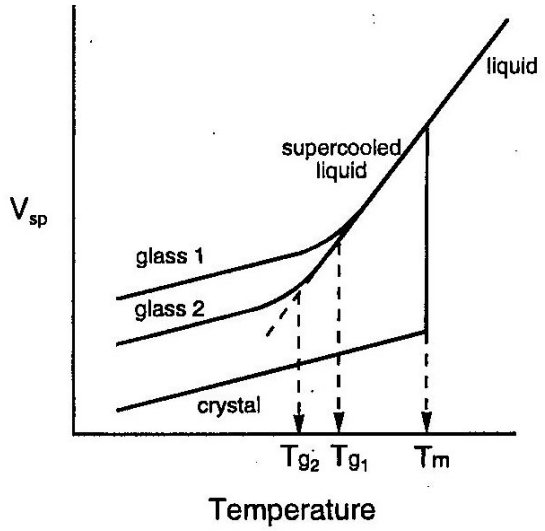

Figure 1.5: *Schematic representation of the specific volume as a function of temperature for a liquid which can both crystallize and form a glass. Figure taken from reference [7].*

Figure 1.5 shows schematically the behavior of the specific volume as a function of temperature in a thermal system. The state of the system below the transition temperature T_m depends on the cooling rate, having the possibility of being a supercooled liquid, a glass or a crystal.

Concerning vibrated granular materials, figure 1.6 shows the stationary packing fraction as a function of vibration intensity Γ on an experiment where a granular column was vertically shaken. The intensity of vibration was characterized by the peak acceleration a of the container normalized by the acceleration of gravity g: $\Gamma = a/g$ (see the inset in figure 1.6). At each value of Γ, the system was tapped 10^5 times and at the end the density of the system, ρ, was measured. Then the vibration intensity was changed by $\Delta\Gamma = 0.5$. After a transient, the system arrives to a branch where there is a well defined reversible value of the density for each vibration intensity. Nowak et al. report in reference [9] that the low Γ part of the reversible branch could only be attained by slowly reducing the intensity of vibration ($\Delta\Gamma = 0.5$), a

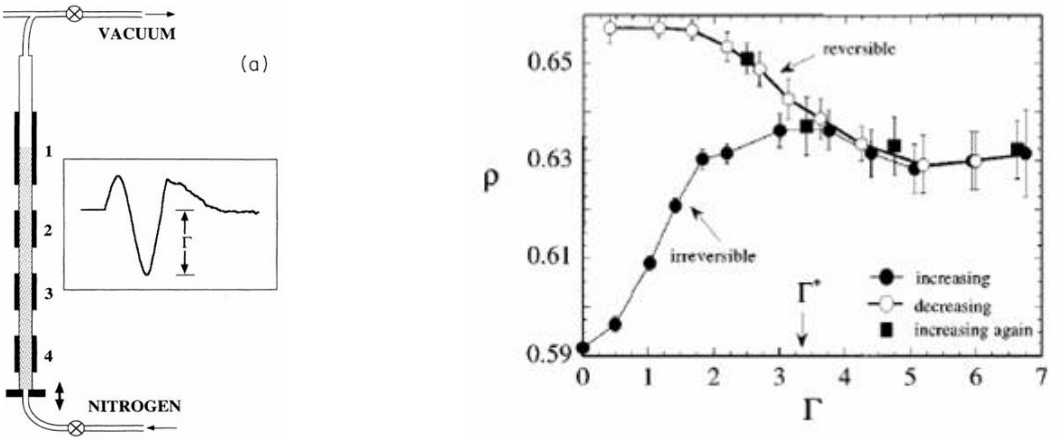

Figure 1.6: *Left: A schematic drawing of the shaken granular column and the four capacitors used to measure density. The inset shows the acceleration induced by a tap of intensity* Γ. *Figure taken from reference [8]. Right: At each value of* Γ, *the system was tapped* 10^5 *times and at the end the density of the system,* ρ, *was measured. Figure taken from reference [9].*

process that is known as 'annealing'. When the vibration was reduced faster, the system fell out of the reversible branch. This behavior seems to be similar to the response of liquids to cooling presented in figure 1.5, though Nowak et al. do not talk about crystallization.

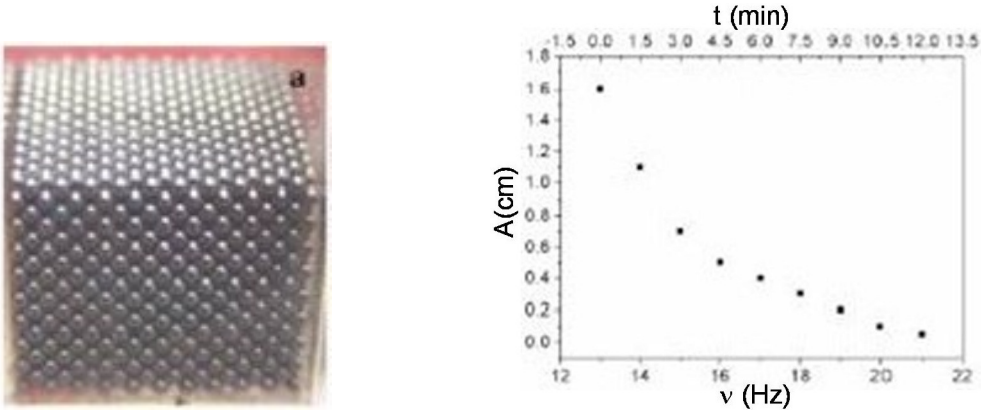

Figure 1.7: *Left: fcc structure obtained by annealing using ball bearings of* $d = 1.6mm$ *in a square confinement of* $24mm$. *Right: Cooling rate for the annealing process. Amplitude and linear frequency for a square vibration as a function of time. Figures taken from reference [10].*

In a more recent work, Ruiz et al. [10] managed to create granular crystals by vibrational annealing (figure 1.7). If the 'cooling' was fast, the crystal was not formed. It would be interesting to try to reconstruct in this system a diagram like the one presented in figure 1.5.

In section 3.4 we present a quasi reversible state of density found in our set up in compaction experiments.

1.4.2 Kovacs effect

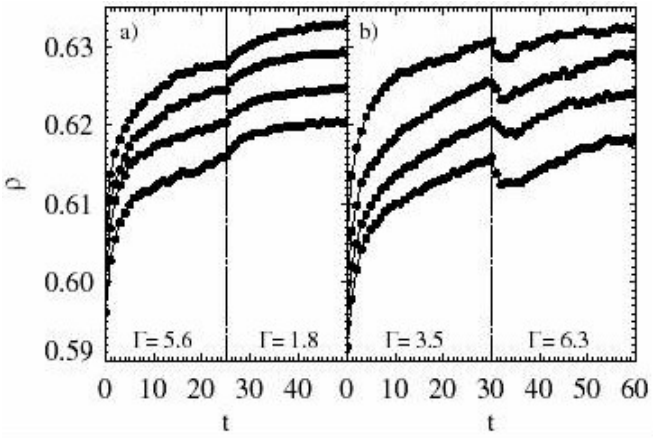

Figure 1.8: *Response of the packing fraction, ρ, to variations of vibration intensity, Γ, as a function of tap number, t, at four heights in the column (see figure 1.6). Curves for different heights are shifted for clarity. Vibration intensity decreases in a) and increases in b). Figure taken from reference [11].*

Another experimental evidence of the analogies between blocked thermal systems and dense granular materials was found by Josserand et al. [11] in the same system described in figure 1.6. The response of the packing fraction to variations on the intensity of vibration is similar to the response of some observables to temperature variations in thermal systems out of equilibrium[2]. In particular, the transient dilation observed in figure 1.8 when the vibration intensity was increased is analogous to the 'Kovacs effect', observed in thermal glassy systems when the temperature is changed abruptly [12]. In our set up we also observed the Kovacs effect (section 3.4).

1.4.3 Cage effect

Molecules in a glassy system have a peculiar dynamics characterized by the so called 'cage effect'. According to this model, a particle in a glassy environment is free to move at the interior of a cage from which it can only eventually escape. This kind of dynamics was proposed to explain the multiple characteristic times observed in glassy systems, and it was finally observed in real space by Weeks et al. in a colloidal system by means of a confocal microscopy method [13].

Concerning granular systems, the cage effect has been observed in shearing experiments in three dimensions by Pouliquen et al. [15], and more recently in two dimensions by Marty and

[2]For example the magnetic susceptibility in spin glasses

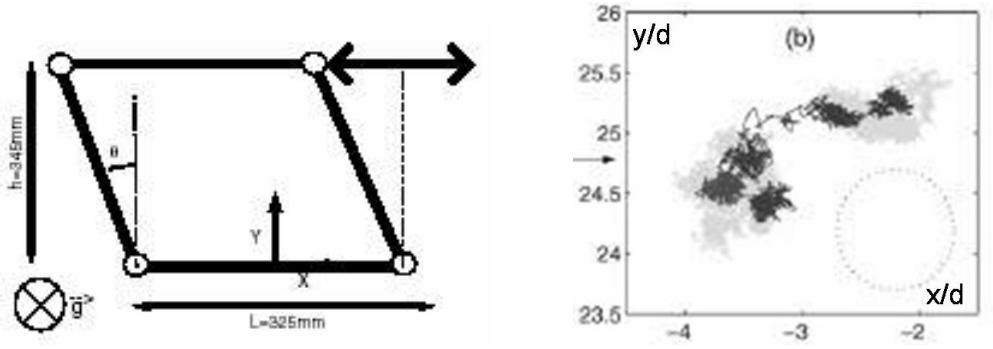

Figure 1.9: *Left: A horizontal deformable paralelogram was used to quasistatically shear a bidisperse granular material. Right: In gray, a trajectory of* 10000 *cycles of a typical particle. The coordinates* x *and* y *are normalized by the mean diameter of the particles (the circle in the figure represents the size of a particle). In black, the first* 2000 *cycles of the same trajectory. The particle follows a cage-like dynamics with a typical size of the cage of* $0.3d$*. Figures taken from reference [14].*

Dauchot [14]. The set up of this later work is shown in figure 1.9. A horizontal deformable paralelogram was used to quasistatically shear a bidisperse granular material composed of metallic cylinders of 4 and $5mm$. The shear was periodic with an amplitude $\Theta_{max} = \pm 10^o$ and the position of 500 particles was registered each time the system was back to $\Theta = 0$. The plot in the right of figure 1.9 shows in gray a trajectory of 10000 cycles of a typical particle and in black the first 2000 cycles. It can be seen that, indeed, the particle presents cage-like dynamics.

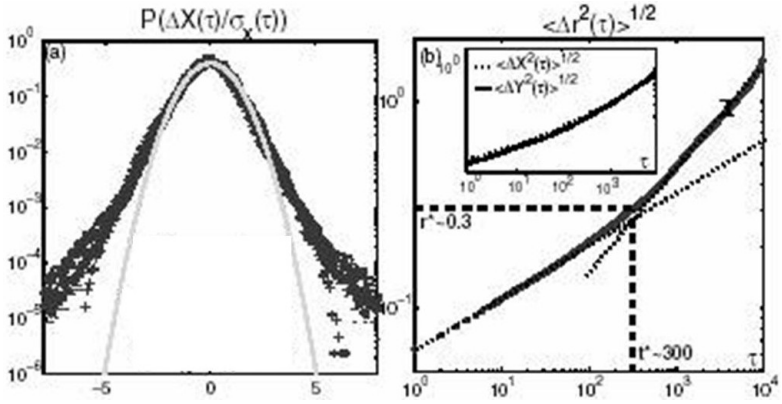

Figure 1.10: *Left: Probability distribution of the size of jumps in the* X *direction for a time* τ*. Right: Root mean squared displacement of the trajectories. Figure taken from reference [14].*

The statistical properties of the trajectories of particles in the experiment by Marty and Dauchot are very similar to those of molecules in glass forming systems [14]. The left plot in figure 1.10 shows the probability distribution of the size of jumps in the X direction for

a time τ, $\Delta X(\tau) = X(t+\tau) - X(t)$, normalized by the root mean squared displacement $\sigma_x = \sqrt{\langle \Delta X^2(\tau) \rangle}$. The exponential tails of the distribution are characteristic of intermittent dynamics in blocked systems [14]. The right plot of the same figure is the ensemble average of the root mean squared displacement of the trajectories. In a normal diffusion process, this quantity should grow like $\tau^{1/2}$. However, it can be seen that for short times $\langle \Delta r^2(\tau) \rangle^{1/2}$ goes as $\tau^{1/4}$, i.e. a sub diffusive behavior. Marty and Dauchot interpret the transition from subdiffusive to normal diffusion as the escape of particles from the cage. In this way they estimate the size of the cage as $r^* \approx 0.3d$, where the corresponding time needed to escape from it is $t^* \approx 300$ cycles. We will see later in chapter 4 that we obtained similar results in our set up when analyzing the trajectories of boundary particles.

1.4.4 Granular temperature

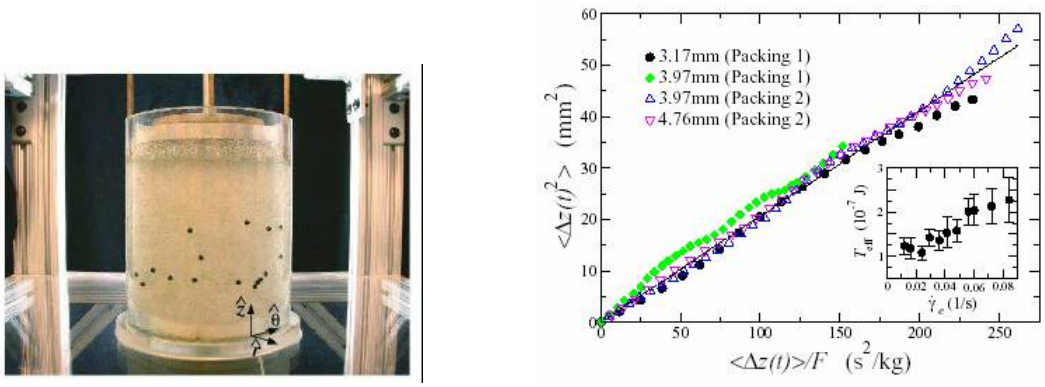

Figure 1.11: *Left: experimental set up: two coaxial cylinders where the interior one rotates. A granular material together with a fluid that matches the refractive index and the density of grains are between cylinders. Tracers of different density are put into the system. Right: The diffusivity and mobility of tracers define an effective temperature. Figures taken from reference [16].*

Makse et al. [16] designed a Couette-Taylor set up in which they measured the effective granular temperature T_{eff} following the idea of applying fluctuation-dissipation relations to granular materials. These ideas can be found in reference [6] and they were briefly described in section 1.3 of the present work. The left image in figure 1.11 shows the experimental set up: two coaxial cylinders where the interior one rotates. A granular material consisting of a bidisperse mixture of acrylic particles is put between the cylinders together with a fluid which matches the refractive index and the density of the particles ($\rho_a = 1.19g/mm$). Tracer particles of slightly different density ($\rho_n = 1.12g/mm$ and $\rho_d = 1.36g/mm$) are put into the system and their trajectories are followed while shearing the granular material. There is an external vertical force on the tracers $F = \Delta\rho V g$, where $\Delta\rho$ is the difference of density

between the tracer and the particles of the medium, V is the volume of the tracers and g is the acceleration of gravity. From the trajectories of the tracer particles, a diffusivity $D = \langle [z(t+t_0) - z(t_0)]^2 \rangle / 2t$ and a mobility $\chi = \langle z(t+t_0) - z(t_0) \rangle / Ft$ can be evaluated. The effective granular temperature is then obtained from $T_{eff} = D/\chi$, shown in the left plot in figure 1.11 as a function of shearing rate. Interestingly, the same temperature is obtained for different sizes of grains and different kinds of tracers.

1.5 Granular drag force; previous works

The motivation of the present work is to study the properties of granular matter near the jamming transition zone. In other words, we wanted to know more about the rheology of dense granular systems near blockage. The rheology of grains can be studied in two general ways: by applying to the system boundary or body forces, and by dragging objects through the system. Examples of the first method are a shearing Couette-Taylor cell and avalanches in an inclined plane. A great number of experimental, numerical and theoretical works have been done in relation to this kind of systems. For a detailed summary and compilation of much of the findings on this subject see the collective work by the GDRMidi French group [17].

Dragging objects through granular materials has not been studied so extensively in the physics community. Two pioneering works on this subject are due to Wieghardt in 1975 [18] and to Zik et al. in 1992 [19]. Both of them studied the drag force as a function of velocity, but in regimes that were far from jamming. The velocities investigated by Wieghardt were big enough to fluidize the granular material, while Zik et al. drove a particle through a strongly vibrated granular material when the system was in the free fall phase of the vibration.

A more recent work that studied the granular drag force was performed by Chehata et al. [20], where they investigated the flow around a fixed cylinder immersed in a uniform granular flow. Among their findings are that the drag force was independent of the mean flow velocity, that it scaled with the asymptotic static stress states in a tall granular bed and that the drag acting on the cylinder was strongly affected by the surrounding channel geometry. Again, since Chehata et al. were more interested in the transition 'liquid-gas' of the flow, they worked in velocity regimes that were far from jamming, so that comparison with our results should be done carefully.

Closer to the jamming transition on which we are interested are the works by Schiffer et al. [21] and by Geng and Behringer [22]. A schematic representation of the experimental set up used by Schiffer et al. is shown in figure 1.12. A vertical cylinder was extended into

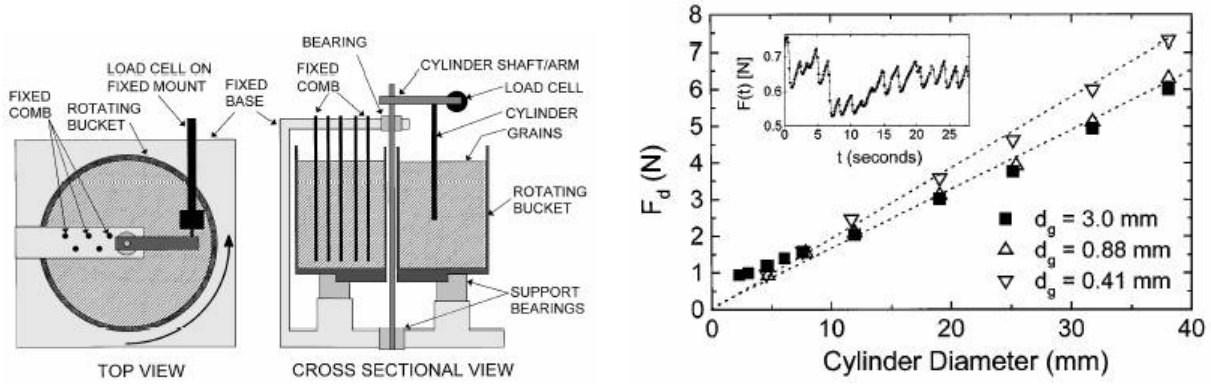

Figure 1.12: *Left: experimental set up: a vertical cylinder was extended into a bucket of granular material and held fixed while the bucket was slowly rotated. Right: dependence of the drag force on the diameter of the cylinder for a velocity of* $1.4mm/s$. *Data for different sizes of grains* d_g *are presented. Figures taken from reference [21].*

a bucket of granular material and held fixed while the bucket was slowly rotated. The arm holding the cylinder was held fixed by the sensor of a load cell which measured the drag force F_d. In order to prevent the cylinder from repeatedly traveling through a trough created by previous rotations, the granular environment was randomized by mixing the medium with a fixed 'comb' consisting of a series of thin steel rods. Millimetric glass spheres were used. Schiffer et al. found no dependence of the drag force on the dragging rate, while the effect on F_d of varying the diameter of the cylinder is shown in figure 1.12. A linear relation was found[3] with deviations from it for thin cylinders. The authors explain this deviation by the fact that even a very thin cylinder encounters resistance from the medium to move, thus the limit of the drag force when the diameter goes to zero must be a non zero constant.

The dragging experiment by Geng and Behringer [22] was, in a sense, the two dimensional version of the experiment by Schiffer et al. presented above, though there are two substantial differences. First, the particles used by Geng and Behringer are very smooth (a photoelastic material was used) compared to the glass beads used by Schiffer et al. Second, the two dimensional experiment is done at constant 'volume', while in the $3D$ version the surface is free. A schematic representation of the set up of Geng and Behringer is shown in figure 1.13, and the plots with the drag force that they measured as a function of drag velocity and of the size of the intruder are shown in figure 1.14. It can be seen that the drag force changed with the drag velocity, in contrast with the results by Schiffer et al. [21]. Geng and Behringer explain that the dependence on rate of the drag force appeared because the softness of the particles introduced a characteristic time that was not present in the experiment with glass

[3]Though it is difficult to be sure of the linearity with less than one decade of variation of the cylinder diameter.

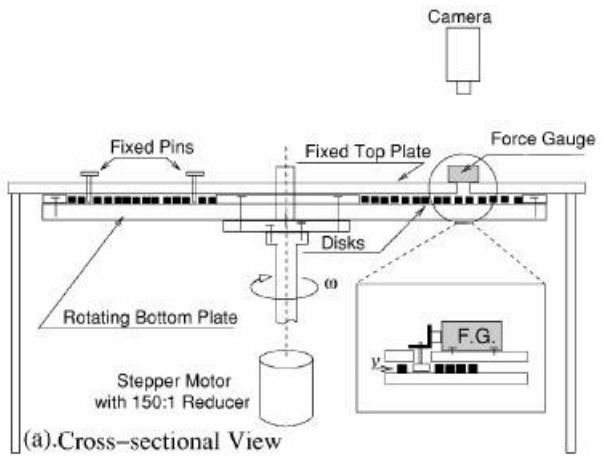

Figure 1.13: *Schematic cross-sectional view of the set up used by Geng and Behringer. The apparatus has circular symmetry in the horizontal plane, and the bottom plate, together with the particles, rotate as a rigid body at a slow velocity. The inset shows how a digital force gauge is mounted o the top plate and connected with an intruder particle through the force gauge hole. Figure taken from reference [22].*

beads by Schiffer et al. [22]. Concerning the variation of the drag force as a function of the size of the intruder, the range of sizes explored by Geng and Behringer, compared to the size of the grains of the medium, coincide with the range in which Shiffer et al. found deviations from linearity.

Finally, figure 1.15 shows the power spectra $P(\omega)$, from force time series at different rotation rates ω_0. The power spectra and frequency are scaled with the rotation rate. The fact that the curves for different rotation rates collapse means that fluctuations of force are rate independent. On the other hand, the shape of the spectra is Lorentzian, which implies that there is a characteristic length beyond which there is no correlation on the drag force [22].

Our own results of dragging an object through a granular material are presented in chapter 5, where the similarities and differences with the experiments by Schiffer et al. and by Geng and Behringer are discussed.

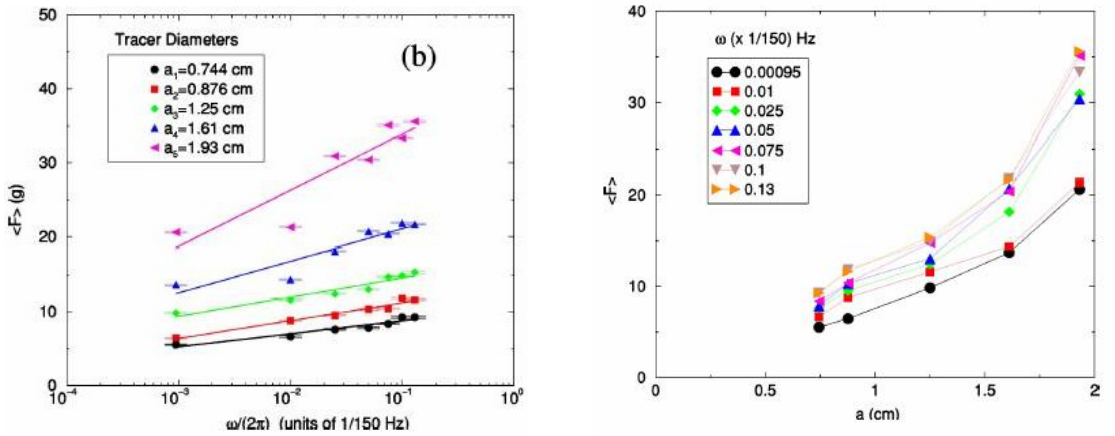

Figure 1.14: *Left: The mean drag force, $\langle F \rangle$, as a function of rotation rate, ω, for intruder particles with different sizes. Right: The mean drag force as a function of the intruder particle diameter, a, for different rotation rates. As a reference, the mean diameter of the background particles is* $0.763cm$. *Figures taken from reference [22].*

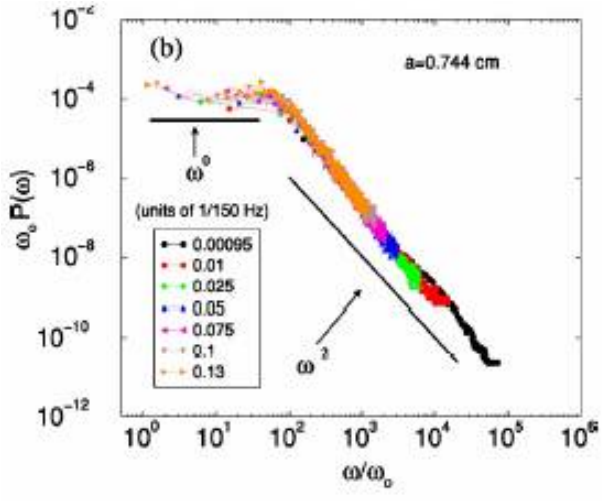

Figure 1.15: *Power spectra, $P(\omega)$, from force time series at different rotation rates. The scaling frequency, ω_0 is the rotation rate. Figure taken from reference [22].*

Chapter 2

Weak random vibration

In the present chapter we describe the experimental set up that we designed with the idea of studying the mechanical properties of a dense granular material under random vibration near the jamming transition. We show how we managed to create a weak and disordered vibration without convection. This last point was important since it allowed to study compaction phenomena and rheological behavior without interference of convective flows.

There are also presented systematic measurements of the acceleration and kinetic energy in the bulk induced on the medium by the piezoelectric transducers as a function of frequency and voltage of the input signal. The measurements were done with an accelerometer buried in the granular medium.

2.1 Experimental set up

Figure 2.1 schematically shows the experimental setup. A rectangular glass container is closed at its bottom by seven piezoelectric transducers, each one glued by its extremes to a plastic base in a way that the ceramic membrane is free to vibrate, being directly in contact with the grains and with nothing else (figure 2.1, lateral view). The plastic bases of the transducers as well as the glass container are all fixed to a main plastic support. The container is filled with a binary mixture of glass beads of 1 and $1.5mm$[1], and each piezoelectric is excited by a square signal of frequency[2] f which is out of phase by π compared to that of its neighbors. With this setup, the agitation created in the bulk is disordered and weak compared to typical experiments of vibrated granular materials [9, 23, 24] where all the container is shaken with accelerations of the order of or greater than gravity. In contrast, in our set up the root mean

[1] The mean diameter of the grains is $d = 1.2mm$ and the dispersion of the diameter of each of the species of the binary mixture is of 10%.

[2] f takes values between 100 and $2000Hz$.

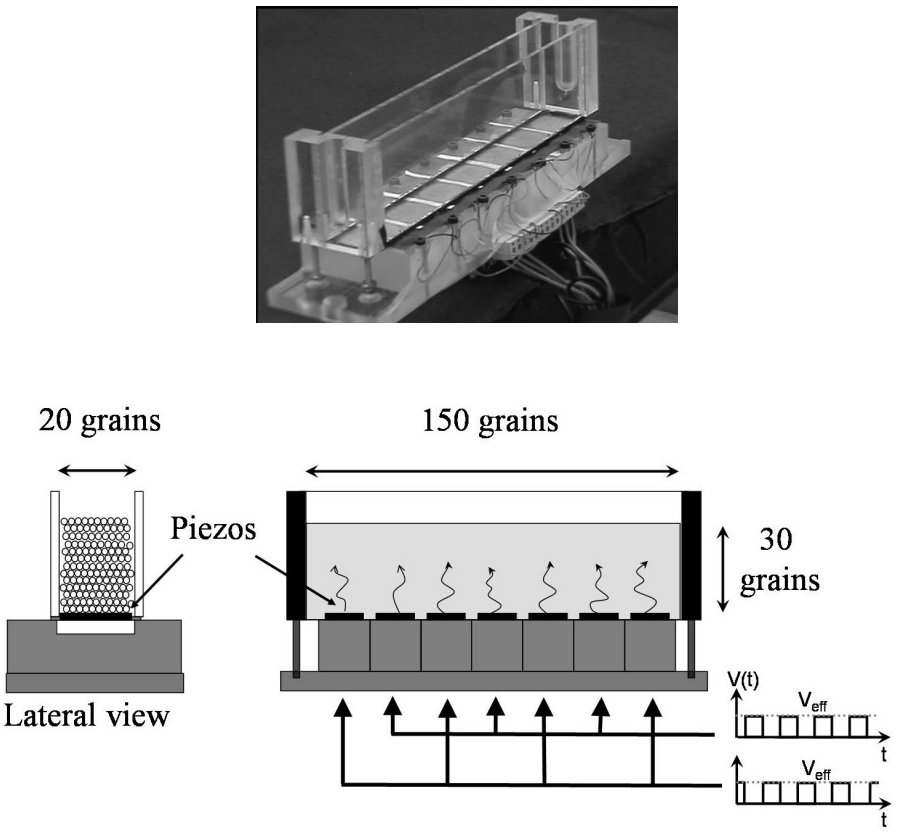

Figure 2.1: *Experimental setup. A glass container is closed at its bottom by seven piezoelectric transducers. The container is filled with a bidisperse mixture of glass beads of 1 and* $1.5mm$ *that are in direct contact with the transducers. Each piezoelectric is excited by a square signal of frequency* f *that is out of phase by* π *compared to that of its neighbors.*

squared acceleration γ_{rms} induced in the bulk, measured by means of an accelerometer buried in the granular material, is always smaller than gravity. With such a weak excitation, the main mode excited in the system is the rotation of grains and re-organization of granular contacts.

2.2 Different measurements

Besides the disordered agitation created by the independent transducers being in direct contact with the grains, a great advantage of our set up is that the container is fixed and the vibrations are very weak, so it is possible to perform very precise measurements of the granular packing

while vibrating. Below, the techniques used to extensively characterize the response of the system to vibration as well as some of its rheological properties, are briefly described.

Agitation measured in the bulk

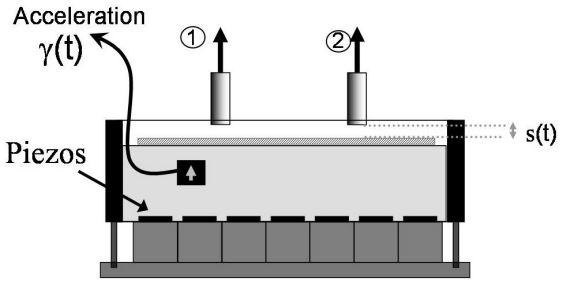

Figure 2.2: *Acceleration in the bulk measured by means of a buried accelerometer. The packing fraction is obtained from the position of a metallic lid on the surface of the pile given by two proximity sensors.*

In the best of our knowledge, in all granular vibration experiments done until now, what is measured and controlled is the vibration of the container by placing an accelerometer on it or simply by adjusting the amplitude and frequency of the shaker. In our set up, we were able to bury an accelerometer into the bulk and take measurements while vibrating (see figure 2.2). This allowed us to fully characterize the state of agitation of the system for different vibration conditions as far as transmission of momentum is concerned. We obtained, for example, the root mean squared acceleration γ_{rms} and mean kinetic energy $\langle \epsilon_k \rangle$ for different frequencies and voltages of the input signal of the transducers. The details of this technique and the main results obtained are described in section 2.3.

Packing fraction

The packing fraction ϕ or, in other words, the average density of the system (represented as ρ in figure 1.6), is obtained by measuring the height of the pile, which, knowing the dimensions of the container, gives the total volume occupied by the grains. To know the height, a thin metallic lid is placed on the surface of the grains and two inductive proximity sensors measure the position of the lid (see figure 2.2). The weight of the lid is equivalent to five layers of beads in the container and, since it is rigid, what we obtain is an averaged measurement of the height of the pile. The resolution of the sensors is of the order of micrometers, so they can detect very small density variations. However, the precision on the absolute value of the packing fraction is not better than 3% (see equation 3.1).

With this set up we were able to study the evolution in time of the density for different vibration conditions in very long experiments. We could also observe the response of the system to abrupt changes in the vibration intensity. Moreover, the density was measured at the same time that measurements of particle tracking and diffusion of light (described below) were performed. A detailed description of this technique and the main results obtained are found in chapter 3.

Particle tracking

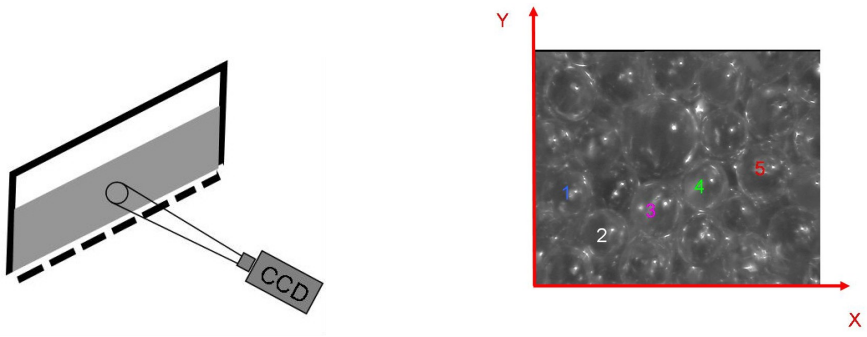

Figure 2.3: *During compaction experiments, a CCD camera filmed a small region of approximately* $5d \times 5d$ *next to a lateral transparent wall at a rate of one image each minute. Vertical* $y(t)$ *and horizontal* $x(t)$ *positions of particles were obtained by image analysis.*

The transparent walls of the glass container allowed to directly see the beads that were next to the wall. We took advantage of this and filmed a small zoomed region of a lateral wall with a CCD camera during long time vibration experiments. Even our strongest vibration intensities were so weak that the system did not seem to move when viewed in real time. However, when images were taken during times of the order of hours, one could see that particles actually had moved, and that the structural configuration of the system continuously changed while compacting. The movement of the particles was quite random though the zone of exploration was rather small. Consequently, particles that were in our vision field at the beginning of the experiments did not get out of it even after ten days of vibration. Then, from image analysis, we were able to extract the position of seven particles as a function of time. These boundary particles gave us an idea of the microscopic dynamics of the system which we could relate with macroscopic features like global compaction. Nevertheless, what we observed were boundary particles, whose dynamics could differ from particles in the bulk. Chapter 4 develops in detail this technique and the results obtained.

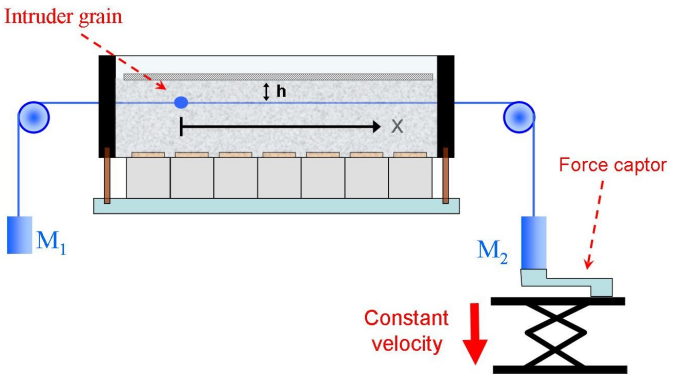

Figure 2.4: *The resistance force of the granular medium to the movement of an object dragged at constant velocity through it is measured by using an Atwood like machine.*

Dragging an intruder grain

The two narrow lateral walls of the container had a small slit thinner than the bead size. A thin metallic thread was made to pass through the slits and the granular matter, and an Atwood like machine (see figure 2.4) was used to test the resistance to motion inside the dense granular medium. The heaviest mass of the machine rested on a force probe that was moved downwards at a constant velocity. Additionally, an intruder grain could be glued to the thread. With this set up we were able to drag the thread alone or the thread together with the intruder grain at constant velocity and to measure the resistance to movement opposed by the granular material very precisely. We extensively studied the dependence of this drag force as a function of the driving velocity, the size of the intruder and the intensity of vibration. We found interesting analogies with solid-solid friction and with the behavior of complex fluids characterized by a yield stress. The range of slow velocities as well as the vibration conditions explored make this experiment novel with respect to previous similar studies [19, 21, 22, 25]. These experiments are the subject of chapter 5.

Diffusion of light

The idea of the Diffusing Wave Spectroscopy (DWS) is to shine a coherent light through a disordered sample where the light is multiply scattered. Therefore, when this light is recovered out of the sample it forms a random interference pattern known as 'speckle' pattern. When the scatterers of the sample move, the interference pattern changes and, in this way, it is possible to obtain information of the dynamics of the sample by studying the temporal correlations of the speckle pattern [26]. This technique was developed for dense suspensions colloids and foams, where it can successfully give quantitative information about the mean squared

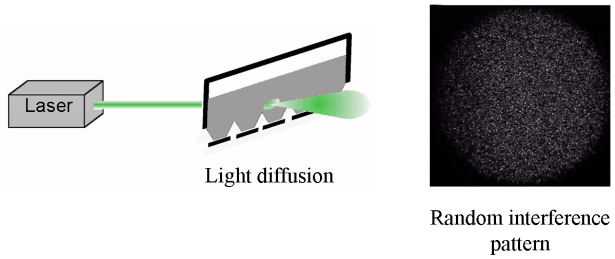

Figure 2.5: DWS measure.

displacement of the scatterers and, thus, is a powerful tool for studying transport properties of complex systems. However, when DWS is applied to granular materials, some of the main assumptions of the theory are not fulfilled any more and the quantitative interpretation in terms of particle displacements is not easy [24]. Nevertheless, very valuable information can still be obtained concerning the characteristic times of the granular dynamics that are not attainable with other techniques given its extreme sensitivity to small movements.

We largely worked on this technique at the beginning of the project, and we were able to obtain interesting preliminary results concerning intermittent dynamics, aging and rejuvenation processes. However, we decided not to include them in this work since none of these results were conclusive.

2.3 Characterization of vibration

2.3.1 Acceleration in the bulk

An accelerometer buried in the granular material allowed the measurement of the acceleration in the bulk induced by the vibration of the transducers. The *Brüel & Kjaer* accelerometer was a $1ml$ cube with a piezoelectric that detected the acceleration of the cube in one direction, which was indicated by an arrow on one of the faces. The electric signal was transmitted to an amplifier through a cable that was attached to the accelerometer on one of the faces of the cube in a way that the orientation of the cable was perpendicular to the direction of measurement of the accelerometer. The accelerometer was buried in the pile in such a way that the direction of measurement was vertical and with the cable going out of the container at one of its extremes (see figure 2.2).

Figure 2.6 shows a typical measurement of acceleration $\gamma(t)$ for an input square signal of frequency $f = 400Hz$ and voltage $V = 10V$. It also shows the vertical velocity $v(t)$ obtained

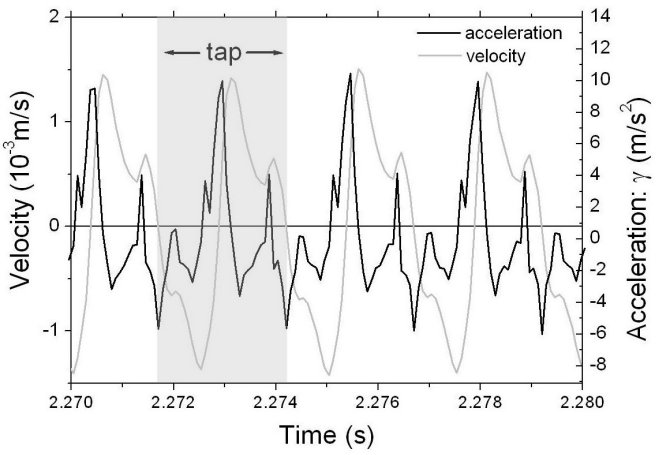

Figure 2.6: *Acceleration measured by the accelerometer buried in the bulk for a signal of frequency $f = 400Hz$ and voltage $V = 10V$. The velocity is obtained by integration of the acceleration signal (equation 2.1). A tap is defined as one cycle of the movement of the transducers.*

by integration of $\gamma(t)$

$$v(t) = \int_0^t \gamma(\tau) d\tau. \tag{2.1}$$

From the velocity signal it was possible to obtain the kinetic energy density $\epsilon_k \equiv (1/2)\rho_{acc} v^2$, where ρ_{acc} is the mass density of the accelerometer. Then, the mean kinetic energy density during vibration is

$$\langle \epsilon_k \rangle = \frac{\rho_{acc}}{2T} \int_0^T v^2(t) dt, \tag{2.2}$$

with $T >> 1/f$. Note that two signals of different frequency f but equal $\langle \epsilon_k \rangle$ did not inject the same energy to the system each tap, where a tap is defined in figure 2.6.

A reference energy to which $\langle \epsilon_k \rangle$ can be compared is the potential energy density of the granular material at a height of one grain diameter d:

$$\epsilon_p \equiv \rho_p g d, \tag{2.3}$$

where ρ_p is the mass density of the granular material, i.e. $\rho_p = \rho\phi$, with ρ the density of glass and ϕ the packing fraction of the pile. In our system $d = 1.2mm$, $\phi \approx 0.6$ and $\rho = 2.6g/cm^3$, then we get $\epsilon_p \approx 20J/m^3$.

It is important to note here that even if the measurements with the accelerometer were directly done in the bulk, they did not give the exact acceleration of the grains, since the accelerometer cube had a different density and geometry.

The voltage and frequency of the input signal to the transducers are the parameters that we can control. Now, we would like to translate them into the energy and acceleration induced in the grains by the transducers since these are more general parameters that can be used for comparison with other experiments.

2.3.2 Acceleration and energy vs frequency

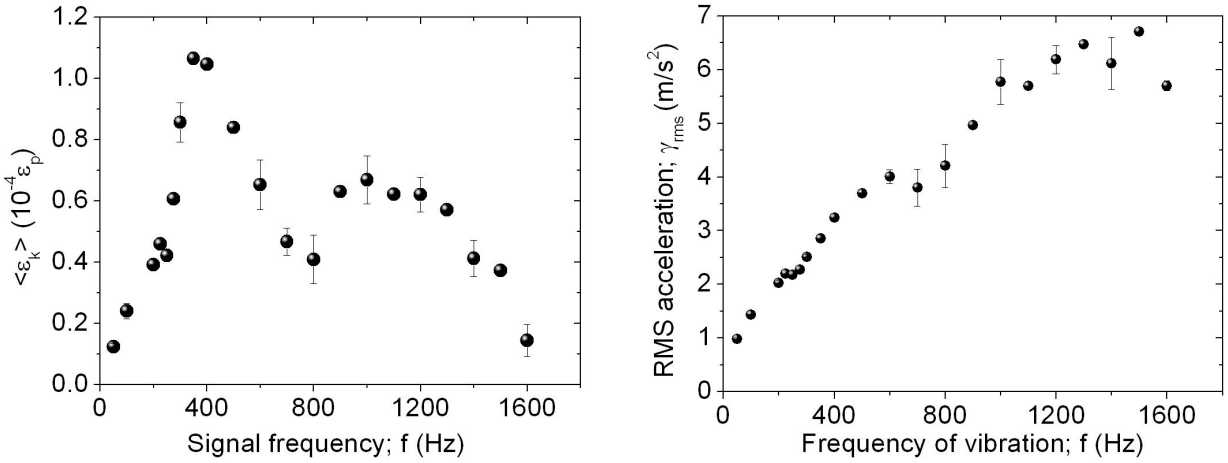

Figure 2.7: *Left: Mean kinetic energy density $\langle\epsilon_k\rangle$ as a function of input signal frequency at the maximum input voltage ($10V$). $\epsilon_p = \rho_p g d$ is the potential energy density for a height d, the mean diameter of grains. Right: RMS acceleration as a function of frequency.*

Figure 2.7 shows the mean kinetic energy density $\langle\epsilon_k\rangle$ (plot in the left), and the root mean squared acceleration $\gamma_{rms} = \sqrt{<\gamma^2>}$ (plot in the right) as a function of input signal frequency f. For these measurements the accelerometer was placed at a depth of $1cm$, which corresponds to the depth at which the drag force experiments were done (chapter 5), and the signal voltage used corresponds to the maximum limit for our set up ($10V$). Before taking these data, the system was vibrated at the maximum intensity ($400Hz$ and $10V$) for three hours in order to avoid the initial regime of strong compaction. However, we verified that the acceleration in the bulk does not change considerably either with packing fraction nor with the depth of the accelerometer in the pile.

The kinetic energy density is expressed in terms of the potential energy density ϵ_p defined above (equation 2.3). From the energy plot we can see that the maximum energy that could be injected in average to the granular medium corresponded to a signal of around $400Hz$ at $10V$. Moreover, the value of this maximum energy was of $10^{-4}\epsilon_p$, which is equivalent in potential energy to a height of $0.1\mu m$ ($10^{-4}\epsilon_p = \rho_g g(10^{-4}d)$; $10^{-4}d \cong 0.1\mu m$). Interestingly,

this height is comparable to the r.m.s. amplitude of sinusoidal oscillation of the piezoelectric transducers at $400Hz$ with $\gamma_{rms} = 3m/s^2$, which is approximately $0.5\mu m$.

2.3.3 Acceleration and energy vs voltage

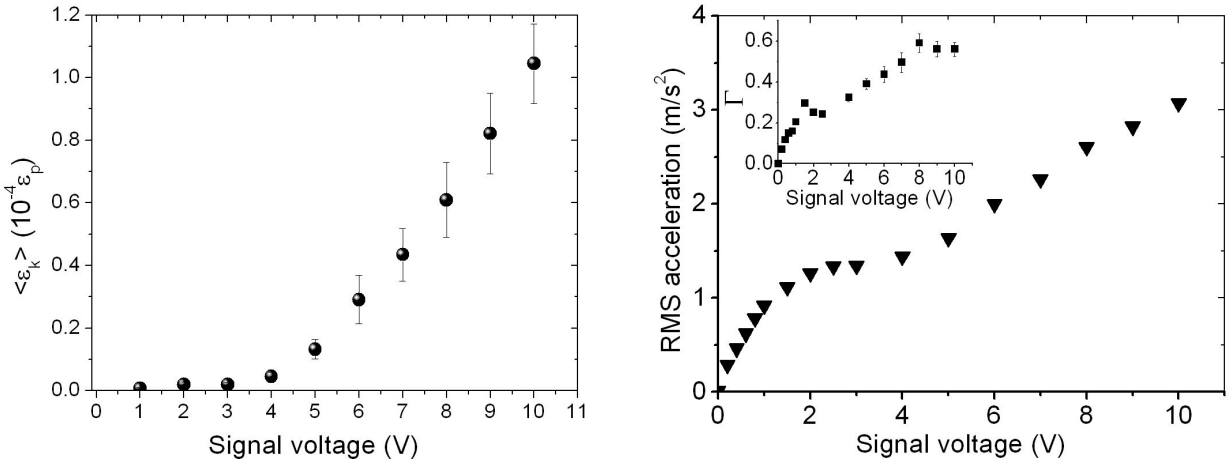

Figure 2.8: *Left: Kinetic energy density $\langle \epsilon_k \rangle$ as a function of input signal voltage. Right: RMS acceleration as a function of voltage (inset: $\Gamma =< Min(\gamma(t)) > /g$). Data on both plots were taken at $f = 400Hz$.*

Figure 2.8 shows the dependence of the energy (plot in the left) and the acceleration (plot in the right) measured in the bulk on the input signal voltage. The measurements were done at $f = 400Hz$ because it was this frequency of vibration for which the injection of energy was maximal for the highest voltage. Noteworthy is the different behavior for low and high voltages, with a transition around $4V$. This abrupt change in behavior might correspond to the threshold voltage at which the transducers manage to break the force network that resists the motion of grains relative to the walls of the container.

2.3.4 Absence of convection

It has been shown that convection, when present, plays an important roll in the evolution of compaction in strong vibration experiments [23]. Moreover, it could be that the steady states that have been obtained would correspond to an interplay between compaction and convection. For this reason we wanted to make a vibration experiment which would present compaction but no convection. To verify if our system presented convection for long time experiments, we put in the system two layers of the same glass beads but colored. One of these layers was at the middle height of the pile and the other at the surface. We then vibrated the system at the maximum intensity for 14 hours, and registered images of a lateral wall all

along the experiments. Figure 2.9 shows the first and the last of these images where it can be clearly seen that the colored layers were not destroyed, showing that there is not flux of particles. Moreover, this shows that particles barely move and that they stay close to their initial neighbors. This experiment was repeated several times giving always the same result: there is no convection in the system!

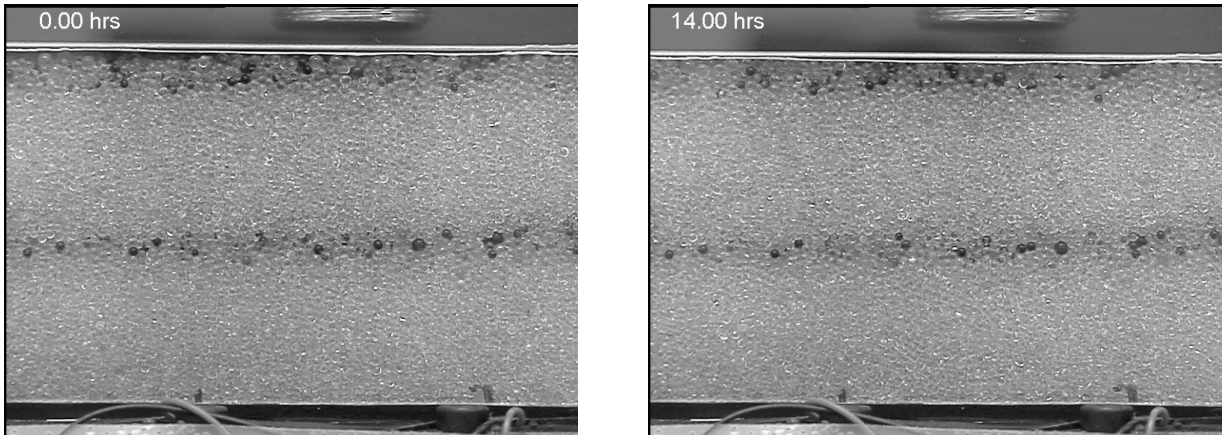

Figure 2.9: *First and last images of a sequence of images taken each three minutes on a* 14 *hour experiment of vibration at the maximum intensity. Two layers of colored particles were still present at the end of the experiment, showing that there was no flux of particles and, therefore, there was no convection.*

Even though there is no net flux of particles, the full sequence of images shows that important changes in the structural configuration of the pile exist. In fact, it can be seen that the dominant motion induced on the particles is rotation, and that such movement is far from being homogeneous. A single particle can present moments of intense activity together with long periods of rest. One can also identify regions of different rotational mobility. The study of rotation of particles would be an interesting analysis to gain information of the microscopic dynamics of the system.

2.4 Conclusions

We constructed a novel experimental set up that vibrates a granular material: a weak and disordered agitation was obtained by using independent piezoelectric transducers. The main motion excited on the grains was rotation and, most importantly, there is no convection in the system.

The energy injected to the system as well as the acceleration induced in the granular matter by the transducers was directly measured in the bulk by means of an accelerometer.

Both acceleration and energy were systematically measured as a function of frequency and input signal voltage.

The fact that vibration was weak and that the container was not shaken, allowed very precise measurements during vibration. The design of the set up allowed measurements of the packing fraction, to see boundary particles directly, to measure the drag force on an intruder grain and, finally, to make Diffusing Wave Spectroscopy measurements.

Chapter 3

Packing fraction

This chapter presents the relaxation of the packing fraction in long time vibration experiments for different vibration conditions. We investigated the effect of the r.m.s. acceleration and the kinetic energy on the relaxation of the density of the pile and we found that it is the energy which determines the compaction rate.

We also studied the response of the packing fraction to variations in the vibration intensity and we found a quasi reversible regime of the density as a function of vibration intensity as well as interesting analogies with the response of thermal systems to changes in temperature like the Kovacs effect.

3.1 Measuring the packing fraction

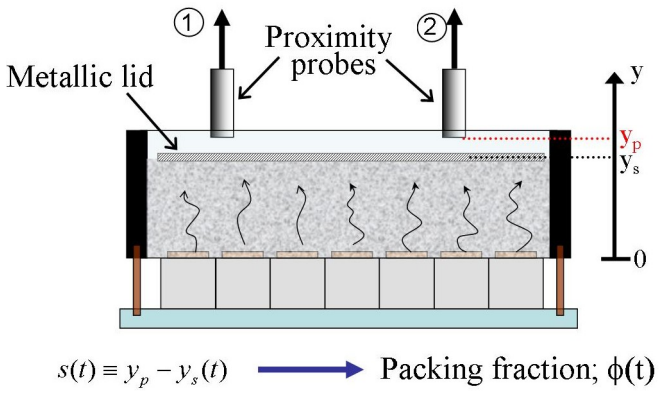

Figure 3.1: Packing fraction is measured with two inductive proximity probes that give the separation $y_p - y_s$ between the probes and a thin metallic lid that rests on the surface of the grains.

The packing fraction ϕ of a granular pile is defined as the ratio of the volume occupied by the grains V_g, and V_T, the total volume of the pack. V_g is easily obtained by knowing the total mass of the pack M_g and the mass density of the constituent material of the grains ρ, so that $V_g = M_g/\rho$. For the particular case of our experiment $M_g = 265 \pm 0.1g$ and $\rho = 2.59 \pm 0.02g/cm^3$, which makes $V_g = 102.3 \pm 0.8cm^3$. On the other hand, V_T for a rectangular packing is the product of the horizontal cross section of the container, S, and the height of the packing surface y_s. In our set up $S = (19 \pm 0.05cm)(2.3 \pm 0.05cm) = 43.7 \pm 0.9cm^2$ and the height of the pile is obtained by using two inductive proximity probes (Pepperl+Fuch's I15-18GM-I3) that measure $s \equiv y_p - y_s$, the separation between the probes and a thin metallic lid that rests on the surface of the packing (see figure 3.1). The resolution of the sensors is of the order of $5\mu m$ and we use two of them to take into account the deviations of the lid from the horizontal. Then, $y_s = y_p - s$ where $s = 1/2(s_1 + s_2)$ (measurements from both sensors) and $y_p = 42.5 \pm 0.2mm$. Thus, the final expression for the packing fraction is

$$\phi = \frac{V_g}{V_T} = \frac{M_g/\rho}{S y_s} = \frac{M_g}{\rho S(y_p - s)}. \tag{3.1}$$

The uncertainty on the absolute value of ϕ when using equation 3.1 is of the order of 3% for a typical value of $\phi = 0.6$.

The metallic lid used had a weight which was equivalent to five layers of glass beads and its shape coincided with the horizontal cross section of the container, but it was slightly smaller in such a way that it did not touch the container walls but at the same time the beads could not pass or get stuck between the lid and the container. Since the lid was not flexible, what we obtained with this technique was an averaged measurement of the height of the pile. In fact, at the beginning of each experiment, the irregularity of the surface of the pile made that the lid did not touch the whole surface. However, after some time of vibration, the surface became regular and the lid touched it everywhere, giving a good measurement of the mean height of the pile. Deviations from logarithmic behavior for short times of the curves in figure 3.4 are consequence of the irregularity of the surface.

3.2 Long time logarithmic compaction

Figure 3.2 shows the time evolution of the packing height and the packing fraction when vibrating at a maximum vibration intensity ($10V$ and $400Hz$) for ten days. It can be seen that the vibration intensity is so small that it induces an extremely slow logarithmic compaction and even after ten days of vibration there is no saturation observed at a final steady volume. The

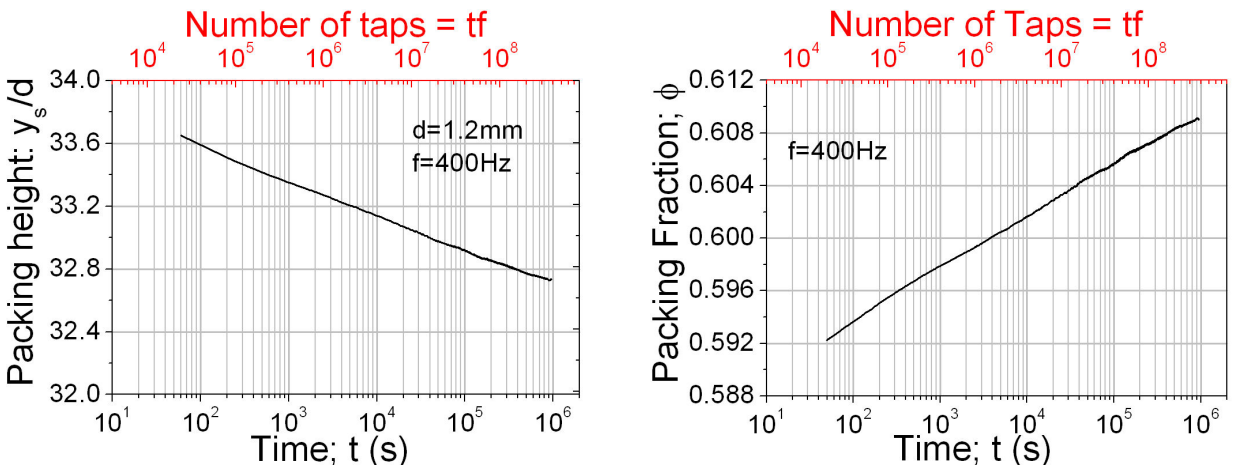

Figure 3.2: *Packing height and packing fraction as a function of time for ten days of vibration at the maximum intensity*$(10V$ *and* $400Hz)$*. The packing height* y_s *is normalized by the mean grains diameter* $d = 1.2mm$*. The number of taps* tf *are also shown.*

total packing fraction variation at maximum vibration intensity is of 3%, which is comparable to the compaction of 5% found by Nowak et al. [9] for much stronger vibration intensity ($\Gamma = 6.8$), and the 4% reported by Pouliquen et al. [15] obtained by shearing.

From figure 3.2 we see that a good fit for the height of the pile is the function

$$y_s(t) = y_{s0}\left(1 - \beta ln(1 + \frac{t}{\tau_0})\right), \tag{3.2}$$

where the parameter β depends on vibration intensity, $\tau_0 = 1s$, and $y_{s0} = y_s(t = 0)$. For our system $\beta \leq 2.5 \times 10^{-3}$, which corresponds to the experiment at the maximum vibration intensity shown in figure 3.2. Since $0 < \beta ln(1 + \frac{t}{\tau_0}) < 1$, from equations 3.1 and 3.2 follows that

$$\phi(t) = \frac{M_g}{S\rho y_{s0}}\left(\frac{1}{1 - \beta ln(1 + \frac{t}{\tau_0})}\right) = \phi_0\left(1 + \beta ln(1 + \frac{t}{\tau_0})\right) + O\left(\left(\beta ln(1 + \frac{t}{\tau_0})\right)^2\right), \tag{3.3}$$

where $\phi_0 \equiv M_g/S\rho y_{s0}$. It is important to note that equations 3.2 and 3.3 diverge for infinite times, which means that they are only valid when the time needed to reach a final steady density is much bigger than experimental times.

The number of taps in figure 3.2 is obtained as the product of the time t and the frequency f of the input signal. This defines a tap as one cycle of the movement of the piezoelectric transducers (see figure 2.6).

3.3 Relevant parameter for compaction: energy.

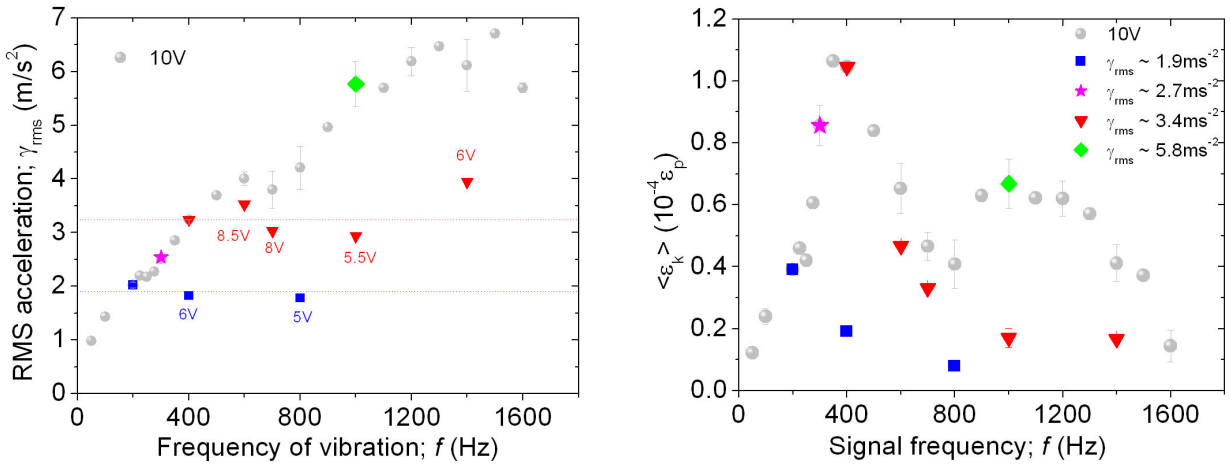

Figure 3.3: *Acceleration and energy as functions of frequency. Superposed to the* $10V$ *measurements are groups of points which have the same acceleration but different energy. These points indicate the vibration conditions of the compaction experiments in figure 3.4.*

In standard vibration experiments [9, 23, 27], the control parameter used to characterize the vibration intensity is the peak acceleration attained by the container of the grains. However, energy can be injected into a granular medium in very different ways, and the peak acceleration might not be the most pertinent and general parameter to be used [23]. In order to explore this issue in our system we performed a set of compaction experiments at different vibration conditions to see the dependence of β (equation 3.3) on the mean kinetic energy density $\langle \epsilon_k \rangle$ and on the r.m.s. acceleration γ_{rms}.

The way in which we proceeded was to perform long compaction experiments (at least 4 days of vibration) at vibration conditions which had the same r.m.s. acceleration but different energy. Figure 3.3 shows the approximately constant acceleration obtained for several frequencies at appropriate voltages as well as the energy associated to each of these vibration conditions. Compaction curves for the vibration conditions indicated by the group of points in figure 3.3 are shown in figure 3.4. Solid lines are fitted to the data using equation 3.3. These fits allow to obtain $\beta(\langle \epsilon_k \rangle)$, which is plotted in figure 3.5. From these results it is clear that the compaction dynamics is governed by the mean kinetic energy of the grains but not by their acceleration. Moreover, as discussed in section 2.3.1 (equation 2.2), the energy injected to the system per tap is not the same for two different vibration frequencies with equal $\langle \epsilon_k \rangle$. Therefore, in this kind of weak continuous vibration, the energy injected to the system per tap is not the relevant parameter.

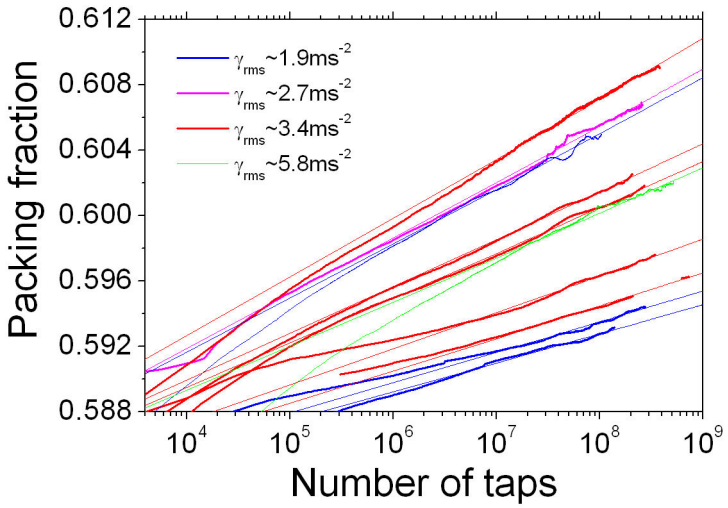

Figure 3.4: *Long compaction experiments for different vibration conditions. Curves of the same color have the same r.m.s. acceleration but different energy $\beta(\langle\epsilon_k\rangle)$. Solid lines are the fits using equation 3.3.*

The noise of these measurements does not allow to determine the exact relationship between β and $\langle\epsilon_k\rangle$. We found that the functions that fitted the best to the data were a power law of the form $\beta = C\langle\epsilon_k\rangle^{\alpha}$ with C a constant and $\alpha = 1/4$, and the logarithmic function shown in figure 3.5, with a characteristic beta $\beta_{char} \approx 4.7 \times 10^{-4}$, and a characteristic energy $\epsilon_{char} \approx 6.4 \times 10^{-7}\epsilon_p$. The logarithmic fit turns out to be statistically better than the power law. However, it is still not clear for us the physical meaning of β_{char} and ϵ_{char}.

3.4 Reversibility of the packing fraction. Kovacs effect

At the end of the long compaction experiments shown in figure 3.4, variations in the intensity of vibration were performed to study the response of the packing fraction. In the following, the reference vibration energy that will be used is the maximum kinetic energy possible with our set up, $\epsilon_{max} = 1.04 \times 10^{-4}\epsilon_p$, which corresponds to an input signal of 10 volt at $400Hz$. Figure 3.6 shows the results of one of these experiments, where the energy variation sequence and the time of vibration in each of these energies were arbitrarily chosen. After ten days of vibration at $300Hz$ at mean kinetic energy $\epsilon_{k1} = 0.8\epsilon_{max}$ (magenta curve in figure 3.4), the energy was lowered down to $\epsilon_{k2} = 0.2\epsilon_{max}$ for 4 hours, then it was set to $\epsilon_{k3} = 0.06\epsilon_{max}$ for 4 hours and finally it was raised up again to ϵ_{k1} for 24 hours. Then the same energy variation sequence was repeated. The right plot in figure 3.6 shows the relative variations of packing fraction $\Delta\phi(\epsilon_{ki} \to \epsilon_{kj}) = \phi(t) - \phi(t_{i\to j})$ when the energy was changed from ϵ_{ki} to ϵ_{kj} at time

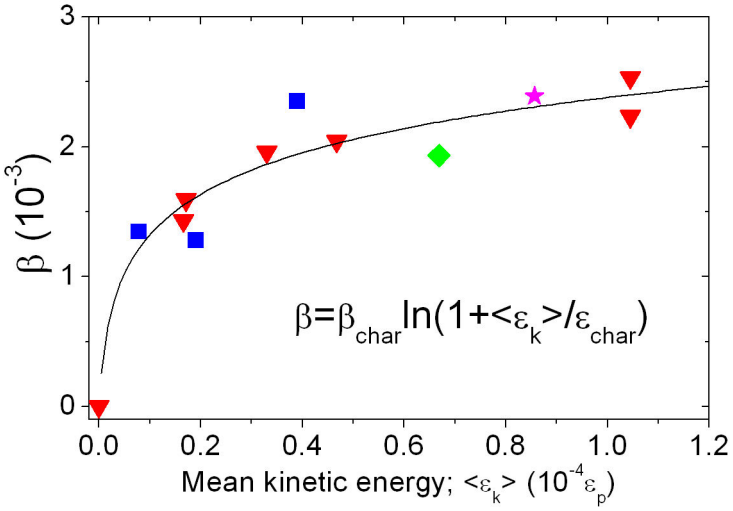

Figure 3.5: *Parameter β from equation 3.2 as a function of the mean kinetic energy density. The r.m.s. acceleration of each point can be known by comparing symbols in this figure with those in figure 3.3. These results show that the relevant parameter for compaction is the kinetic energy of the grains and not their acceleration.*

$t_{i\to j}$ (with $i, j = 1, 2, 3$). The first energy variation sequence is shown in blue and the second sequence in gray.

The behavior of the packing fraction is consistent with the results obtained by Nowak et al. [9] in the sense that for lower vibration intensities the density of the packing increases. This means that in this long time experiment the system is not far from the reversible branch of the density vs intensity of vibration curve in reference [9]. In other words, there is a unique and well defined relative value of the density for each vibration intensity.

In contrast with the behavior of density in figure 3.6, figure 3.7 shows the results of a vibration energy variation sequence done at the end of a six days initial vibration at $1400Hz$ and energy $\epsilon_{k5} = 0.16\epsilon_{max}$. Then, the energy was changed as follows: $\epsilon_{k5} \to \epsilon_{k4} \to \epsilon_{k5} \to \epsilon_{k4} \to \epsilon_{k5} \to \epsilon_{max}(400Hz)$, where $\epsilon_{k4} = 0.4\epsilon_{max}$. Note that at the end of the long time vibration the system was looser than in the experiment at $300Hz$ presented above (figure 3.6), and the response of the density to energy variations was always to increase, except for a small dilation transient in the second change from ϵ_{k5} to ϵ_{k4}, which can be better seen in figure 3.8. This transient dilation is analogue to the 'Kovacs effect' observed in thermal glassy systems when the temperature is changed abruptly [12] and it was previously observed in granular systems by Josserand et al. [11]. Noteworthy, there is not a transient dilation either on the first change of energy from ϵ_{k5} to ϵ_{k4}, nor in the last change from ϵ_{k5} to ϵ_{max}.

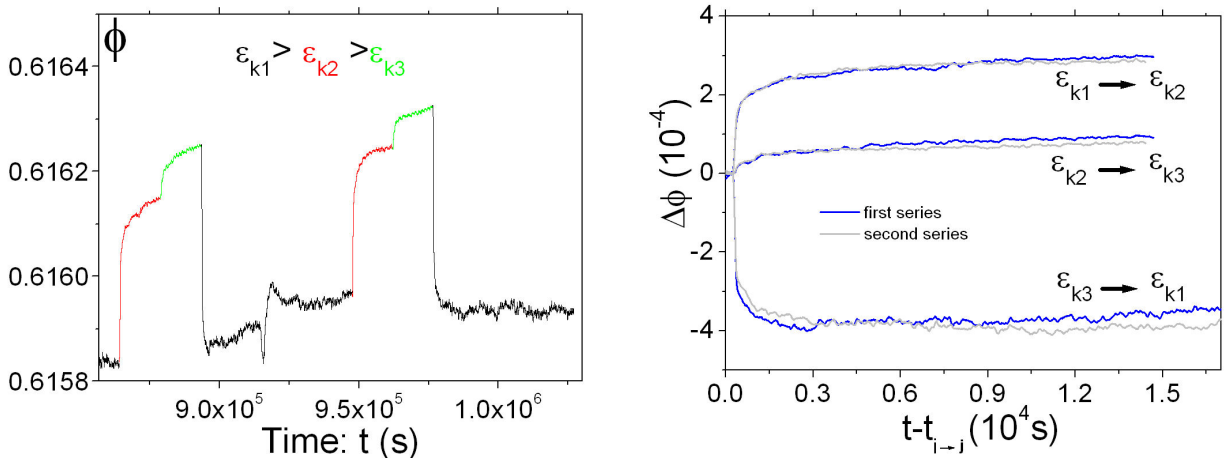

Figure 3.6: *After ten days of vibration at* $300Hz$ *at energy* ϵ_{k1}*, the intensity of vibration was changed to see the response of the density. Right: relative variations of packing fraction* $\Delta\phi(\epsilon_{ki} \rightarrow \epsilon_{kj})$*. A quasi reversible state is seen with denser packs for lower vibration intensities.*

Many features of granular compaction are also found in glassy systems [28, 29, 30, 31] and some of them are successfully described by the reversible Parking Lot Model (PLM) [32, 33, 34] or the nonlinear diffusion model by Arenzon et al. [35].

It is important to note here that it was not obvious *a priori* that these results were to be recovered with our set up, even though they have been observed in other compaction experiments [9, 11, 23], since there are profound differences in the agitation methods. Ours is a high frequency continuous weak vibration without convection while usually people work with discrete strong taps. Therefore, these results support the robustness of the main features of compaction. An advantage of our set up is that the evolution of density with time can be measured very precisely for very weak vibration intensities with, on the other hand, the disadvantage of not having access to stronger shaking.

3.5 Conclusions

In this chapter, an extensive study of the relaxation of the packing fraction of the weakly vibrated granular material was presented. A neat logarithmic compaction for all vibration intensities and frequencies studied was observed. Due to the weakness of the agitation, a saturation of the density was never attained, even after ten days of vibration at our strongest vibration intensity.

It was found that the relevant parameter that controls the rate of compaction of the granular pile is the mean kinetic energy and not the r.m.s. acceleration. This is important because in vibration experiments in granular materials the acceleration is often used as the

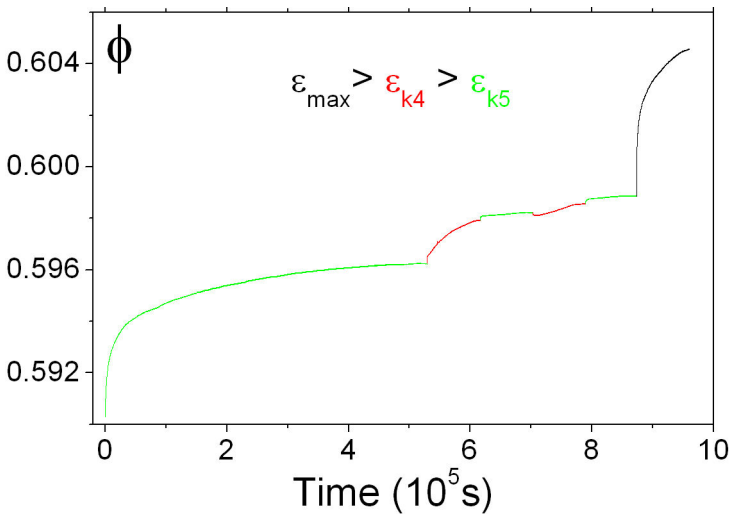

Figure 3.7: *Vibration intensity variations at the end of a long time experiment at* $1400Hz$ *and energy* $\epsilon_{k5} = 0.16\epsilon_{max}$. *The system is so loose that it becomes always more compact when the energy changes.*

control parameter. However, vibration is usually applied in the form of discrete strong taps, while ours is a weak continuous agitation.

A quasi reversible packing fraction state was observed where, for each intensity of vibration, corresponded a well defined relative value of density.

When vibration intensity variations were applied to looser packs, the response of the packing fraction was analogous to thermal systems under temperature variations, like the Kovacs effect.

Both the reversibility of the packing fraction as well as the Kovac effect had already been observed in granular materials [9, 11]. However, the system and vibration method used in those cases were very different from ours. Thus, the fact that we have also found them shows the robustness of the compaction features. Moreover, our set up allows the measurement of the relative variations of density in a very precise way, which makes it possible to study relaxation processes and transient phases very accurately.

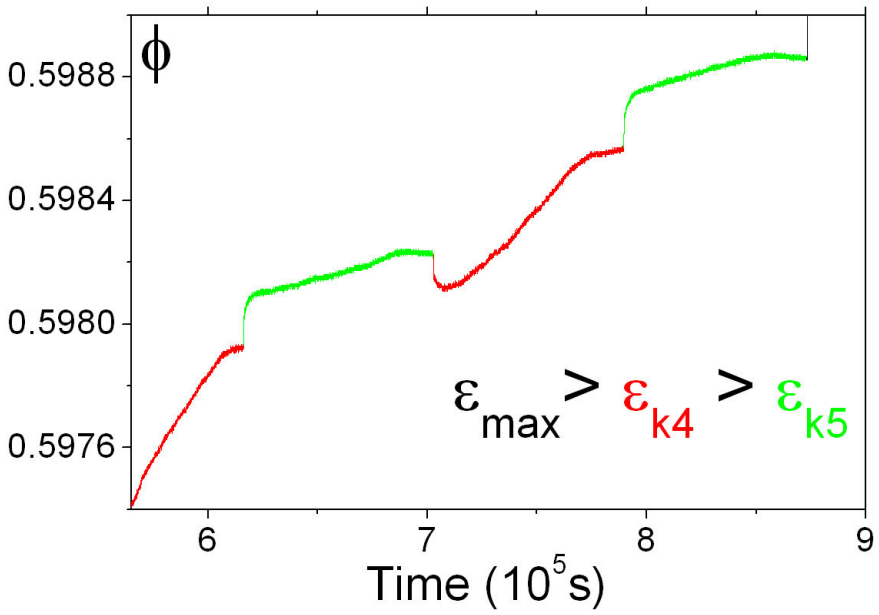

Figure 3.8: *Zoom to the energy variations of experiment in figure 3.7. A transient dilation analogue to the 'Kovac effect' is observed when the energy changes from* ϵ_{k5} *to* ϵ_{k4}.

Chapter 4

Particle tracking

Direct observation of boundary particles allowed to follow and study their trajectories during long time compaction experiments. The results of these experiments are the subject of the present chapter.

The statistical characteristics of the trajectories of these boundary particles are analyzed and it is shown that they present a cage-like dynamics, like glassy thermal systems. It is even estimated the size of the cages. It is also shown that the dynamics of these particles is homogeneous in time while the compaction is continuously increasing, an astonishing result that suggests that compaction results from collective modes of the system.

Of course, all these results are valid for particles that are next to the wall, and we do not know to what extent their dynamics resemble the dynamics of particles in the bulk. Nevertheless, we believe that they do not differ considerably because the width of the system is only twenty times the diameter of the grains and also because the intensity of vibration is strong enough to brake the contacts between particles and walls (see section 2.3.3).

4.1 Tracking individual grains

In the previous chapter we presented long time vibration experiments where the evolution in time of the packing fraction of the system was studied. Density is an intensive macroscopic quantity that would be interesting to relate to microscopic local features the way it is done in statistical mechanics. Here, of course, microscopic refers to the size of a grain. With this in mind, during compaction experiments we filmed a small region of approximately $5d \times 5d$ next to a lateral transparent wall with a CCD camera. Figure 4.1 shows one of these images during vibration. Images were recorded at a rate of one image per minute all along the duration of

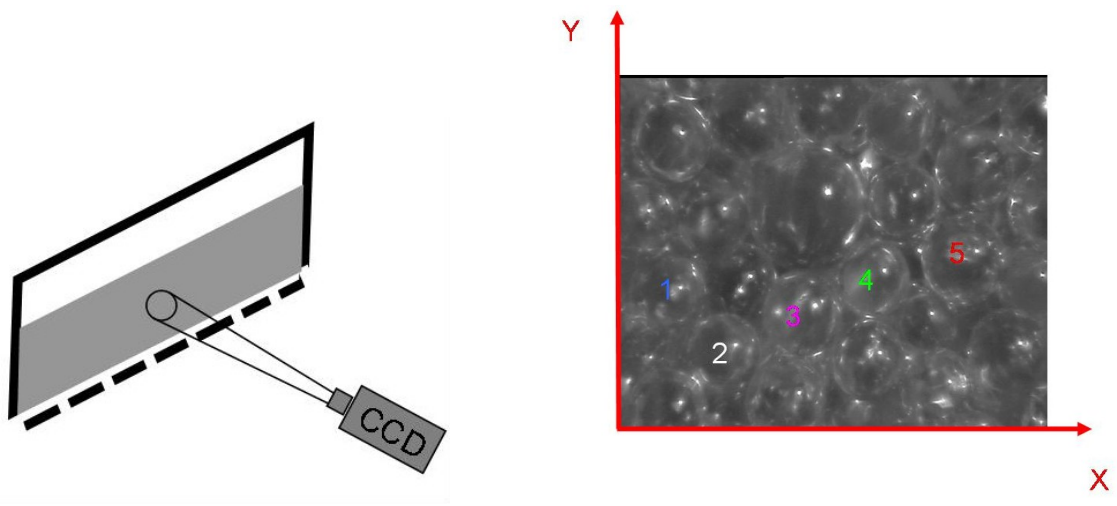

Figure 4.1: *During compaction experiments, a CCD camera filmed a small region of approximately* $5d \times 5d$ *next to a lateral transparent wall at a rate of one image per minute. Vertical* $y(t)$ *and horizontal* $x(t)$ *positions of numerated particles were obtained by image analysis.*

the experiments. By image analysis it was possible to obtain the position of each particle in each image, i.e. the position of particles as a function of time.

The way in which images were analyzed was by tracking the position of the bright spots that appeared in the upper left portion of the particles. These spots are due to the reflection of a fixed light source situated far away from the packing (approximately two meters). Given the small size of the grains, the light can be considered as coming from a single point infinitely far and, therefore, the relative position of the spot with respect to the center of the grain is constant for any practical purpose. Thus, the position of a grain in an image corresponds to the center of the spot. The determination of the position of the spot was made by using the Particle Tracking Script of the ImageJ software. This script gives the central pixel of all the pixels occupied by the spot, which implies that the resolution of this analysis technique can not be less than one pixel (pix). The mean size of the spots was around $4pix \times 4pix$. In order to assess the precision of the image analysis method we mounted the camera on a support that allowed micrometric horizontal displacements. We took images of a static granular pack at constant displacement steps of the camera of $10\mu m$. The set up was under similar lighting and optical conditions than in the experiments. Figure 4.2 shows the position obtained by image analysis of one grain while moving the camera. From the best linear fit of the measurements made on several grains we obtained a relation of $145 \pm 15 pix/mm$, which means that the size of one pixel in the image is of $6.9 \pm 0.7 \mu m$. In figure 4.2 a plot of the deviations from the best linear fit for each measurement is also shown. These divisions are all smaller than one pixel.

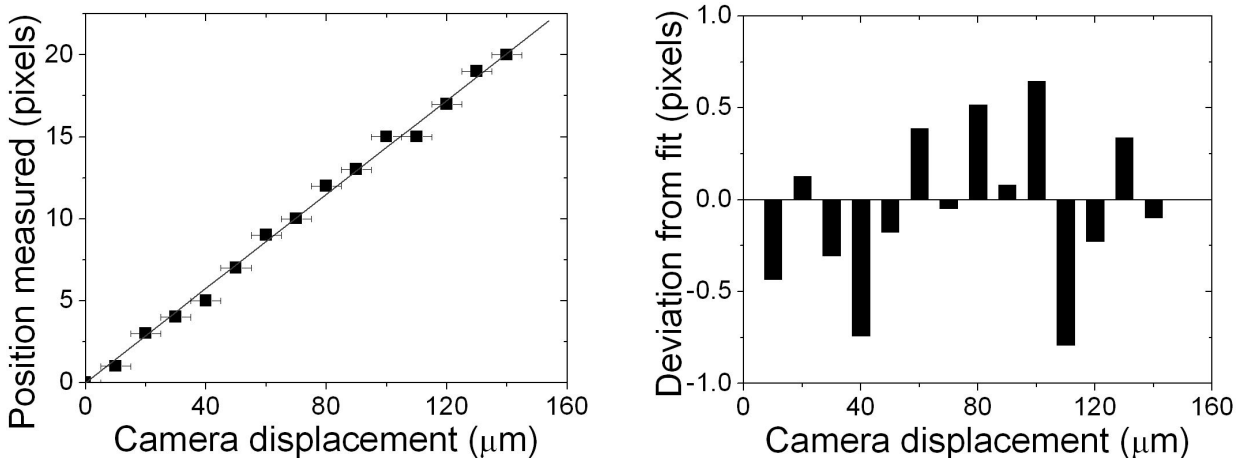

Figure 4.2: *Calibration of the image acquisition and analysis set up. The camera was displaced horizontally at steps of* $10\mu m$*, at each step recording an image of an static packing.*

4.2 Trajectories in long time experiments

Figure 4.3 shows the trajectories of the five particles numerated in figure 4.1 during a ten days vibration experiment at $300Hz$ and $10V$. The corresponding packing fraction curve of this experiment is the bright green curve in figure 3.4. The origin of the vertical coordinate y is taken at the bottom of the container (see figure 3.1) while $x = 0$ corresponds to the left border of the image. Both x and y are normalized by the mean particle diameter $d = 1.2mm$. Note that the filmed region was at a height of around 26 particle diameters, i.e. at a depth of $1cm$ from the surface. This position was chosen because it is more or less the same depth at which the intruder particles are dragged in the experiments described in chapter 5. Trajectories of particles bear a strong erratic component and it can be seen that after an initially big downwards displacement related to a strong initial compaction, particles become trapped in a small region compared to the particle size.

Plots in figure 4.4 show the horizontal and vertical coordinates as a function of time for the five particles of figure 4.3. Interestingly, the position of individual particles is highly fluctuating in both directions, though the exploration surface is small compared to the grain size. The horizontal dynamics of the particles seems very much like random walks without any preferred direction, and at the same time, correlations between different particles are obvious. On the other hand, the vertical displacements present a logarithmic downwards drift which seems to be consistent with the global logarithmic compaction of the packing. Now we proceed to characterize quantitatively this rich microscopic dynamics and to relate it to macroscopic features.

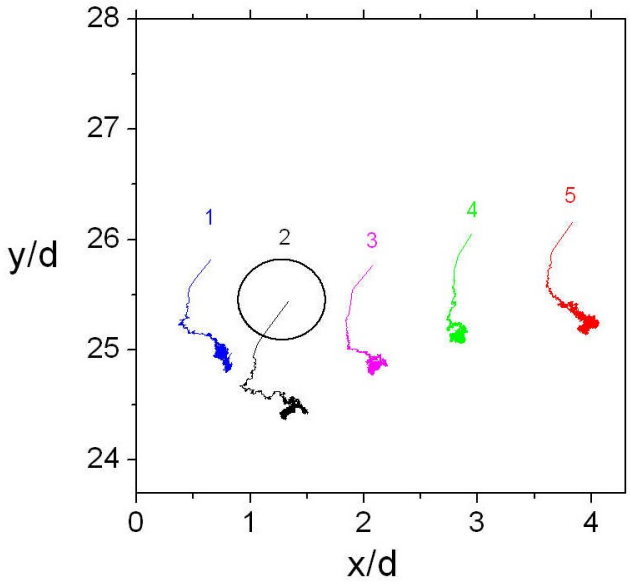

Figure 4.3: *Trajectories of numerated particles in figure 4.1 for a ten days vibration experiment at* $300Hz$ *and* $10V$*. The origin of the vertical coordinate* y *is at the bottom of the container (see figure 3.1) while* $x = 0$ *corresponds to the left border of the image. Both* x *and* y *are normalized by the mean particle diameter* $d = 1.2mm$*. The size of a small grain is illustrated by the circle near particle* 1*.*

4.3 Homogeneous vertical compaction

Combining the measurement of the surface height with the lateral particle tracking it is possible to test the vertical homogeneity of the compaction. We can think of the packing as composed of several horizontal slices[1], each one of them squeezing an amount $\epsilon(y, \Delta t)$ for a vibration of duration $\Delta t = t_2 - t_1$. The total displacement $\Delta y = y(t_2) - y(t_1)$ of a particle at a height y would be

$$\Delta y(\Delta t) = \int_0^{y_1} \epsilon(y, \Delta t) dy. \tag{4.1}$$

An homogeneous vertical deformation would imply that $\epsilon = \epsilon(\Delta t)$, and thus $\Delta y(\Delta t) = \epsilon(\Delta t) y_1$. This relation is true for any horizontal slice and in particular, it is true for the surface height y_s. Then

$$\frac{\Delta y(\Delta t)}{y_1} = \frac{\Delta y_s(\Delta t)}{y_{s1}}. \tag{4.2}$$

[1]Imagine slices of width of the order of two or three particle diameters that would be thiner the more compact is the system.

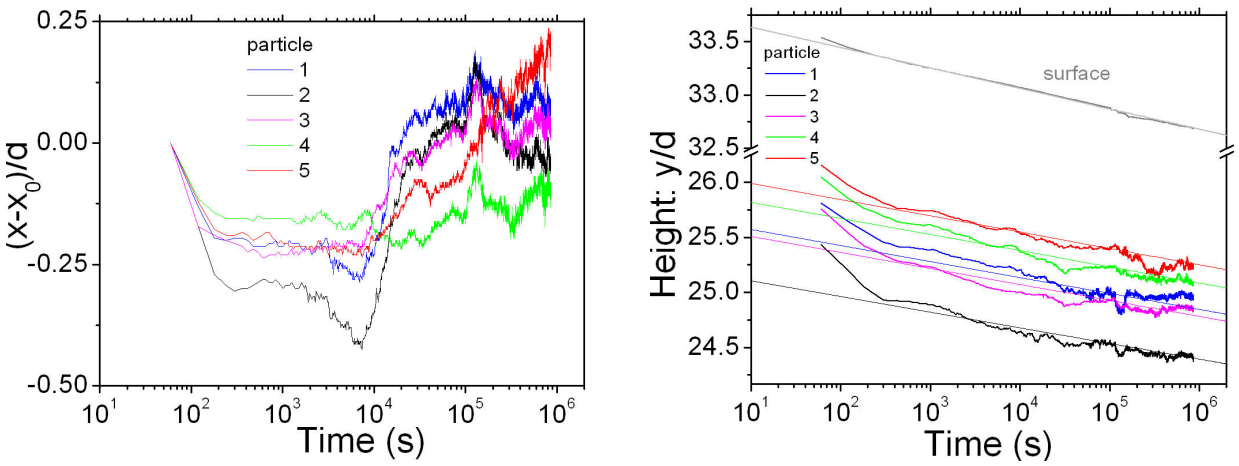

Figure 4.4: *Horizontal and vertical coordinates as a function of time for the five analyzed particles. Horizontal origins are put together for comparison. In the y plot, the position of the surface together with the fits from equation 4.3 is also shown.*

The surface position is well described by equation 3.2, which together with 4.2 gives the position of any horizontal slice in the pack if the deformation is homogeneous:

$$\Delta y(t_1, t_2) = -\left(\frac{y_1}{y_{s1}}\right) y_{s0}\beta ln\left(\frac{1+t_2/\tau_0}{1+t_1/\tau_0}\right). \tag{4.3}$$

The individual lateral particles that we tracked belong to some of these horizontal slices so, if deformation is vertically homogeneous during vibration, it is expected that their height follow equation 4.3. Figure 4.4 shows the evolution in time of the height of the particles together with the height of the surface. The solid line that passes through the surface data is the fit using equation 3.2, while solid lines through particles heights correspond to equation 4.3 with $t_1 = 10^5 s$ and $t_2 = t$. The good agreement between data and equation 4.3 suggests that the compaction of the pack is indeed vertically homogeneous.

In the following, we will be interested in the statistical characteristics of the fluctuations in the position of the particles. Thus we will subtract the vertical drift due to the logarithmic compaction (the drift shown in figure 4.4).

4.4 Position fluctuations

In the context of the analogy between vibrated granular packings and thermal systems, a central quantity to look at is the squared displacement as a function of a lag time τ,

$$\Delta r^2 = (r(t+\tau) - r(t))^2. \tag{4.4}$$

The ensemble average of Δr^2 for a Brownian particle grows linearly with lag time τ and in two dimensions it is given by $\langle \Delta r^2(\tau) \rangle = 4D\tau$, with $D = k_B T / 6\pi\eta a$, D being the diffusion coefficient, T the temperature, k_B Boltzman's constant, η the viscosity of the fluid, and a the size of the particle. Complex fluids usually present deviations from this behavior that are related to complex macroscopic rheology [36].

4.4.1 Ensemble dynamics

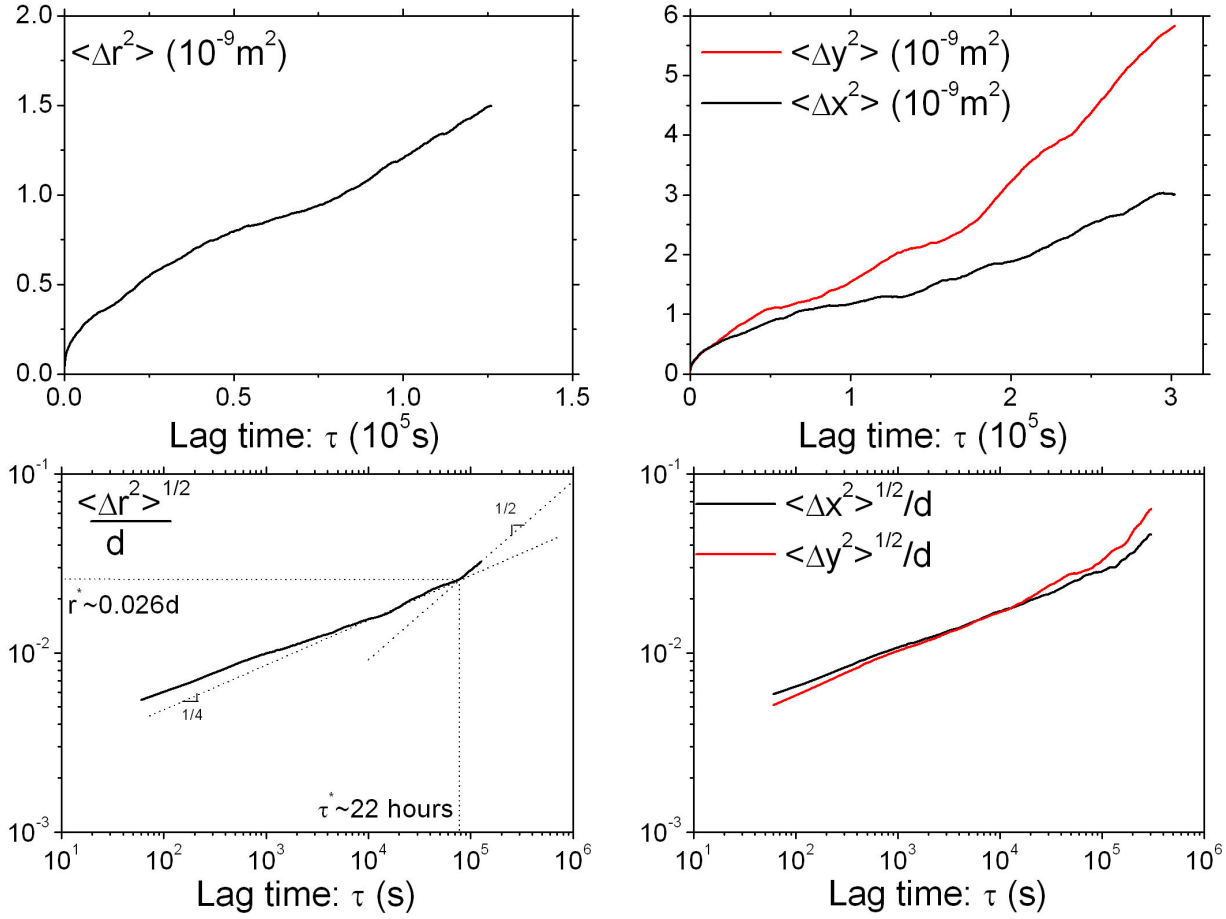

Figure 4.5: *Left: Time and ensemble averaged mean squared displacement of the particles* $\langle \Delta r^2(\tau) \rangle$ *in linear scale, and root mean squared displacement* $\langle \Delta r^2(\tau) \rangle^{1/2}$ *in log-log scale for* $t > 3$ *days. A sub diffusive behavior for short times becomes diffusive at* τ^**, which defines a cage size* r^**. Right: The same but for each of the coordinates* x *and* y*. It shows an asymmetry between vertical and horizontal mobility.*

Since we only have data for five particles, ensemble averages are statistically very poor so, in order to improve the statistics, first we made time averages on the data of each particle and then we averaged between particles. For a discrete series of time $r_i \equiv r(t_i)$ for $i = 1, 2, ..., N$,

where $\delta t \equiv t_{i+1} - t_i$ is constant, we calculated the root mean-squared displacement σ as a function of lag time $\tau = s\delta t$, with s an integer, as

$$\sigma(\tau) \equiv \left\langle \Delta r^2(\tau) \right\rangle^{1/2} \equiv \sqrt{\frac{1}{N-s}\sum_{i=1}^{N-s}(r_{i+s} - r_i)^2}. \tag{4.5}$$

In addition, $\sigma(\tau)$ can also be averaged over the five particles, i.e. an ensemble average. Time and ensemble average are equivalent for a stationary process where there is no privileged time. As we will see later, ours is a quasi stationary system, so one expects that time and ensemble averages to not differ considerably. Left plots in figure 4.5 show the time and ensemble average of $\sigma^2(\tau)$ in linear scale and $\sigma(\tau)$ in log-log scale. Time average was done for $t > 3$ days in order to avoid transient effects from the initial strong compaction. The logarithmic compaction drift was subtracted from the y coordinate. For short times the dynamics is clearly sub diffusive since $\sigma(\tau)$ grows with a power law with exponent smaller than 1/2. However, for longer times there seems to be a change of regime and the dynamics becomes diffusive, though there is no enough data to make any definite conclusion. However, this behavior qualitatively coincides with the results by Marty and Dauchot [14] where they suggest that the short time sub diffusive dynamics correspond to the particles trapped in a cage and the long time diffusion comes from particles going from cage to cage. Thus, the crossover between both regimes defines a cage size r^* and a cage lifetime τ^* [14]. It can be seen from figure 4.5 that for our experiment $r^* \approx 0.026d$ and $\tau^* \approx 22$ days or, equivalently, $\tau^* \approx 24 \times 10^6$ taps. These values contrast with those reported by Marty and Dauchot in reference [14] of $r^* \approx 0.3d$ and $\tau^* \approx 300$ shearing cycles. The way in which we can understand such great discrepancies is by referring to the results by Pouliquen et al. [15] where they made particle tracking in a three dimensional shearing experiment and, even though they did not get a precise size of a cage, they showed that the value of the packing fraction was related to the size of the cage and that they both changed with the shearing angle: a bigger shearing angle made the cage size bigger and more dilated the packing. Therefore, since the size of the cage in our experiment is one order of magnitude smaller than the one found by Marty and Dauchot we can say that the vibration in our experiment is one order of magnitude weaker than their shear. However, the validity of this comparison is not clear since the set up of Marty and Dauchot is a two dimensional horizontal system where there is no effect of gravity.

On the right plots of figure 4.5 are shown the root mean-squared displacements in x $\left(\sigma_x(\tau) = \langle \Delta x^2(\tau) \rangle^{1/2}\right)$ and y $\left(\sigma_y(\tau) = \langle \Delta y^2(\tau) \rangle^{1/2}\right)$. Both coordinates have the same dynamics though particles seem to be more mobile in the vertical direction despite the fact that the logarithmic compaction drift was subtracted. This asymmetry might be caused by the

vertical shaking and could be equivalent to the asymmetries encountered both by Marty and Dauchot [14] and Pouliquen et al. [15] in the direction of shear.

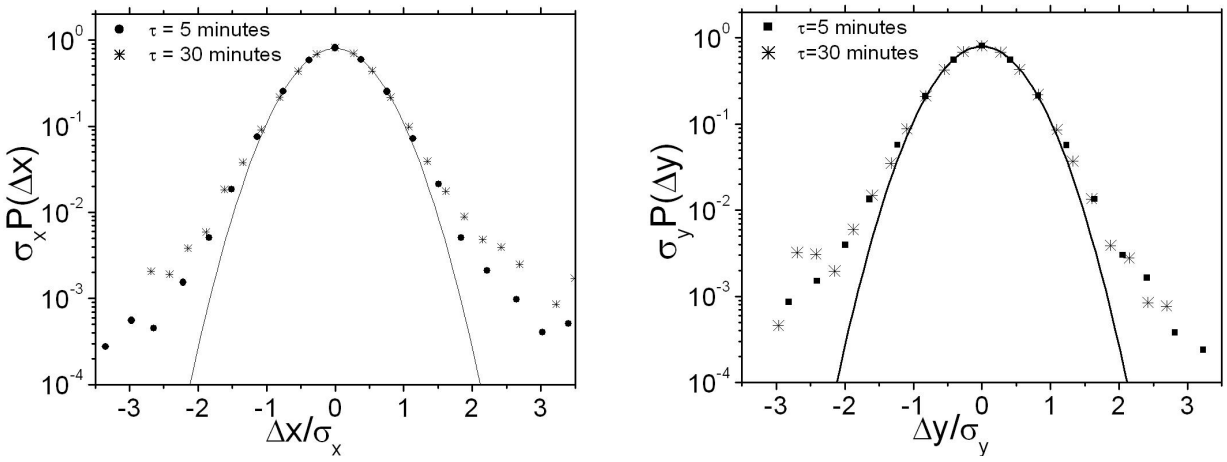

Figure 4.6: *Ensemble averaged jump probability distributions for $t > 3$ days and for two different lag times τ. Exponential tails are characteristics of intermittent dynamics [14].*

Figure 4.6 shows the ensemble averaged probability distributions of the jumps $\Delta x = x(t+\tau) - x(t)$ and $\Delta y = y(t+\tau) - y(t)$ for $t > 3$ days and $\tau = 5$ and 30 minutes. The Gaussian curve is plot for comparison. The distributions of jumps are similar to those reported by Marty and Dauchot [14] and, as they point out, the exponential tails are characteristics of intermittent dynamics and might be related to the cage effect.

4.4.2 Spatial and temporal inhomogeneities

Sub diffusive dynamics is also found in thermal jammed system like actin [36] or glass forming systems which present aging, memory effects and spatial and temporal heterogeneities [7]. So far, we have studied ensemble quasi-stationary features of the microscopic dynamics of our system by averaging over five different particles and for $t > 3$ days. Now, we will see that the dynamics of individual particles differ from each other and from the ensemble behavior and that they are not homogeneous in time.

Figure 4.7 shows the mean squared horizontal displacement σ_x^2 and the probability distribution of ΔX for the five different particles and for $t > 3$ days. It can be seen that the behavior of each particle is very different ranging from very blocked particles with nearly Gaussian distributions like particle 2, to very mobile particles whose probability distributions have important exponential tails, like particle 5. Figure 4.7 only shows the horizontal coordinate but similar plots result for the y coordinate. Thus, these differences can be interpreted as particle 2 being trapped in a single cage while particle 5 belonging to a more mobile region

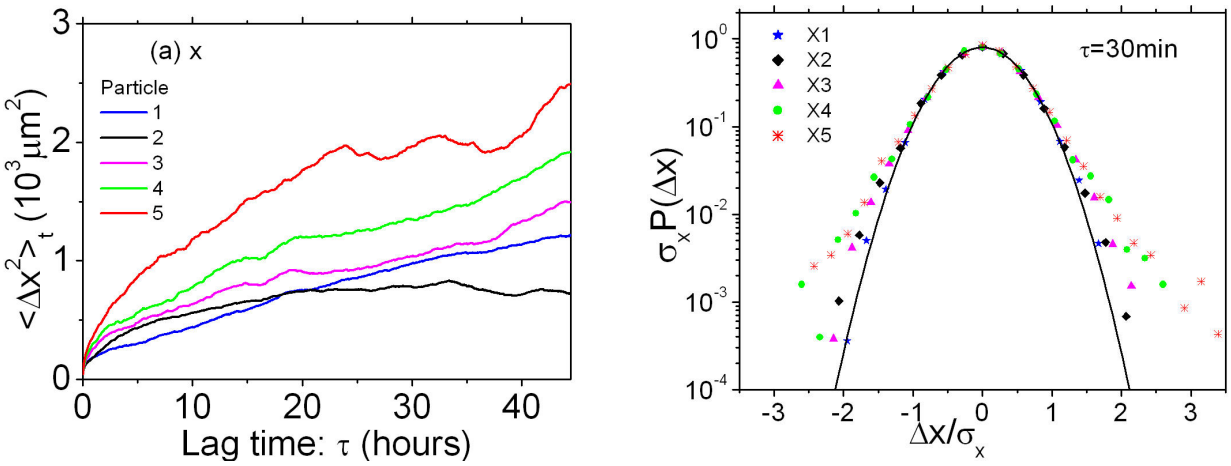

Figure 4.7: *Mean squared x displacement and probability distribution of ΔX for the five different particles for $t > 3$ days. Differences between particles imply important spatial heterogeneities.*

which allows it to change cage and diffuse, thus having a more intermittent and inhomogeneous dynamics. The existence of regions of different mobility would be analogous to the results of Valentine et al. [36] when doing particle tracking on actin and agarose.

The evolution in time of the dynamics can be seen in figure 4.8, which shows the ensemble average of $\sigma_x(\tau) = \langle \Delta x^2(\tau) \rangle^{1/2}$ as a function of the packing fraction ϕ for $\tau = 30, 90$ and 500 minutes. To get this plot we analyzed data on time intervals of varying sizes such that the relative variation of density for each interval was the same: $\Delta\phi = 5 \times 10^{-4}$. Therefore, the statistics for lower densities is poorer than for higher densities, which explains the huge fluctuations. However, for higher densities it is clear that fluctuations in horizontal jumps saturate to a constant value which is smaller than the cage size r^*.

This result may look counter-intuitive at a first glance. Indeed, we do not see any 'aging' of the fluctuation dynamics with the waiting time. This may look contradictory to the fact that the system is compacting. Moreover, there are moments where, surprisingly, something more like rejuvenation events can be seen. This result is not an accident because it was consistently found in different independent experiments and, moreover, it could be associated to the behavior observed by Kabla and Debregeas [24] using a DWS probe. It simply may say that the relevant scale associated to the compaction dynamics is not a local one, i.e. the size of few grains. It could be associated to the larger scale dynamics akin to the soft modes identified in frictionless isostatic systems [37].

To explore the spatial inhomogeneities in a more quantitative way and to characterize the dynamics at the granular scale, we calculated a local variance $W^2(t_w, \tau)$ in an interval of size

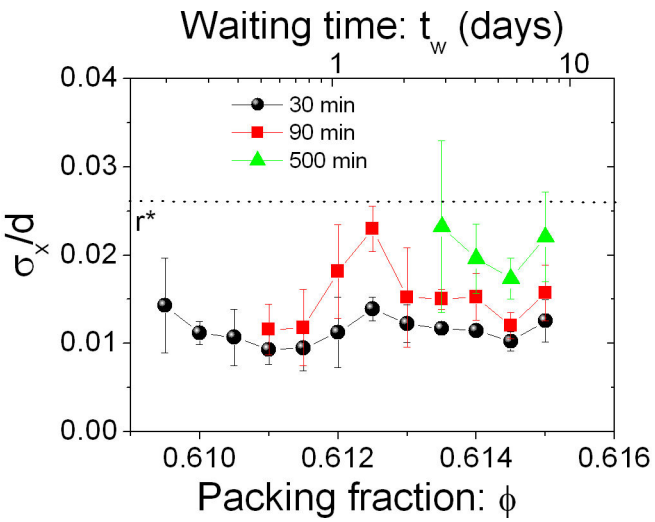

Figure 4.8: *Ensemble averaged* $\sigma_x(\tau) = \langle \Delta x(\tau)^2 \rangle^{1/2}$ *as a function of the packing fraction* ϕ *for* $\tau = 30, 90$ *and* 500 *minutes. The statistics of* Δx *does not seem to change with the increasing density of the system. The cage size* r^* *measured in figure 4.5 is put as a reference.*

τ that begins at the waiting time t_w

$$W^2(t_w, \tau) \equiv \overline{x^2(t)} - \overline{x(t)}^2 \equiv \frac{1}{s}\sum_{i=w}^{w+s} x_i^2 - \left(\frac{1}{s}\sum_{i=w}^{w+s} x_i\right)^2, \tag{4.6}$$

where,

$$\begin{aligned} &t_w \geq t \geq t_w + \tau, \\ &x(t_i) \equiv x_i, \\ &s\delta t \equiv \tau, \\ &\delta t \equiv t_{i+1} - t_i. \end{aligned}$$

This quantity allows the evaluation of a kind of particle 'activity' during the interval $t_w \geq t \geq t_w + \tau$. The left plot in figure 4.9 shows the local variance W_y^2 of the y coordinate as a function of waiting time t_w for the five particles for $\tau = 90$ minutes and $t > 3$ days. The dynamics presents moments of intense activity all along the duration of the experiment. Interestingly, there are important peaks of fluctuations for some particles that occur toward the end of the experiment, contrary to the image of a particle becoming more and more trapped with increasing density [15].

On the right plot of figure 4.9 are shown the probability distributions of W_y^2 for particle 2 for $t > 3$ days and for different interval sizes τ. All curves collapse when normalized by

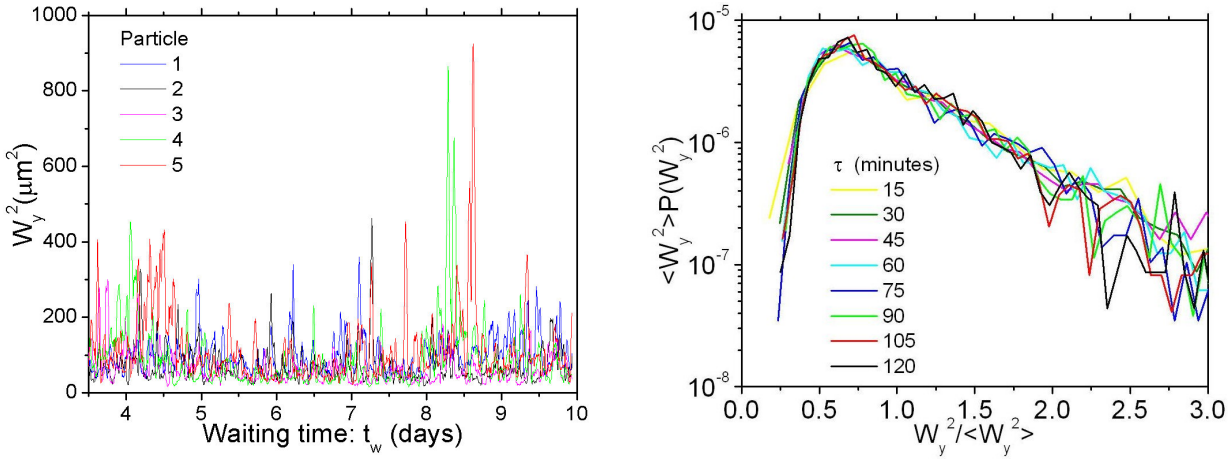

Figure 4.9: *Left: local variance* W_y^2 *(equation 4.6) for the five particles for* $\tau = 90$ *minutes and* $t_w > 3.5$ *days. Right: probability distribution of* W_y^2 *for particle number two as a typical case. Distributions for different interval sizes* Δt *collapse when normalized by* $\langle W^2 \rangle$.

the mean value $\langle W^2 \rangle$ giving a unique probability distribution curve that is characteristic of this specific particle in the vertical direction. It turns out that the distributions for each coordinate and each particle are not all the same curve. These differences between particles become clearer when we look at mean value $\langle W^2 \rangle$ as a function of interval size τ, shown in figure 4.10 for x and y for the five particles and $t > 3$ days. Data are well fitted by an expression of the form $\langle W^2 \rangle = C\tau^\alpha$, where C is a constant and $\alpha < 1$. The exponent α differs between particles and even between x and y for the same particle, as is the case for particles 1 and 2. This is, again, result of the strong sub diffusive dynamics of particles, since the expected value of α for a Brownian process is 1.

So far we have interpreted the different values of α for different particles and coordinates x and y as a signature of the spatial inhomogeneity of the dynamics. However, we wanted to know to which extent this parameter α really characterizes the dynamics of a particle and how much it depends on the time interval in which it was calculated. Thus, we calculated α on one day intervals for $t > 3$ days. The results of this analysis are shown in figure 4.11. It can be seen that in general the values of α for all particles take more or less the same values, which means that statistically they all have similar diffusion dynamics. Nonetheless, looking carefully to the left plot in figure 4.11 it can be seen that coordinate x of particle 1 is consistently smaller than that of particle 5, revealing that in fact the dynamics of different particles have not necessarily the same diffusion characteristics. Interestingly, the separation distance between particles 1 and 5 is the biggest of the interparticle distances.

In order to show in a clearer representation than in figure 4.9 the behavior in time of the dynamics of different particles, we analyzed the data in a binary way: we defined as 'active

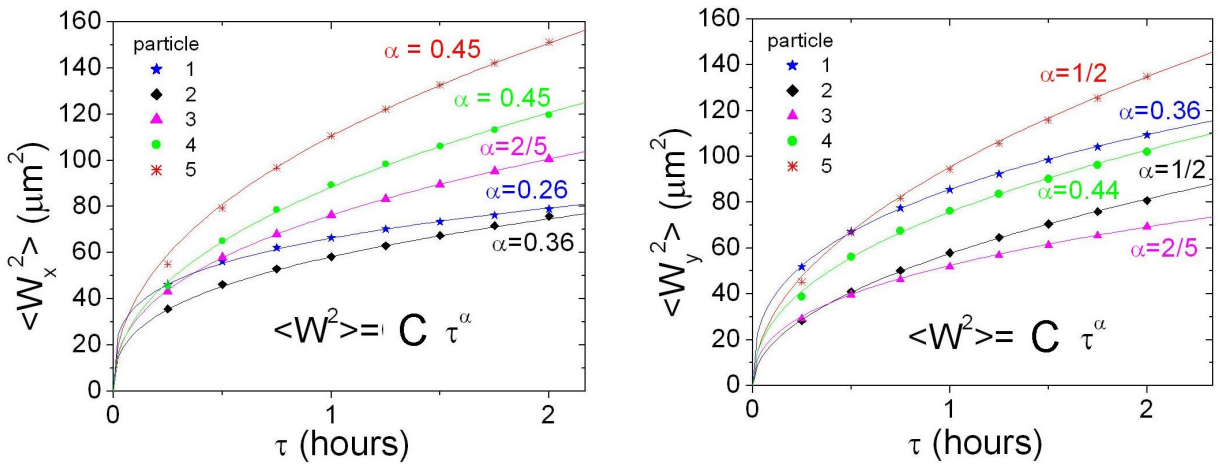

Figure 4.10: *Behavior of the mean x and y variances W_x^2 and W_y^2 as a function of τ for $t > 3$ days. Parameter C is a constant and exponent $\alpha < 1$ means sub diffusive dynamics and the variability between α of different particles is due to spatial inhomogeneities.*

intervals' those with $W^2 \geq \langle W^2 \rangle$ and we assigned to them the value 1. All other intervals got the value 0. Figure 4.12 shows these plots for x and y of all particles and for $\tau = 90$ minutes.

The binary representation of the activity of the particles shown in figure 4.12, allows to objectively evaluate the temporal homogeneity of the dynamics for each particle. The way in which it was done was by computing the probability distributions of the sizes Δt of active and inactive intervals[2] (see figure 4.13). If the dynamics was inhomogeneous in time one would expect long periods of time during which particles would be trapped and consequently $W^2 < \langle W^2 \rangle$. This would result in important deviations of $P(\Delta t)$ from an exponential distribution, which is not the case for any of the distributions in figure 4.13. In fact, we see that besides some extreme events identified in the tails of $P(\Delta t)$, the distributions of active and inactive interval sizes are essentially exponential. However, the statistics on extreme events is too weak to draw any conclusion.

4.5 Conclusions

Direct observation of boundary particles allowed to follow and study their trajectories during long compaction experiments. These trajectories were consistent with an homogeneous vertical compaction of the pile.

All five analyzed particles showed sub diffusive dynamics for short times and, as an average ensemble behavior, particles seemed to diffuse normally for longer times. This behavior

[2]The size Δt of an active (inactive) interval is the time during which the particle is active (inactive) between two inactive (active) events.

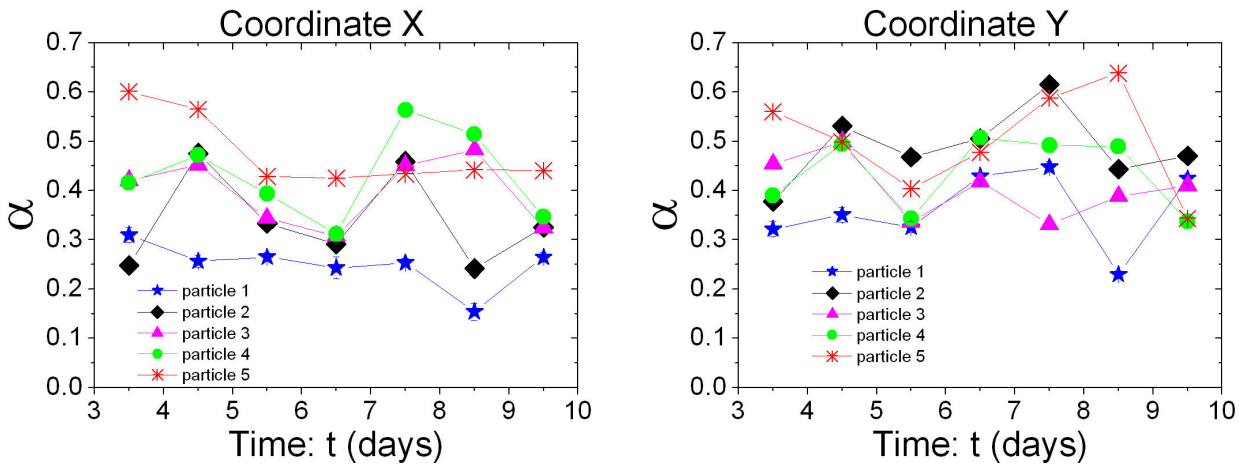

Figure 4.11: *Exponent α (defined in figure 4.10) calculated on one day intervals for $t > 3$ days. This shows to what extent α characterizes the dynamics of a particle.*

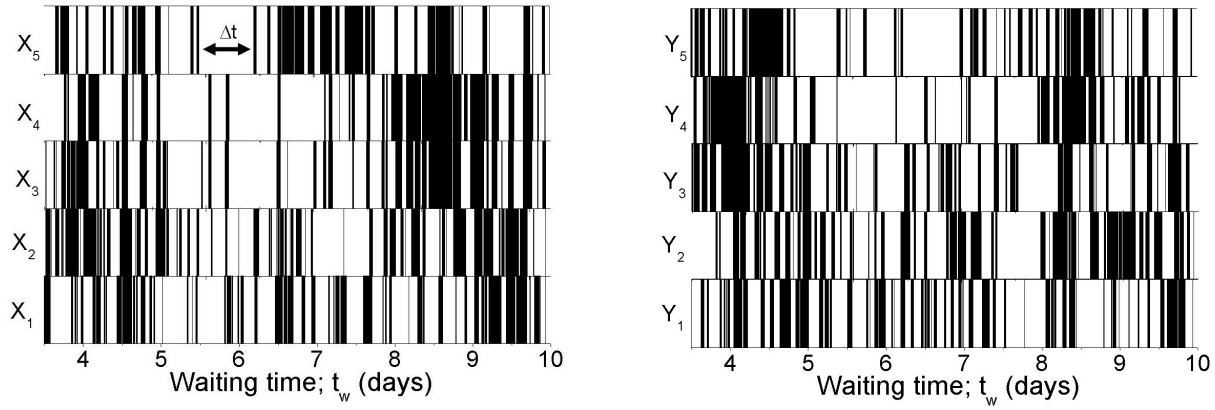

Figure 4.12: *Binary analysis of the particle 'activity'. A black line points out an interval of size $\tau = 90$ minutes where $W^2(t_w, \tau) \geq \langle W^2(t_w, \tau) \rangle$.*

was identified with the cage effect found in glasses, and it was even possible to get a rough estimation of the cage size ($r^* \approx 0.026d$).

Differences in the diffusion characteristics of different particles revealed spatial inhomogeneities, which are also found in thermal blocked systems. Different diffusion properties were only found between the two particles whose separation was the biggest (there were approximately three particles between them), which could be related to a correlation length that would be worthy to study.

It was a surprise to find that the dynamics of the particles was homogeneous in time. Since the system was continuously compacting, one would expect that individual particles became more and more blocked. As this is not the case, the compaction must then result from collective modes.

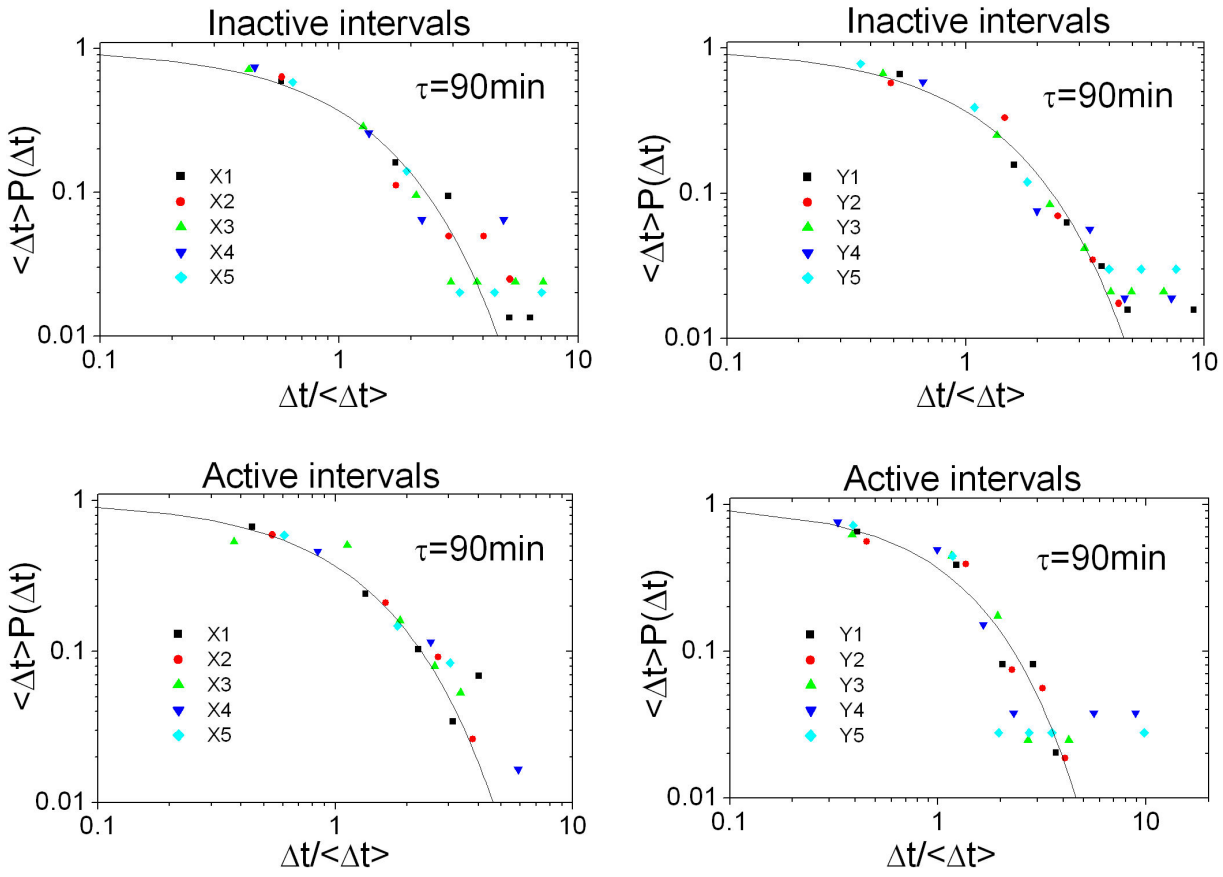

Figure 4.13: *Probability distributions of the sizes Δt of active and inactive intervals of figure 4.12. Solid lines are the exponential distributions.*

Chapter 5

Rheology of the weakly vibrated phase

The present chapter shows rheology experiments where the granular drag force was measured while dragging quasi statically a thread and an intruder grain through the granular material at constant velocity. An exhaustive study of the drag force as a function of velocity, intruder size and vibration intensity is presented.

It is shown the way in which we managed to separate the contributions to the drag force that came from the thread and those that came from the intruder grain. There were profound differences in the rheology of the thread alone and the intruders, and we found that the vibrated system does not behave like a Newtonian fluid. Interestingly, the rheology of the intruders dragged through the vibrated phase shared features with solid - solid friction, which suggests that thermal activated processes models could be used to describe granular drag force.

An analysis of the fluctuations of the drag force is also included, where it is shown that the size of the fluctuations were independent of the size of the intruder. The power spectra of the force fluctuations showed to be Lorentzian, with a characteristic length that coincides with the mean diameter of the grains of the medium. Finally, it is developed a simple model based on an Ornstein-Uhlenbeck process which recovers the principal features of the fluctuations of the drag force.

5.1 Rheology set up

Figure 5.1 shows the experimental setup used to measure the mobility of the system by driving an intruder grain at constant velocity v. A tense ($M_1 < M_2$) metallic $100\mu m$ thick thread supported by two pulleys passed through the container filled with grains. The heaviest mass M_2 rested on a force gauge that was attached to a step motor which moved vertically at

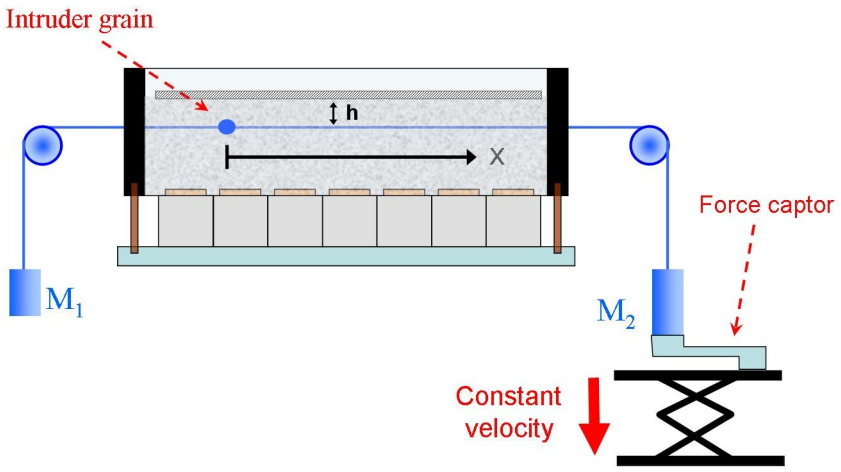

Figure 5.1: *An Attwood-like machine is used to measure the drag force that results of driving an intruder bead glued to a metallic thread through the granular medium.*

constant velocity. This allowed to measure the drag force that resisted the motion of the thread and the intruder grain. The drag force was measured as a function of driving velocity, intensity of vibration and size of the intruder.

The mobility experiment protocol was the following : $265g$ of a mixture of glass beads of 1 and $1.5mm$ were poured in the container trying to make the upper surface as horizontal as possible without tapping the container. Then, the thread with the intruder grain was made to pass through the grains at a depth $h = 13mm$ from the surface of the pile (the total height was around $40mm$). The metallic lid was gently placed on the surface of the pile and the piezoelectric transducers were turned on at their maximum intensity ($10V$ at $400Hz$). After 4 hours of vibration the intruder grain was driven at constant velocity along ten centimeters. Then, the grains were taken out of the container and the intruder grain was driven through the same path as before and at the same velocity, but this time with the container empty. This last step gave us a reference control measure which accounted for the friction forces inherent to our set up that it is well known, depend on the driving velocity [38]. In this way, the resistance force due to the granular material was obtained relatively to the control measurement.

Figure 5.2 shows typical measures of the force that the granular material opposes to the displacement of the thread with an intruder bead glued to it and also to the thread alone. There are curves for different intensities of vibration, all of them at $400Hz$. In fact, all the rheological experiments were done at this frequency in order to be able to go from no vibration to the maximum input of energy without changing the frequency (see figure 2.7). Note that the scale of force in both plots are different. The resistance forces for the thread alone is approximately three times smaller than those for the intruder bead of $6mm$ in diameter. Data

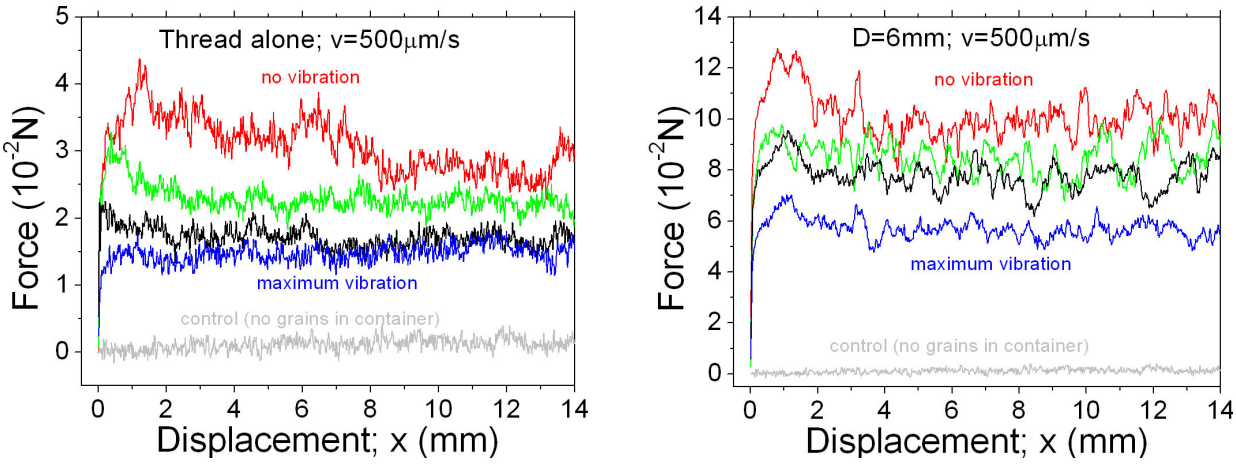

Figure 5.2: *Typical raw data of force as a function of displacement x. Experiments at constant velocity $v = 500\mu m/s$ for several intensities of vibrations at $400Hz$ are shown for the thread alone and for an intruder of diameter $D = 6mm$. Control experiments without grains in the container shows the level of noise of the set up.*

are presented as a function of displacement of the intruder, which is equivalent to time since the driving is done at constant velocity. However, we will see that for comparison between experiments done at different velocities it is more convenient to think in terms of displacement. Note in figure 5.2 that fluctuations in force are of the order of 30% of the mean value. These fluctuations come from the interaction of the thread and the intruder bead wih the granular material as can be seen when compared to the control experiment done without grains in the container.

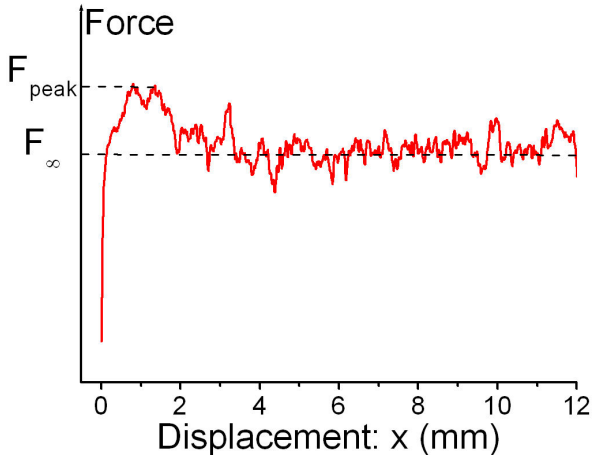

Figure 5.3: *Typical data of force vs displacement to show what we call the mean steady force F_∞ and the peak force F_{peak}.*

Notice that the force as a function of displacement presents an initial rapid increase to a maximum value F_{peak}, to relax afterward to a mean constant steady value F_∞. This kind of behavior is also found in complex fluids that present a yield stress below which the material behaves like a fragile elasto-plastic solid [39, 40]. Thus, in order to make the connection between these kind of materials and granular packings, we have interest to well characterize the behavior of F_{peak} and F_∞ as a function of dragging velocity, intensity of vibration and size of the intruder. We determined F_{peak} as the maximum value of $F(x)$ whereas F_∞ was calculated as the mean value of $F(x)$ for $x > 20mm$. The reported values of F_∞ that we show in the following sections result from the average of three independent realizations of the experiment and the associated errors correspond to the dispersion of such an average and that should not be confused with the fluctuations of the force versus displacement given by

$$\delta F = \sqrt{\left(F(x) - \overline{F}\right)^2}. \tag{5.1}$$

Interestingly, δF is usually bigger than the average dispersion except for some cases where the poor statistic yields exceptionally big standard deviations. In normal cases, δF was of the order of 20% of the absolute value while average deviations were of the order of 15%. We were obliged to work with only three realizations because of the long time required for the experiments at low velocities, specially if considered that for each experiments there was a control run done at the same velocity.

A quantity that will be interesting to study is the effective friction coefficient μ that we define as the ratio of the drag force and the hydrostatic force on the intruder if the granular material was a fluid with the same density. Therefore,

$$\mu(x) = \frac{F(x)}{SP} = \frac{F(x)}{S(\rho_p g h + P_l)}, \tag{5.2}$$

where S is the surface of the dragged object, $\rho_p = \phi\rho$ is the mass density of the packing being $\phi \approx 0.6$ the packing fraction and ρ the density of glass. $P_l = 46Pa$ is the pressure due to the metallic lid. This made a total pressure of $P = 244Pa$. Again, we will be interested in the peak friction coefficient $\mu_{peak} = F_{peak}/SP$ and in the mean steady value $\mu_\infty = F_\infty/SP$.

Before studying the dragging of an intruder bead glued to the thread, we would like to begin with the simpler case of the thread alone.

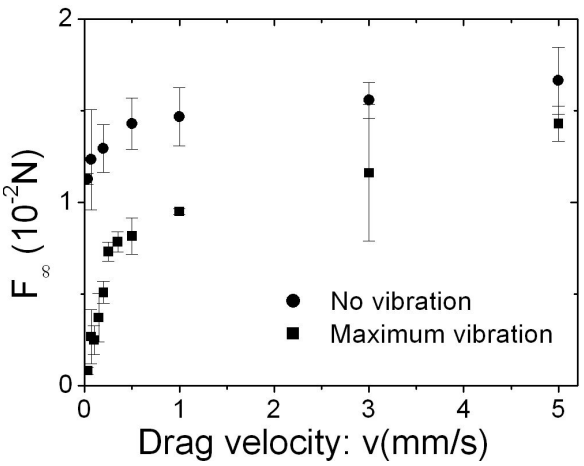

Figure 5.4: *Steady mean force versus drag velocity for the thread alone.*

5.2 Rheology of the thread alone

Figure 5.4 shows F_∞ as a function of drag velocity for the maximum vibration intensity and also without vibration for the thread alone, i.e. the thread driven through the granular material without an intruder bead glued on it. The linear regime found for low velocities can be seen when the system is vibrated. At higher velocities the relation is not longer linear, going from one regime to the other with an abrupt transition at about $v \approx 0.3mm/s$. When the system is not vibrated, the relation between force and velocity is not linear even for low drag velocities and it is hard to distinguish from the experimental data if the relation is either logarithmic or a power law, but what is clear is that it is not constant as one would have expected from Coulomb friction [41].

Before trying to understand the non trivial F_∞ vs v relation of figure 5.4, note that the resistance force that we measured when dragging the thread was tangential with respect to the surface of the thread. Therefore, the shear stress is directly obtained from the ratio of the measured force and thread's surface: $\sigma_\infty = F_\infty / S_{thread}$, with $S_{thread} \approx 6 \times 10^{-5} m^2$. If now we define the strain rate as the drag velocity divided by the mean grain size, $\dot{\gamma} \equiv v/d$, we obtain the strain-stress relation, which is shown in figure 5.5. Interestingly, these results are very similar to the results obtained by Sollich et al. [42] in the context of a model aimed to describe in a general way the rheology of the so called 'soft glassy materials', referring to materials like foams, pastes, emulsions and slurries. They found that for low strain rates and temperatures below the glass transition temperature T_g, the stress-strain relation followed the Herschel-Bulkeley equation

$$\sigma = A + B\dot{\gamma}^n, \tag{5.3}$$

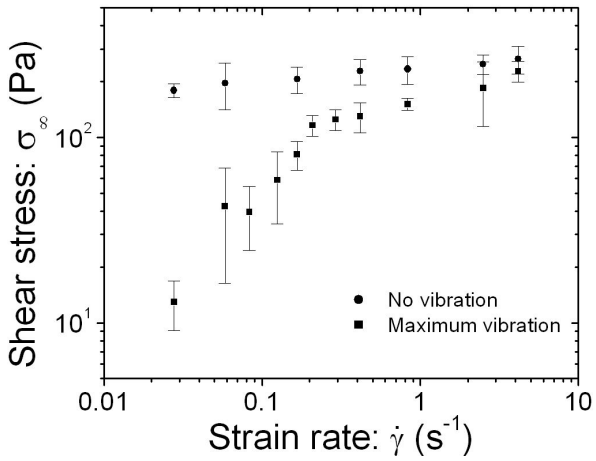

Figure 5.5: *Same data as in figure 5.4 but in terms of shear stress* $\sigma_\infty = F_\infty/S_{thread}$ *and strain rate* $\dot{\gamma} \equiv v/d$.

which is commonly used to fit experimental data from the soft materials mentioned before [42]. Note that equation 5.3 implies the existence of a finite yield stress $\sigma_y \equiv \sigma(\dot{\gamma} \to 0)$. Sollich et al. found also a power law fluid behavior for temperatures slightly higher than T_g, but without a yield stress ($A = 0$ in equation 5.3). For temperatures even higher, the fluid was Newtonian. For high strain rates ($\dot{\gamma} > 1$), Sollich et al. reported that $\sigma \approx (Tln(\dot{\gamma}))^{1/2}$, where T was a mean-field noise temperature. It is not a minor issue to see that our results follow closely the features of this model, being the vibration in our system the source of noise that would play the same role as a temperature in the model. This suggests that it is indeed a power law and not a logarithmic behavior what we found for the experiments with no vibration (figures 5.4 and 5.5). Supposing that this is correct, our data still do not allow us to discern the existence or not of a yield stress. However, it can be seen from figure 5.5 that if it is considered that there is no yield stress, the strain rate for which the stress would become close to zero (of the order of the uncertainty bars, for example) is extremely low ($\dot{\gamma} << 0.01$). Thus, in practice, for our data there is a finite dynamic yield stress, whose value we propose to be $\sigma_y \approx 130Pa$, the extrapolation of our data to a strain rate of 10^{-3}. Given this value of σ_y we obtain by fitting equation 5.3 that $\sigma_\infty \approx 130Pa(1 + 0.8\dot{\gamma}^{0.17\pm0.01})$.

Up to here we concentrated our attention on the stationary values of force and stress (F_∞ and σ_∞). However, our set up allowed us to to study the transitory features of the force at the beginning of the driving of the thread. We defined in section 5.1 a peak force F_{peak} as the maximum value attained by the force during the dragging. It was also defined the corresponding friction coefficient μ_{peak} in equation 5.2 with $S = S_{thread}$. Figure 5.6 shows the peak and the stationary values of the friction coefficient as a function of the energy input for

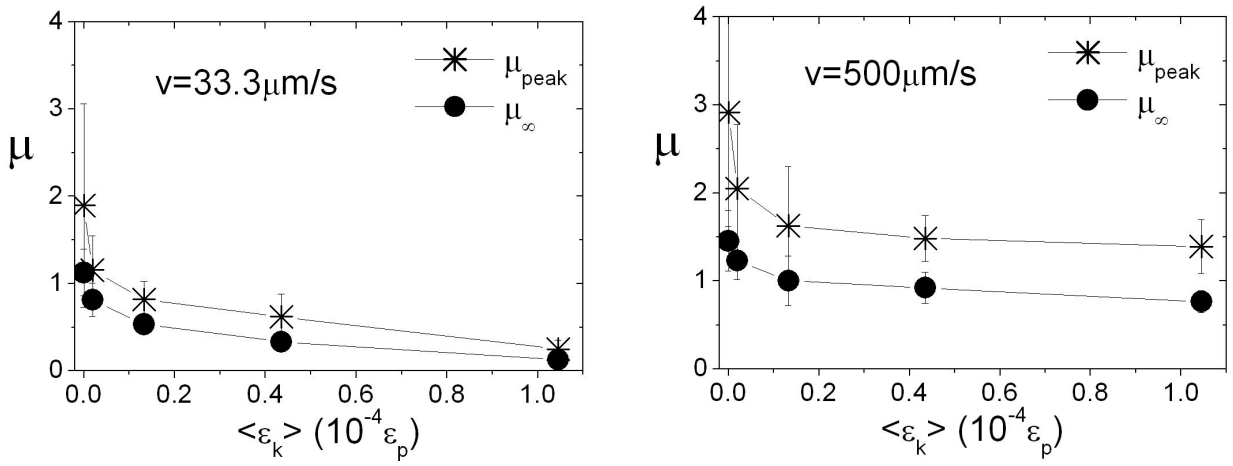

Figure 5.6: *Peak and stationary friction coefficients as a function of vibration energy for two different velocities: the lower velocity corresponds to the linear regime in figure 5.4 while the other is in the non linear part.*

two different velocities: the lower velocity corresponds to the linear regime in figure 5.4 while the other is in the non linear part. Significant differences between μ_{peak} and μ_∞ are coherent with the picture of a complex fluid behavior with an elastic-like response of the material for small strains up to a point where the system yields and begins to flow [40, 43]. That would be the case for the high velocity plot in figure 5.6 independently of the vibration energy whereas for the low velocity plot there is a transition from a fluid like behavior at high vibration energy where there is no μ_{peak} to a yield regime with μ_{peak} different from μ_∞.

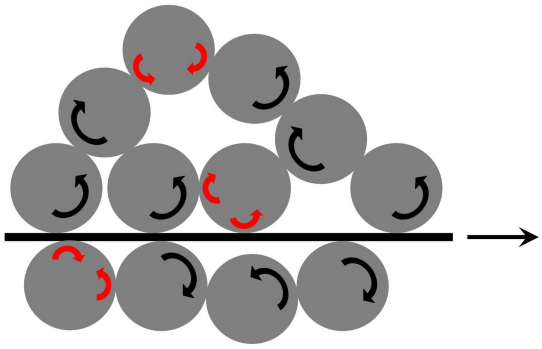

Figure 5.7: *Two dimensional schematic representation of a thread moving through a granular material. Frictional forces appear in sliding contacts due to frustrated rotations.*

Now, let us develop a picture of the microscopic processes occurring around the driven thread. When dragging the tense thread through the granular material, rotations are induced in the grains that are in the neighborhood of the thread. However, as shown schematically in figure 5.7, the disordered configuration of the grains make some of these rotations to be

'frustrated' [1], i.e. the sense of rotation induced on a particle by one of its neighbors is incompatible with the sense of rotation induced by another one. Some of these cases are represented by the particles with two arrows in figure 5.7. Consequently, frustrated particles slide and rub against their neighbors, opposing a resistance to the motion of the thread that is governed by the physics of solid-solid friction. On the other hand, since grains are not perfectly spherical, their rotation induce small reorganizations (compared to the size of the grains) on the configuration of the granular edifice. Additionally, the system can be vibrated. The resulting shear stress on the thread comes from a complicated interplay of all these processes.

The situation of the driven thread pictured in figure 5.7 contrasts with the case of an intruder bead moving through the pile in the sense that the reorganizations induced by the dragging intruder are much bigger than the size of the grains. We will see in the next section that in fact the rheology for the thread with and without an intruder is qualitatively very different.

5.3 Rheology of an intruder bead

5.3.1 Steady force

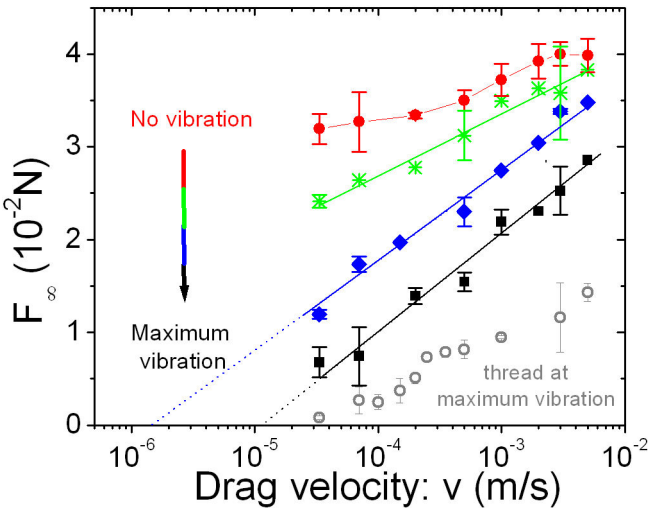

Figure 5.8: *Drag force versus drag velocity for a 2mm intruder bead*

The steady drag force F_∞ as a function of velocity for a $2mm$ intruder glued to the thread for different vibration intensities is shown in figure 5.8. The case of the thread alone for the maximum vibration is also included for comparison and it corresponds to the data in figure 5.4. The scale of the plot is lin-log, so the logarithmic variation of the force can be seen as

well as its dependence on the vibration intensity. Note that when there is no vibration, F_∞ seems to saturates to a constant value both at high and at low velocities.

Figure 5.9 shows also F_∞ as a function of the velocity but for different intruder sizes. Again, it can be seen the nearly constant behavior of the force when there is not vibration and the logarithmic relation for the maximum vibration. In these series of experiments, much lower velocities were explored for the case of the $2mm$ intruder at the maximum vibration intensity.

The steady force F_∞ of figures 5.8 and 5.9 is the total force measured by the force gauge, which means that it is the result of the combined interaction of both the thread and the intruder with the granular material. In the previous section we studied the behavior of the thread alone, so now, we can study the effect of the intruder by looking at the deviations from measurements done with the thread only.

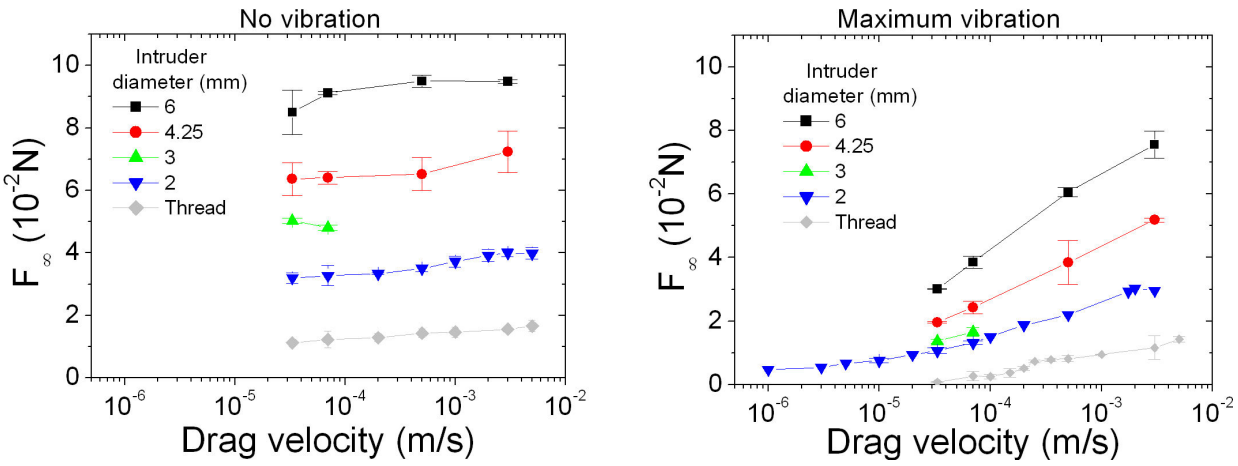

Figure 5.9: *Mean friction force as a function of velocity for different intruder sizes and the thread alone.*

5.3.2 Decoupling intruder and thread

Deviations of the drag force measured with an intruder glued to the thread from the force measured with the thread alone account for the interaction of the intruder with the granular material[1]. In order to isolate this interaction from that of the thread, we define the force on the intruder as the difference between the total force measured and the force on the thread alone measured at the same drag velocity and intensity of vibration, $F_\infty^{(int)} \equiv F_\infty - F_\infty^{(thr)}$.

[1]Although the presence of the dragging thread certainly perturbed the measurement in comparison with the dragging of an intruder alone

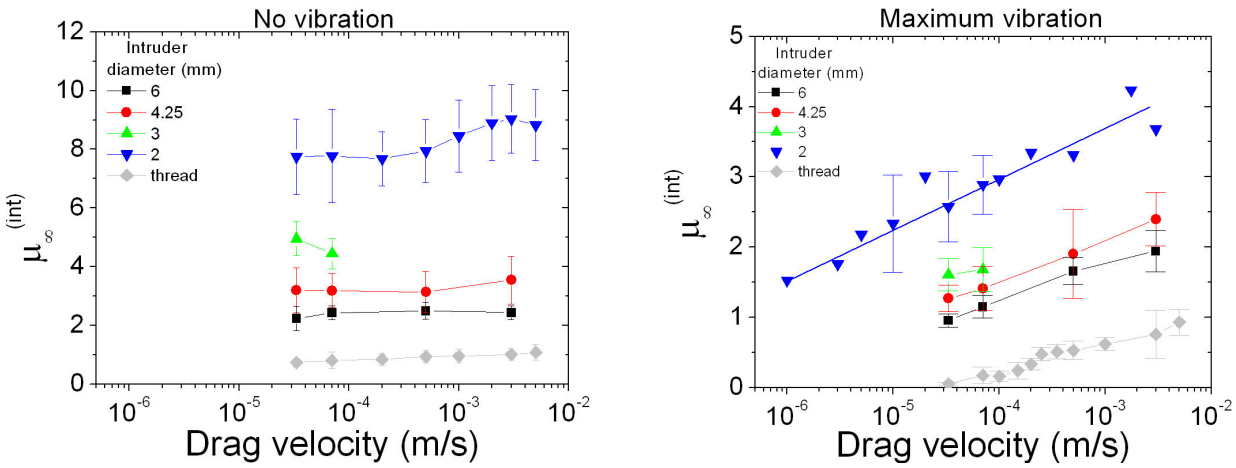

Figure 5.10: *Friction coefficient of the intruder with the thread contribution removed.*

Therefore, the corresponding friction coefficient is:

$$\mu_\infty^{(int)} \equiv \frac{F_\infty^{(int)}}{S_{intr}P} = \frac{F_\infty - F_\infty^{(thr)}}{\pi D^2 P}, \tag{5.4}$$

with D the diameter of the intruder. Figure 5.10 shows $\mu_\infty^{(int)}$ as a function of the drag velocity for the maximum vibration and without vibration for different intruder diameters. We also show the experiments with the thread alone.

In spite of the big uncertainties due to the small amount of repetitions for each point, we observe in figure 5.10, that without vibration, the friction coefficient is relatively constant, which is consistent with the results by Albert et al. [21], who dragged a cylinder perpendicular to its axis in a non vibrated granular material at different velocities. At the maximum vibration intensity a logarithmic relation was found for all intruder sizes. This kind of behavior is characteristic of macroscopic solid-solid friction where $\mu(v) = \mu(v_{ref}) + O(ln(v/v_{ref}))$ [38, 44, 45] and also on atomic force microscope experiments of nanoscale single-asperity contacts [46, 47, 48] where $\mu(v) = \mu(v_{ref}) + O((Tln(v/v_{ref}))^{2/3})$, being T the absolute temperature. From our data it is difficult to distinguish between which of these behaviors is closer to our results. Interestingly, the models that correctly describe the logarithmic dependence of friction on velocity, namely the model by Rice and Ruina [49] for the macroscopic friction and the Prandtl-Tomlinson model [50, 51] for the nanoscale case, are both based on thermally activated processes. This suggests that the mechanisms governing the drag force in our experiment are similar to those at microscopic scale in solid-solid friction with the vibration of grains playing the role of temperature.

Another interesting result from figure 5.10 is that the friction coefficient $\mu_{\infty}^{(int)}$ varies with the size of the intruder, which implies, from equation 5.4, that the drag force does not scale with the surface area of the intruder. For the vibrated experiments, there is an important separation of the curve for the $2mm$ intruder with respect to the other sizes. This indicates that when the size of the intruder becomes comparable to the size of the grains of the medium, the drag force on the intruder is relatively more important.

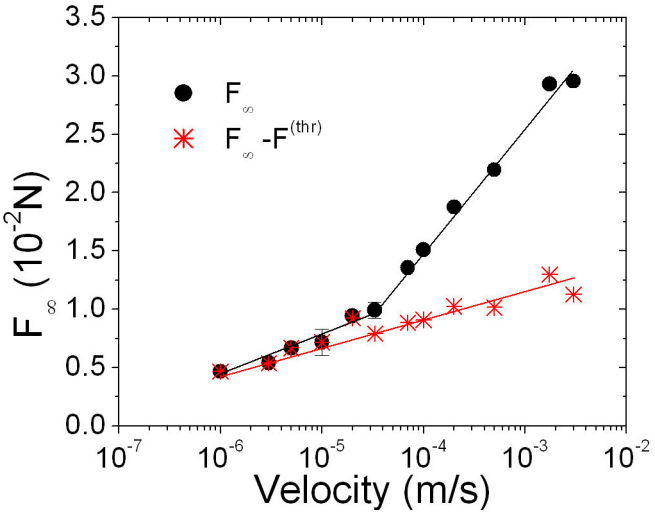

Figure 5.11: *Force versus velocity for a* $2mm$ *intruder bead at the maximum vibration intensity. The total drag force measured is shown together with the force due to the intruder, that is, the difference between the total force and the force with the thread alone.*

In the previous section a linear relation was found between shear stress and strain rate for the thread alone at low velocities when the grains were vibrated at the maximum intensity. This result would suggest that at such low velocities, the granular system behaved like an effective Newtonian fluid with a well defined viscosity. If this was really the case, dragging the thread together with an intruder at low velocities should also result in a force linearly increasing with velocity. Figure 5.11 presents the results of experiments done with a $2mm$ bead glued to the thread. The steady force on the intruder varies logarithmically even in the low velocity range where we had previously found a viscous-like regime (figure 5.4). Therefore, the linear relation between force and velocity found with the thread alone is not the result of a Newtonian rheology of the vibrated granular system. Instead, it is result of the peculiar conditions of shearing, maybe related to the fact that the reorganizations induced on the granular packing by driving the thread are small compared to the size of the grains. On the other hand, dragging a bead implies a large deformation at the granular scale.

5.3.3 Role of vibration intensity

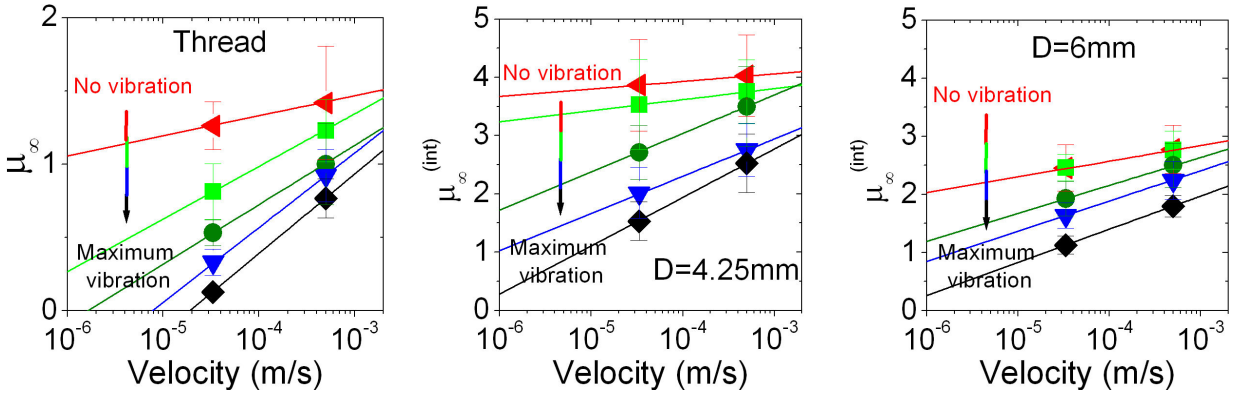

Figure 5.12: *Steady friction coefficient for different vibration intensities.*

It was found from figure 5.10 that, for the maximum vibration intensity, the steady friction was of the form

$$\mu(v) = \mu(v_{ref}) + Aln(v/v_{ref}). \tag{5.5}$$

This kind of behavior is typically observed in solid-solid friction, where the logarithmic term in equation 5.5 is known as the 'direct effect' in the context of the model by Rice and Ruina [49, 45]. Figure 5.12 presents experiments done to systematically study the effect of the vibration intensity on the 'direct effect' parameter A. Intruders of size $4mm$ and a $6mm$ as well as the thread alone were dragged at different vibration intensities. Unfortunately we only do the measurements for two different velocities because, as we had mentioned before, each realization of these experiments took a lot of time. These two velocities were enough to get a rough estimation of A from equation 5.5.

Figure 5.13 shows the 'direct effect' parameter A, defined in equation 5.5 and obtained from experiments in figure 5.12, as a function of the energy density of vibration. Note that the uncertainty in the determination of A is very big due to the big uncertainties in the data of figure 5.12. The values of A that we found are slightly bigger than those measured by Baumberger et al. in polymer glasses [45], where they find a substantial increase of A when the temperature approaches from below the glass transition temperature. We do not found such a divergence, though it is difficult to compare our results in terms of energy to those by Baumberger et al. [45] in terms of temperature, specially with the big uncertainties present in the measurements on both works.

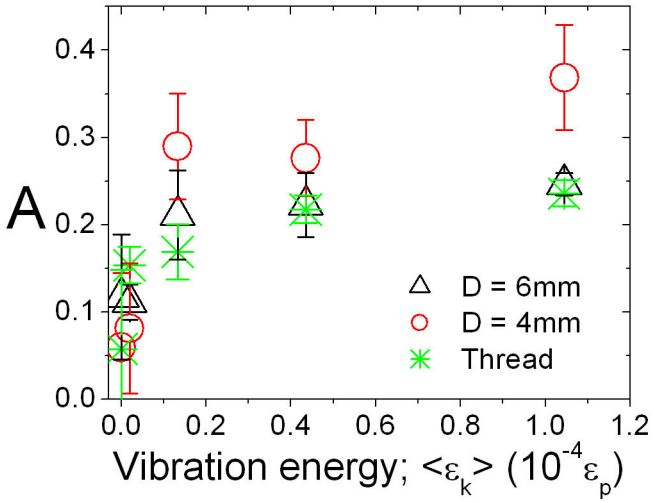

Figure 5.13: *Direct effect parameter A, defined in equation 5.5 obtained from figure 5.12.*

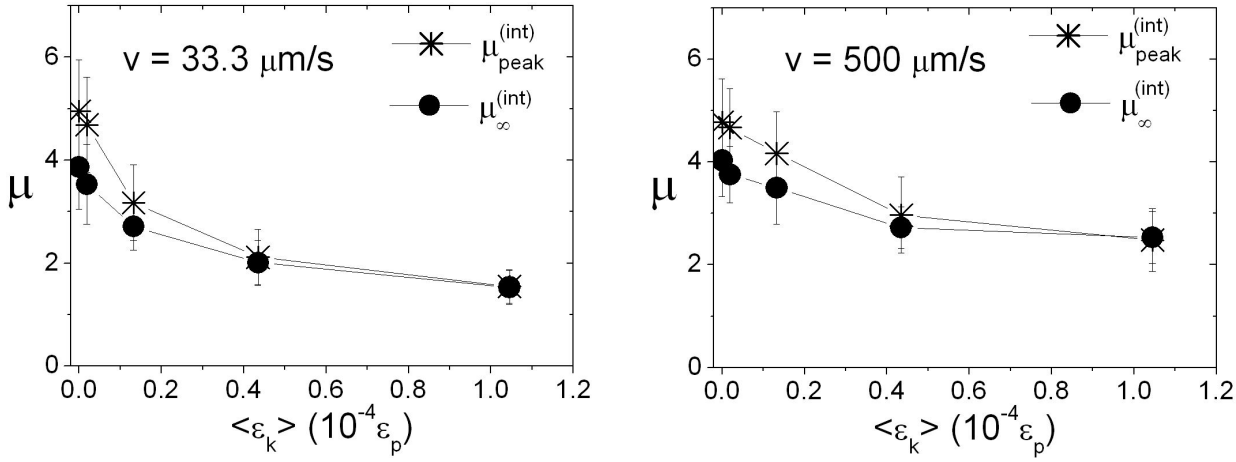

Figure 5.14: *Steady and peak friction coefficient for a* 4.25*mm intruder.*

5.3.4 Disappearance of the stress peak

It was mentioned at the beginning of the present chapter that under certain vibration conditions and drag velocities, the granular system could behave like many complex fluids in the sense that the drag force increases to a peak value F_{peak} at the beginning of the drag to further relax to a stationary value F_∞ (section 5.1; figure 5.3). It was also shown for the thread alone that at low velocities showed a transition from a Newtonian-like regime with no μ_{peak} to a complex fluid behavior having a peak yield stress when the vibration energy was decreased.

Now, when an intruder bead is dragged together with the thread, the peak friction coefficient that corresponds to the intruder, $\mu_{peak}^{(int)}$, is obtained in the same way that $\mu_\infty^{(int)}$ in equation 5.4 but using F_{peak}. Figure 5.14 shows together $\mu_{peak}^{(int)}$ and $\mu_\infty^{(int)}$ as a function of

vibration energy for a $4.25mm$ intruder at two different velocities. Again, we observe the progressive disappearance of the peak stress beyond a value of the agitation energy. However, in contrast with the thread alone, the intruder also presents this transition at $500\mu m/s$. This is another manifestation of the qualitatively different rheologies for the thread alone and for the intruders. Interestingly, the effect of increasing energy of agitation is a softening of the granular system, which resembles the softening of complex fluids due to an increase of temperature [40].

5.3.5 Varying the intruder size

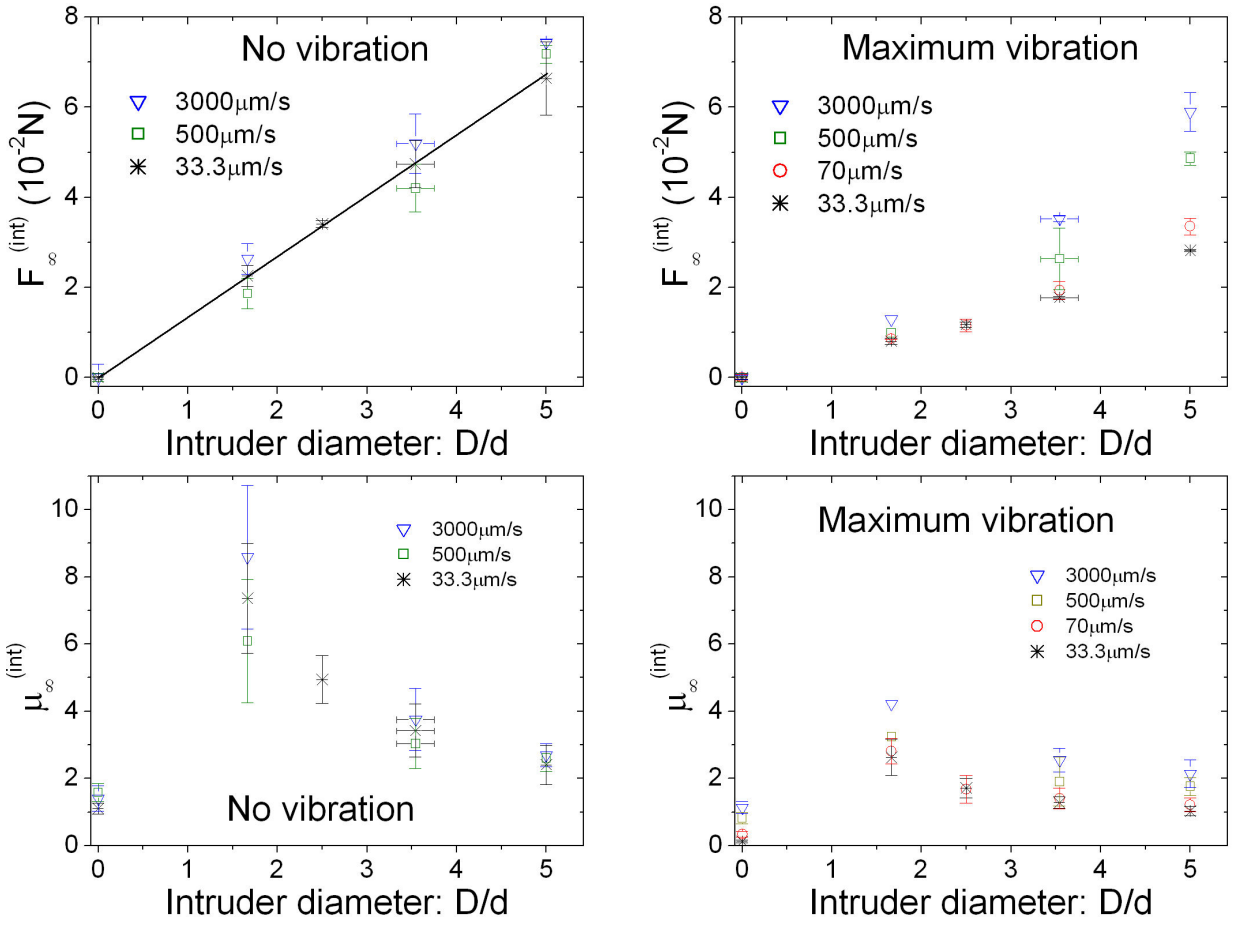

Figure 5.15: *Effect of the size of the intruder on the stationary drag force and on the effective friction coefficient. D is the diameter of the intruder and $d = 1.2mm$ the mean diameter of the grains of the medium.*

The effect of the size of the intruder on the steady drag force and effective friction coefficient is shown in figure 5.15, both with no vibration and with the maximum vibration for different

dragging rates. The drag force due to the thread alone, which would correspond to $D = 0$, was subtracted from the total force measured.

When the system was not vibrated, the drag force scaled linearly with D, the same way it would scale if the intruder were dragged in a viscous fluid! However, according to Stoke's law, the drag force in a fluid grows also linearly with the dragging rate, while on the non vibrated granular case it is rate independent. This result is indeed a surprise, since the effective friction coefficient turns out to be a decreasing function of the size of the intruder (bottom plots in figure 5.15). A similar result was obtained by Albert et al. [21] where a cylinder was dragged in a non vibrated granular material. They found that the drag force and the cylinder diameter D were linearly related for D bigger than five times the mean size of the grains d which, given the cylindrical geometry, resulted in a constant friction coefficient. However, for $D < 5d$, Albert et al. found deviations from linearity that correspond, like in our experiment, to an effective friction coefficient that increases when D decreases [21]. Therefore, it is a finite size effect where the friction is relatively more important for small objects compared to the size of the grains of the medium.

In contrast with the non vibrated case, when the system was agitated at the maximum intensity, the drag force grew faster than linear with the size of the intruder and it depended on dragging rate. It is noteworthy that this rate dependence was also found by Geng and Behringer [22] in an equivalent two dimensional dragging experiment, though their granular system was not agitated. This could be related to the fact that Geng and Behringer found a logarithmic dependence of the drag force on drag velocity which contrasts with the rate independence found by Albert et al. [21] and by Cheheta et al [20]. Geng and Behringer attribute this discrepancy to the fact that they worked with a very soft photoelastic granular material while Albert et al. and Chehata et al. used rigid glass beads. They propose that there is a relaxation time associated to the smoothness of the particles [22]. In our experiments as well as in that of Albert et al. and Chehata et al., the rigidity of glass beads implies that there is not such a relaxation time. Therefore, the rate dependence obtained in our set up suggests that vibration introduces a relaxation time in our system in an analogue way as smoothness does in Geng and Behringer's experiments [52]. When comparing our results to those by Geng and Behringer it must not be forgotten that theirs was a two dimensional system where the 'volume' was kept constant and with strong wall effects.

5.3.6 Drag force fluctuations

So far, we have focused our attention on the behavior of the stationary mean drag force F_∞. However, it can be seen from figure 5.2 that the force is a highly fluctuating function of position

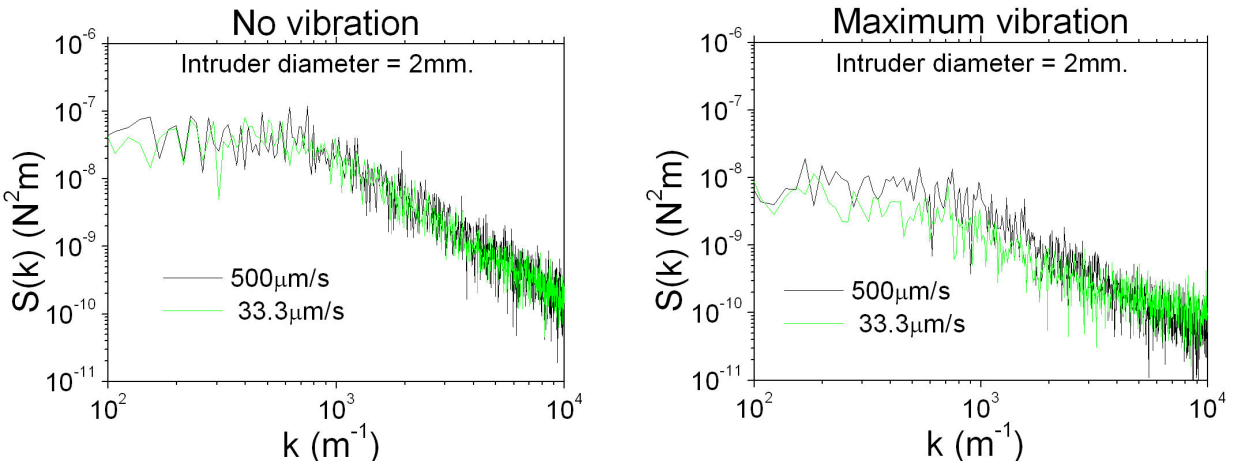

Figure 5.16: *Power spectra in the k domain nearly collapse.*

x or, equivalently, of time t [2]. Interestingly, when viewed as a function of position, fluctuations of force signals from experiments done under the same vibration conditions but at different drag velocities are nearly undistinguishable from each others. To confirm this observation we calculated the power spectrum $S(k)$ in the k domain of the force-position series:

$$S(k) = \left\langle 2 \left| \int_{x>2cm} dx F_f(x) exp(-2\pi i k x) \right|^2 \right\rangle_x , \qquad 0 \leq k < \infty, \tag{5.6}$$

where $F_f(x) \equiv F(x) - F_\infty$ is the fluctuating part of the drag force. Since we were interested on the fluctuations of the force in the stationary regime, we only analyzed $F_f(x)$ for $x > 2cm$. Figure 5.16 shows $S(k)$ for experiments with a $2mm$ intruder with and without vibration at different velocities. The collapse of these curves suggests that the relevant variable to study the force is position instead of time. This drag rate independence of the force fluctuations has been already observed in other granular rheology experiments [22, 53, 54].

In order to study the dependence of force fluctuations on drag velocity we looked at the root mean squared drag force $\delta F_f = \sqrt{(1/N)\sum_{i=1}^{N} F_f^2(x_i)}$. $S(k)$ and δF_f are related by Parseval's theorem:

$$\delta F_f^2 = \int_0^\infty S(k) dk \tag{5.7}$$

Figure 5.17 shows δF_f for different drag rates and intruder sizes. In contrast with results by Geng and Behringer [22], in our system δF_f does not depend on the intruder size. On the other hand, for the vibration case there is a clear logarithmic dependence of δF_f on drag velocity.

[2] It is equivalent to see the force as a function of position x or as a function of time t since the drag is at constant velocity: $x = vt$.

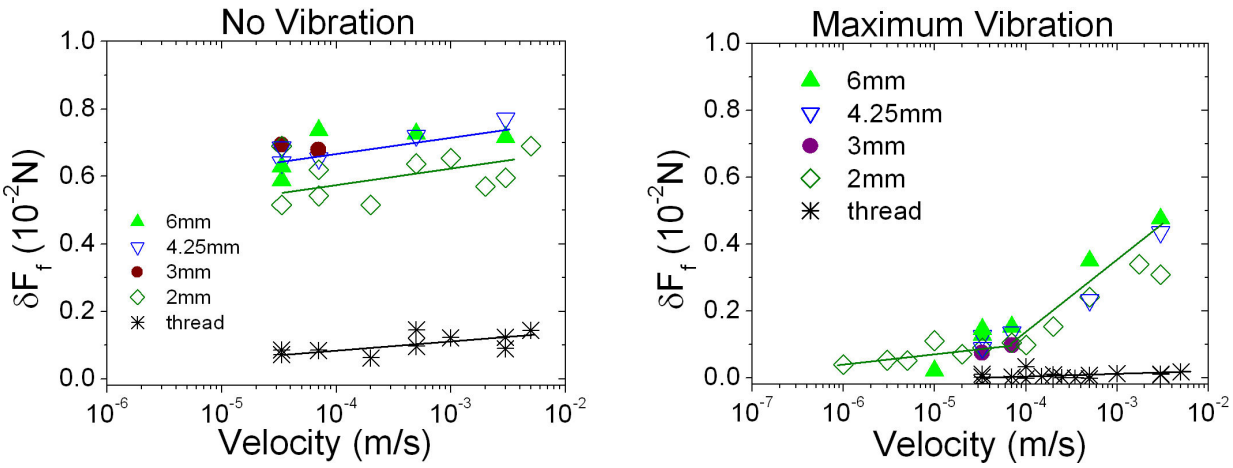

Figure 5.17: *Root mean squared fluctuating drag force δF_f at different drag rates and for intruders of various sizes.*

Another interesting feature of the force spectra is their shape. Figure 5.18 shows $S(k)$ for a $4.25mm$ intruder as a typical case with and without vibration. For large k, $S(k) \propto k^{-2}$, while for low k the spectrum is flat at a level that we call Θ. A clear crossover between these two regimes is observed at a value k_0 which defines a characteristic length k_0^{-1}. These spectra can be fitted by a Lorentzian function of the form:

$$S(k) = \frac{\Theta}{\left(\frac{k}{k_0}\right)^2 + 1}. \tag{5.8}$$

It turns out that for all the experiments with intruder, this characteristic length is a constant $k_0^{-1} = 1.25mm$ approximately, which is the mean diameter of the grains in the medium. Consistently with the invariance of δF_f with intruder size (figure 5.17), the power spectrum is also invariant as can be seen in figure 5.19, where Θ and k_0 remain constant. Again, the thread alone shows a different quantitative and qualitative behavior.

Finally, it can be seen in figure 5.18 that there is an effect of the intensity of vibration on the spectrum: while the characteristic length k_0 remains unchanged, the value of the plateau Θ decreases for stronger agitation. The variation of Θ with vibration energy is related to the variation of δF_f. From Parseval's relation (equation 5.7) and the Lorentzian form of $S(k)$ (equation 5.8) it can be showed that

$$\delta F_f = \sqrt{\frac{\pi}{2}\Theta k_0}. \tag{5.9}$$

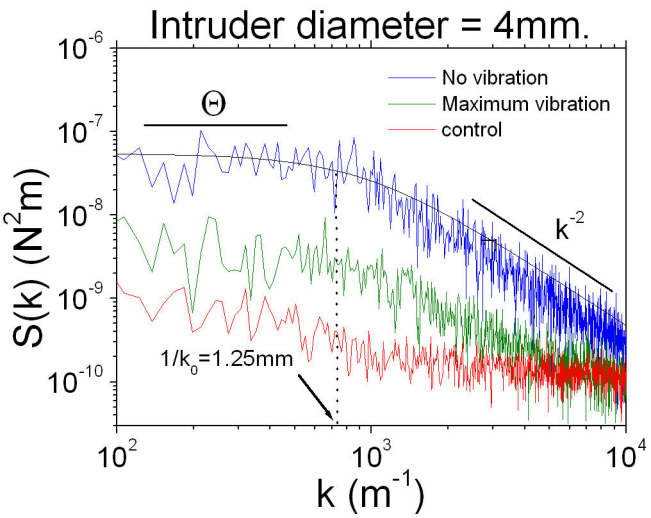

Figure 5.18: *Power spectra of the force signal of a $D = 4.25mm$ intruder. The control spectrum is the noise of the measurement apparatus. Continuous line is a fit with the Lorentzian function (equation 5.8).*

Figure 5.20 shows δF_f as a function of the intensity of vibration for a $2mm$ intruder and the thread alone at two different drag rates.

In summary, the spectrum plateau is a measure of the vibration intensity, $\Theta = \Theta(e_k)$, while the characteristic length does not depend on the vibration or dragging details. Moreover, the constant value found of $k_0^{-1} = 1.25mm$ coincides with the mean diameter d of the grains that constitute the granular medium, which suggests that $k_0 = k_0(d)$.

It is important to note here that the spectrum of the thread alone is qualitatively different from the cases when an intruder is glued to the thread : there is not a well defined plateau nor a characteristic length (see figure 5.19).

An Ornstein-Uhlenbeck process

Now, we will develop a simple model based on an Ornstein-Uhlenbeck process which captures the main features of the fluctuations that we found in our experiments and that were presented above.

Figure 5.21 shows a simplified schematic representation of the drag system where the spring stands for the force gauge that moves at constant velocity v_0. In this context, the equation of motion for the intruder grain is:

$$M\ddot{x} = \kappa(v_0 t - x) - F \tag{5.10}$$

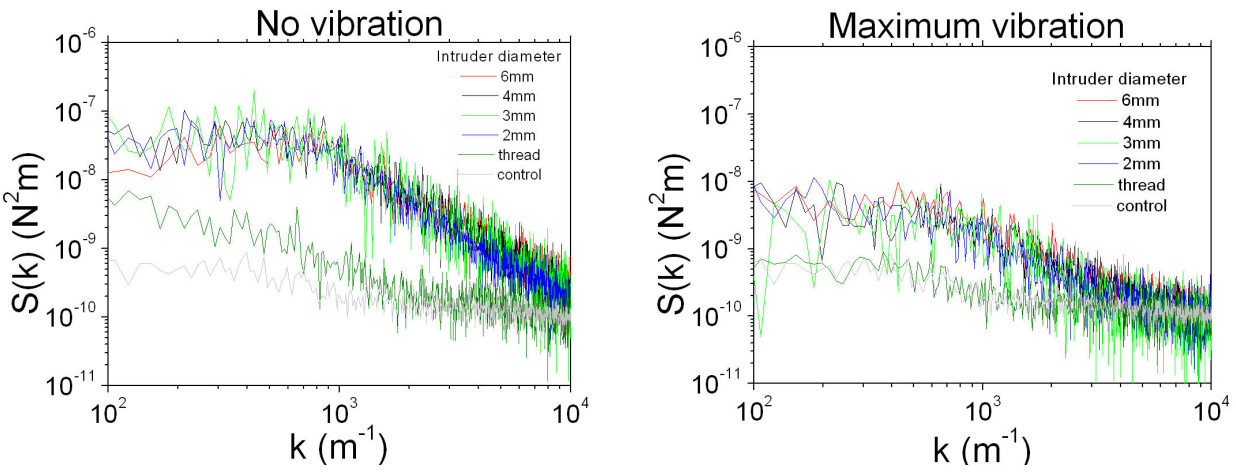

Figure 5.19: *$S(k)$ for different intruder sizes dragged at a rate of $33.3\mu m/s$. Power spectrum does not change with intruder size but it is different for the thread alone.*

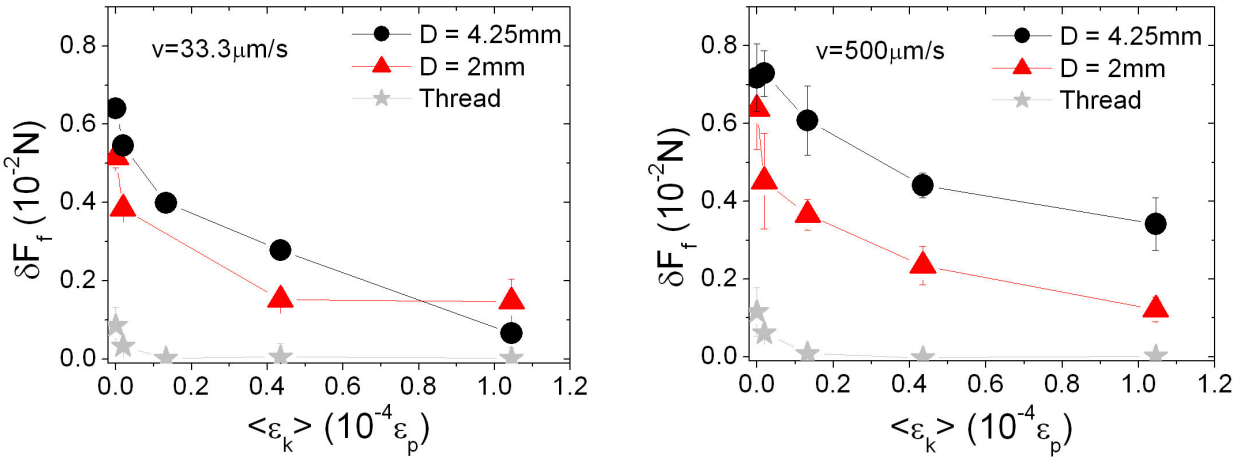

Figure 5.20: *Spectrum plateau as a function of intensity of vibration.*

where M is the mass of the intruder, x is its position, κ is the spring stiffness, and F is a friction force due to the granular medium. The friction force F is what we directly measure (see figure 5.2), so we know that it is a strongly varying quantity whose mean value depends principally on intruder's size D while its fluctuations depend on the position x. Both mean value and fluctuations vary with the intensity of vibration.

As pointed out by Baldassarri et al. [54], the fluctuations in the force results from the disordered landscape of particles and force chains encountered by the intruder which, in turn, modifies such a landscape while moving. It would be expected that for small displacements δx of the intruder, the changes induced in the landscape would be also small as well as the change on the friction force, which would remain correlated. For larger displacements, rearrengments would be large enough to completely decorrelate the force. This considerations

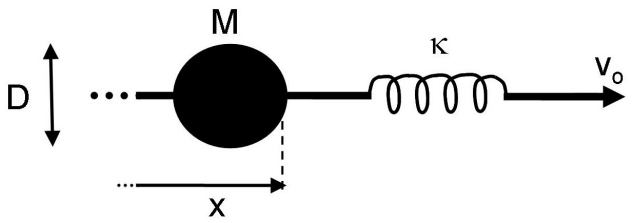

Figure 5.21: Schematic representation of the drag system. The spring of stiffness κ represents the force gauge that is moved at constant velocity v_0. M and D are the mass and diameter of the intruder respectively and x is its horizontal position.

took Baldassarri et al. to propose that the fluctuating part of the friction force can be thought as an Ornstein-Uhlenbeck process with the distance as independent variable:

$$\frac{dF_f}{dx} = \eta(x) - 2\pi k_0 F_f, \tag{5.11}$$

where $< \eta(x)$ is an spatial noise with correlation $< \eta(x)\eta(x') >= C\delta(x-x')$, and the parameter k_0 is the inverse of the characteristic correlation length. The pertinence of this model is supported by looking at the power spectrum of the force signal. The power spectrum that corresponds to equation 5.11 is Lorentzian:

$$S(k) = \left\langle 2 \left| \int_0^\infty dx F_f(x) exp(-2\pi i x k) \right|^2 \right\rangle = \frac{C}{2\pi^2 k_0^2} \left(\frac{1}{\left(\frac{k}{k_0}\right)^2 + 1} \right), \tag{5.12}$$

which we had seen, fits very well the experimental data (see figure 5.18). From equations 5.8 and 5.12 it can be seen that $\Theta = C/2\pi^2 k_0^2$. Thus, the parameter C, which is the variance of the noise η in equation 5.11, depends on the size of the grains d, on drag velocity and on the intensity of vibration, being smaller for higher agitations.

These results can be understood if we consider that the agitation provided by the piezoelectric transducers is, on one hand, so weak that it does not manage to modify, at least for short time scales, the structure or geometrical configuration of the granular pile. Hence, the landscape of grains and force chains in which the intruder moves is very similar to the non vibrated case. On the other hand, the level of agitation is strong enough to facilitate the relative displacement of grains and their reorganization while the intruder is moving. This means that the effect of such a weak agitation would be equivalent to reduce the friction between grains.

It is important to note that the noise $\eta(x)$ in equation 5.11 is a function of position x and it is due to the disordered structure of the granular pile. It should not be mixed up with the 'thermal like' noise that comes from the agitation of the grains. For a weak vibration like ours, the spatial noise $\eta(x)$ is only affected quantitatively by the agitation, not qualitatively.

5.4 Conclusions

We were able to perform rheology experiments in a granular material with the novel characteristic that an object could be dragged through it while vibrating the system. The dragging could be done at a wide range of velocities, including very low ones ($1\mu m/s$), and the measure of the force was very precise.

It turned out that it was possible to separate the contribution of the thread and the intruder, although the presence of the dragging thread certainly perturbed the measurement in comparison with the dragging of an intruder alone. However, the dragging of the thread alone resulted on a very interesting system in itself.

There were profound differences in the rheology of the thread alone and with the intruders. The transition from linear to logarithmic relation between force and velocity found for the thread alone at low velocities was not present any more when an intruder was glued to the thread. This means that the vibrated system does not behave like a Newtonian fluid at low velocities as one would have thought from the experiments with the thread alone.

The rheology of the intruders dragged through the vibrated phase share features with solid-solid friction. Interestingly, the physics behind solid-solid friction is based in thermally activated processes. This means that in our system, vibration plays an analogue role to temperature in activating processes. We were even able to calculate the 'direct effect' parameter of friction models.

The effective friction coefficient was found to be a decreasing function of the size of the intruder, which was attributed to a finite size effect when the intruder approached the mean size of the grains of the medium.

When the system was vibrated, the friction coefficient became drag rate dependent which would be associated to the apparition of a characteristic time that is not present without vibration. Interestingly, another case in which such a characteristic time appears and gives a rate dependent friction coefficient is by working with a soft granular material at constant volume, as was found by Geng and Behringer (see section 1.5 and reference [22]).

The power spectra of the stationary drag forces for the intruders were all Lorentzian, with a characteristic length that corresponded to the mean size of the grains of the medium. The

fluctuations of the force were independent of the size of the intruder. It was proposed a simple model which recovers the Lorentzian power spectrum and that suggests that fluctuations on the force come from the landscape encountered by the intruder while moving. This would explain that fluctuations do not change with the size of the intruder.

Chapter 6

Conclusions and perspectives

6.1 Conclusions

The possibility of a universal description of all the systems that present jamming, even if they are as different as liquids, foams and granular matter, motivated us to design an experimental set up that allowed to study the physics of an ideal granular material near jamming.

We implemented a novel way of shaking the grains, obtaining a more disordered agitation compared to standard compaction experiments and, most important, we managed to avoid convection.

The characteristics of the set up made possible to make a variety of different but complementary measurements that allowed an extensive characterization of the properties of the granular system.

We observed in our system phenomena that had already been observed in other granular experiments, as was the case of the logarithmic compaction, the Kovacs and cage effects, the rate independence of the drag force in non vibrated pack, or the Lorentzian spectra of the fluctuations of the drag force, reinforcing their robustness as properties of granular matter.

There were also novel results, for example, the relation between the mean kinetic energy of the system and its compaction rate. The friction-like behavior of the drag force in vibrated packs was also an interesting result that supports the idea that models of thermally activated processes can be applied to describe the rheology of vibrated granular systems, where agitation would play the role of temperature.

A central result of the present work was the finding of no aging on the dynamics of individual particles while the global density of the packing continued to increase during vibration (section 4.4.2). This astonishing result would support the idea that compaction phenomena result from collective behavior [37].

6.2 Perspectives

Much of the time that has been dedicated to this project was devoted to design, construct and calibrate the set up. Consequently, there are still many crucial tests and experiments that are missing.

Density relaxation processes when varying the intensity of vibration should be studied systematically and more quantitatively. In particular, attention should be paid to the density curves on the Kovacs effect near the vibration intensity change, since its exact form is a discrepancy point between different models that try to capture the physics of this phenomenon [55].

On the particle tracking part, the study of collective modes could be done by taking images from different zones of the boundary at the same time and analyzing correlations between trajectories of particles separated by a distance r. The idea would be to see how such correlations depend on distance r and the way they change with time.

Another possible experiment would be to place intruder particles, heavier than the grains of the medium, on the boundary of the system and follow their motion during long time vibration experiments. This would be equivalent to the experiment by Makse et al. [16], since it would be possible the determination of the effective temperature T_{eff} from the application of fluctuation dissipation relations to the trajectories of the intruders.

Concerning drag experiments, the variation of the confining pressure is an important test that would help on the understanding of the microscopic mechanisms that govern the properties of the granular drag force. Specially interesting would be the effect of confining pressure on the linear regime found for the drag force for the thread alone.

As mentioned in section 2.2, the set up allows to perform Diffusing Wave Spectroscopy measurements. We have already obtained interesting preliminary results using this technique which revealed unexpected evolution of the dynamics with time on long vibration experiments. We think that such findings could be related to the rejuvenation peaks observed when tracking boundary particles and, therefore, this technique could be useful to study collective modes related to compaction.

So far, we have talked about possible experiments and tests to be done on the set up in its present version. However, a modification that would be important to do on it would be increasing the possible agitation intensity. With more energy injected to the system it might be possible to look for a stationary state and to create more reproducible initial states without taking out the grains from the container. It would also allow to study the transition from a fluid-like to a blocked glassy like state, while at present we always work in the blocked phase.

6.3 Final remarks

Our experimental set up shows to be well adapted to study in an novel and extensive way the properties of an ideal granular material around the jamming transition.

With respect to the application of statistical physics concepts to describe granular materials, the present work reinforces with experimental evidence the fact that there are astonishing similitudes between systems that jam, even if they are as different as the non thermal granular matter and thermal systems like glasses and colloids. However, such analogies must be treated carefully. For example, from the linear relation between drag force and velocity that we found with the thread alone, we could have thought that at slow drag rates, the system behaved like a Newtonian fluid, which was further contradicted by the results obtained by dragging intruder beads.

Appendix A

Versión resumida en español

A.1 Resumen

Un sistema granular puede fluir como un líquido bajo la acción de una fuerza externa, pero también puede auto organizarse y atorarse, siendo entonces capaz de soportar hasta cierto punto esfuerzos cortantes, como si fuera un sólido. Los sistemas térmicos pueden también presentar atoramiento, como es el caso del estado vítreo de un fluido. Algunas analogías impresionantes entre las dinámicas de sistemas tan distintos como son los coloides, las espumas y los materiales granulados, cuando se encuentran cerca del atoramiento, motivaron diversas propuestas sobre la posibilidad de describir de forma unificada y general a todos los sistemas que presentan atoramiento.

Con la intención de poner a prueba experimentalmente estas ideas, en el presente trabajo estudiamos las propiedades mecánicas de un sistema granular vibrado de forma débil y desordenada. Al poner en contacto directo esferas de vidrio milimétricas con transductores piezoeléctricos, logramos inyectar energía al material granulado de una forma desordenada y con aceleraciones menores a la de la gravedad, dando como resultado una compactación logarítmica lenta y sin flujos de convección.

El hecho de que el contenedor de los granos no tuviera que ser agitado para vibrar los granos hizo posible, junto con lo débil de la vibración, realizar mediciones muy precisas al mismo tiempo en que los granos estaban en vibración. El diseño del dispositivo permitió: medir la fracción de empaquetamiento; evaluar la agitación de los granos por medio de un acelerómetro enterrado en el medio granular; ver directamente las partículas de borde y seguir su trayectoria; medir la fuerza de arrastre sobre una partícula intrusa jalada a velocidad constante; y, finalmente, hacer experimentos de espectroscopía de difusión de luz coherente (Diffusing Wave Spectroscopy; DWS).

El capítulo 1 es una introducción general sobre los medios granulados y el atoramiento, junto con una breve descripción de algunos trabajos experimentales realizados por otros grupos que ponen en evidencia algunas analogías entre materiales granulares densos y sistemas térmicos atorados. También de otros grupos, se discuten dos experimentos que estudian la fuerza de arrastre granular bajo condiciones que son parecidas a las de nuestro propio experimento.

El dispositivo experimental se describe en el capítulo 2 y se muestra la forma en que logramos crear una vibración débil y desordenda y sin flujos de convección. También se presentan mediciones sistemáticas de la aceleración y de la energía cinética inducidas en el medio granular, como función de la frecuencia y del voltaje de la señal de alimentación de los transductores piezoeléctricos. Estas mediciones fueron hechas con un acelerómetro enterrado en el medio granular.

El capítulo 3 incluye el estudio de la relajación de la densidad del medio granular vibrado, la cual resultó aumentar de manera logarítmica con el tiempo. Un resultado central de estos experimentos fue encontrar que el parámetro relevante que controla la velocidad de compactación es la energía cinética media, y no la aceleración cuadrática media, como normalmente se considera. También se estudió la respuesta de la densidad a cambios repentinos en la intensidad de vibración, en donde encontramos interesantes analogías con la respuesta de sistemas térmicos a cambios en la temperatura.

La observación directa de partículas de borde permitieron seguir y estudiar sus trayectorias a lo largo de experimentos de vibración de larga duración. Los resultados de dichos experimentos son el tema del capítulo 4. Las propiedas de difusión de estas partículas sugiere que su dinámica es similar a la dinámica de 'jaula' característica del estado vítreo, y fue incluso posible dar una estimación del tamaño de la jaula. Un hallazgo sorprendente fue que a pesar de que la densidad del sistema no dejaba de crecer, la dinámica de las partículas no cambiaba con el tiempo, lo cual sugiere que la compactación está gobernada por modos colectivos del sistema.

El capítulo 5 muestra experimentos reológicos en donde un hilo metálico y un grano intruso eran jalados de forma cuasi estática a través del medio granular a velocidad constante y se medía la fuerza de arrastre resultante. Se presenta un estudio exahustivo de la fuerza de arrastre como función de la velocidad, del tamaño del intruso y de la intensidad de la vibración. Las contribuciones a la fuerza dearrastre provenientes del hilo y del grano intruso pudieron ser separadas, y se encontró que la reología de los granos intrusos jalados a través del medio granular vibrado comparte características con la fricción sólido - sólido, lo cual sugiere que podrían usarse modelos de procesos activados térmicamente para describir la fuerza de arrastre granular.

También se incluye en el capítulo 5 un análisis de las fluctuaciones de la fuerza de arrastre, en donde se muestra que su tamaño no depende del diámetro del intruso. Los espectros de potencia de las fluctuaciones de la fuerza resultaron ser de tipo Lorenciano, con una longitud característica que coincide con el diámetro medio de los granos. Finalmente, se presenta un modelo simple basado en un proceso de tipo Ornstein-Uhlenbeck que recupera las características principales de las fluctuaciones de la fuerza de arrastre.

Las conclusiones generales así como las perspectivas del trabajo son discutidas en el capítulo 6.

A.2 Introducción

Un sistema granular está constituido por muchas partículas que interactúan principalmente a través de fuerzas de contacto. Las partículas deben ser suficientemente grandes para que la energía gravitacional sea mucho mayor que la energía térmica k_BT.

Un material granulado puede fluir como un líquido bajo la acción de una fuerza externa (ya sea de borde o de bulto), pero también puede autorganizarse y bloquearse, siendo capaz de resistir ciertos esfuerzos de corte, como si fuera un sólido. Sin embargo, el comportamiento de un material granulado presenta siempre peculiaridades que no permiten hacer una analogía exacta con fluidos o sólidos. El desorden intrínseco a un medio granular y la complejidad inherente a las interacciones altamente disipativas como son las colisiones y fuerzas de fricción que gobiernan la física de estos materiales, no ha permitido hasta hoy desarrollar un marco teórico completo que los describa satisfactoriamente.

La transición entre un estado de flujo y un estado bloqueado de un material granulado, conocida como transición de atoramiento, resulta especialmente interesante ya que se conoce poco sobre las propiedades mecánicas de estos sistemas cerca de esta transición. Además, se han podido constatar sorprendentes analogías entre el comportamiento de medios granulados cerca del atoramiento y sistemas térmicos que también presentan fenómenos de bloqueo, como es el estado vítreo de un fluido.

El objetivo del presente trabajo es el de estudiar la reología, los procesos de relajación y la dinámica de las partículas de un medio granular cerca de la transición de atoramiento.

A partir de las similitudes en el comportamiento de sistemas tan disímiles como un medio granular cerca del atoramiento y un fluido en estado vítreo, algunos autores [3, 4] vieron la posibilidad de describir de forma unificada a todos los sistemas que pueden bloquearse al autorganizarse. Con esta idea, Liu y Nagel [4] propusieron de manera especulativa un

diagrama de fase del atoramiento (figura 1.4), en donde en uno de los ejes se encuentra la temperatura, en otro un forzamiento externo y en el tercero el inverso de la densidad.

Los sistemas atérmicos que presetan atoramiento como espumas o materiales granulares vivirían en el plano de densidad y esfuerzo del diagrama propuesto por Liu y Nagel (figura 1.4). En cambio, en sistemas térmicos la temperatura y el forzamiento juegan papeles equivalentes con respecto al bloqueo y desbloqueo del sistema. El hecho de que todos estos sistemas tan disímiles pudieran ser descritos por el mismo diagrama de fase llevó a Liu y Nagel a preguntarse qué tan similares son la dinámica y las propiedades mecánicas de sistemas térmicos y atérmicos cerca del bloqueo. También plantean la posibilidad de aplicar conceptos de física estadística para describir sistemas atérmicos e incluso se cuestionan sobre la pertinencia de definir una temperatura efectiva para este tipo de sistemas [4].

La búsqueda de analogías entre sistemas granulares densos y sistemas térmicos, así como la posibilidad de definir una temperatura granular, ha motivado una gran cantidad de trabajos teóricos, numéricos y, más recientemente, experimentales. En el capítulo 1 se presentan algunos de estos trabajos experimentales. Se muestra, por ejemplo, la similitud entre la densidad de un medio granular como función de la intensidad de vibración y la transición vítrea de un fluido como función de la temperatura [9, 10]. También se muestra el experimento hecho por Josserand et al. [11] en donde observan en medios granulados el efecto Kovac, efecto que es característico de sistemas vítreos. Marty y Dauchot [14] observaron el efecto 'caja' en la trayectoria de las partículas en un medio granular bidimensional, efecto que es también observado en sistemas vítreos. Finalmente se muestra un experimento por Makse et al. [16] en donde se define y mide una temperatura granular efectiva a partir de aplicar relaciones de fluctuación - disipación a las trayectorias de partículas individuales. Todos estos trabajos refuerzan la idea de comparar y asimilar los sistemas vítreos y granulares. Sin embargo, todavía quedan muchas dudas sobre cuáles de estos fenómenos son específicos de estos dispositivos experimentales y cuáles son fenómenos generales de los medios granulares.

En el contexto del estudio de las propiedades mecánicas de un medio granular cerca de la transición de atoramiento y la comparación con sistemas térmicos, la fuerza de arrastre es una cantidad que puede dar información muy valiosa y que, sorprendentemente, ha sido muy poco estudiada ente los físicos. En el capítulo 1 se presentan dos trabajos experimentales en donde se estudia la fuerza de arrastre en medios granulados en condiciones cercanas a las que nosostros estudiamos en el presente trabajo. El primero de ellos fue realizado por Schiffer et al. [21] y consistió en estudiar la fuerza sobre un cilindro arrastrado en dirección perpendicular a su eje a través de esferas milimétricas de vidrio a velocidad constante. Sus principales resultados fueron que la fuerza no depende de la velocidad de arrastre pero que varía linealmente con el diámetro del cilindro (figura 1.12).

El otro experimento de fuerza de arrastre presentado en el capítulo 1 corresponde a un dispositivo bidimensional en el que Geng y Behringer [22] estudian la fuerza sobre un disco intruso arrastrado a velocidad constante a través de discos compuestos de un material fotoelástico suave. Además, a diferencia del experimento de Schiffer et al., Geng y Behringer trabajan a 'volumen' constante. Esta vez, la fuerza de arrastre aumenta logarítmicamente con la velocidad de arrastre y depende de manera no lineal del diámetro del intruso.

Los resultados que nosotros obtuvimos al jalar un grano intruso a través de nuestro medio granular presentan similitudes y diferencias con respecto a los resultados de Geng y Behringer y de Schiffer et al., las cuales son discutidas en el capítulo 5 y en la sección A.6.

A.3 Vibración débil y desordenada

Con el objetivo de estudiar y comprender mejor las propiedades mecánicas de un medio granular que se encuentra cerca de la transición de atoramiento, diseñamos un dispositivo experimental en el que logramos vibrar de manera débil y desordenada un medio granular ideal.

La figura 2.1 muestra de manera esquemática el dispositivo experimental que consiste en un recipiente rectangular de vidrio cuyo fondo está cerrado por siete transductores piezoeléctricos, fijos a una base de plástico de forma que la pastilla de cerámica de cada transductor es libre de vibrar sin entrar en contacto ni con el recipiente de vidrio ni con la base de plástico. El recipiente es llenado con una mezcla de esferas de vidrio de dos diámetros diferentes: 1 y $1.5mm$. De esta forma, las esferas de vidrio están en contacto directo con los transductores, los cuales vibran al ser excitados por una señal cuadrada de frecuencia f. La frecuencia de excitación es la misma para todos los piezoeléctricos y puede ir desde 100 hasta $2000Hz$, mientras que la vibración de cada transductor está en antifase (diferencia relativa de fase de pi) en relación a la de sus vecinos.

Con este dispositivo, la agitación inducida por los transductores en el material granular es bastante desordenada y débil en comparación con los experimentos estandar de vibración de medios granulados [9, 23, 24], en donde normalmente todo el recipiente es agitado con aceleraciones del orden o mayores a la de la gravedad. La agitación débil y desordenada inducida en nuestro sistema hace que el principal modo excitado sea la rotación de los granos sobre su propio eje, con la consecuente reorganización de los contactos con sus vecinos. Además, gracias a este modo de vibración logramos evitar la convección.

Las características de nuestro dispositivo experimental, así como el tipo de agitación creada en el medio granular permite la realización de muy diversas y complementarias mediciones: : la

agitación al interior del sistema usando un acelerómetro enterrado en los granos; la relajación de la densidad como función de la intensidad de vibración; la dinámica de partículas de borde por visualización directa; la fuerza de arrastre sobre una partícula intrusa jalada a través del medio a velocidad constante; y, finalmente, propiedades colectivas de la dinámica del sistema estudiadas por medio de espectroscopía de difusión de luz coherente (Diffusing Wave Spectroscopy).

Lo primero que se hizo fue caracterizar el tipo de vibración inducida en el medio granular usando un acelerómetro enterrado en los granos. La figura 2.6 muestra una medición típica de la aceleración a la máxima intensidad de vibración. Al integrar la aceleración es posible obtener la velocidad del acelerómetro como función del tiempo, la cual se muestra en la misma figura. A su vez, a partir de la velocidad se puede obtener la densidad de energía cinética media $\langle \epsilon_k \rangle$ (ecuación 2.2), la cual es expresada en términos de la densidad de energía potencial del material granulado ϵ_p (ecuación 2.3), correspondiente a una altura $d = 1.2mm$, el diámetro medio de los granos.

Las gráficas de la figura 2.7 muestran $\langle \epsilon_k \rangle$ y γ_{rms}, la raíz cuadrada de la aceleración cuadrática media, como función de la frecuencia de vibración a 10 volt, el voltaje máximo. En dichas gráficas es claro que la energía cinética no crece con la frecuencia como la aceleración y, en cambio, presenta un máximo alrededor de $f = 400Hz$. Más adelante veremos que el parámetro que gobierna la velocidad de compactación del medio es la energía cinética y no la aceleración, mientras que es este último parámtro el usado normalemente como control en los experimentos granulares de vibración [9, 23].

Para finalizar la caracterización de la vibración se midió la energía y la aceleración en función del voltaje (figura 2.8), encontrándose una transición de comportamiento alrededor de los $4V$, que pudiera ser el voltaje a partir del cual los transductores logran desatorar el medio granular. También se tomaron imágenes de una pared lateral con una cámara digital durante tiempos largos de vibración (de más de diez horas) y con partículas coloreadas para seguir su trayectoria. Se encontró que a pesar de haber cambios locales en la estructura del sistema, los granos en general no cambian de vecinos próximos y no presentan importantes desplazamientos con respecto a su tamaño, por lo que, consecuentemente, no hay convección en el sistema aún a la máxima intensidad de vibración.

A.4 Compactación

El grado de compactación de un material granular puede ser expresado a través de la fracción de empaquetamiento, ϕ, que se define como la razón entre el volumen ocupado por los granos,

V_g, sin tomar en cuenta los espacios vacíos entre éstos, y el volumen total ocupado por el sistema granular, V_T. En nuestro caso, V_g se obtiene a partir de la masa total de granos vertida en el recipiente y la densidad del vidrio que los constituye y es constante durante todo un experimento. V_T, en cambio, se calcula a partir de las dimensiones de la sección transversal del recipiente, que es constante, y la altura total de la pila granular. Para medir la altura de la pila se coloca una delgada placa metálica sobre la superfice de ésta y dos sensores inductivos de proximidad que miden la separación entre la placa y los sensores (ver figura 3.1).

La figura 3.2 muestra la evolución de la fracción de empaquetamiento durante diez días de vibración a la máxima intensidad. La curva obtenida es logarítmica (ecuación 3.3), sin presentar saturación en algún valor estacionario máximo de ϕ. El hecho de que no se haya encontrado un estado estacionario es muestra de la intensidad de vibración tan pequeña con la que trabajamos.

En los experimentos de vibración en medios granulares [9, 23, 27], es común usar la aceleración del recipiente en el que se encuentran los granos como parámetro de control para caracterizar la intensidad de vibración. Sin embargo, a un medio granular se le puede inyectar energía de muy distintas maneras, por lo que la aceleración del recipiente pudiera no ser el parámetro más adecuado y general relacionado con la intensidad de vibración [23].

Con el objetivo de estudiar el papel que juegan la aceleración y la energía cinética en la compactación, obtuvimos curvas de compactación con diferentes voltajes y frecuencias de modo tal que las distintas curvas tuvieran asociada la misma aceleración pero diferente energía cinética. El resultado obtenido fue que la velocidad de compactación, caracterizada por el parámetro β de la ecuación 3.3, depende de la energía cinética media $\langle \epsilon_k \rangle$ y no de la aceleración (ver figura 3.5), como normalmente se supone. Sin embago, al comparar nuestros resultados con otros experimentos de vibración granular es importante tener en cuenta que la vibración creada en nuestro dispositivo es continua, débil y desordenada, en contraste con la vibración discreta, fuerte y de todo el recipiente que es aplicada usualmente.

En el contexto de la comparación entre un medio granular vibrado y un sistema térmico en estado vítreo, una cosa importante de hacer es estudiar la respuesta de la fracción de empaquetamiento ante cambios en la intensidad de vibración, y compararla con la respuesta de distintos observables a cambios en la temperatura en sistemas térmicos.

En la figura 3.6 se muestra la fracción de empaquetamiento como función del tiempo en donde después de diez días de vibración a la máxima intensidad se hicieron dos ciclos de una serie de cambios en la intensidad de vibración. En este caso, el cambio relativo en la densidad correspondiente a cada cambio de intensidad de vibración es el mismo en cada parte del ciclo, lo cual indica que el sistema se encuentra en un estado cuasi estacionario. En contraste con este comportamiento, las figuras 3.7 y 3.8 muestran otro experimento en el que el sistema

fue inicialmente vibrado con una intensidad inferior a la máxima durante seis días, al final de los cuales, una nueva serie de cambios en la intensidad de vibración fue aplicada. Esta vez, debido a que el sistema se encontraba menos denso que en el experimento enterior, el efecto de cada cambio en la intensidad de vibración fue el aumento en la densidad, excepto por una dilatación transitoria en el segundo cambio de intensidad de ϵ_{k5} a ϵ_{k4} (figura 3.8). Dicho transitorio es análogo al efecto Kovacs [12] observado en sistemas térmicos y fue previamente observado en medios granulados por Josserand et al. [11].

Los resultados obtenidos con nuestro dispositivo al variar la intensidad de vibración muestran que lo robusto que son los fenómenos observados en la compactación de medios granulares ya que están presentes en sistemas de vibración tan difrentes como el de Josserand et al. [11] y el nuestro. Además, al tener su contraparte térmica, estos fenómenos apoyan la idéa de describir de manera unificada a todos los sistemas que presentan atoramiento.

Una importante ventaja de nuestro dispositivo experimental es que permite mediciones muy precisas de cambios relativos de densidad durante la vibración, lo cual hace posible el estudio de procesos de relajación de manera muy detallada.

A.5 Trayectoria de partículas de borde

En la secció anterior se presentó la evolución temporal de la densidad en experimentos de varios días de vibración. Las paredes laterales transparentes de nuestro dispositivo experimental permitieron que durante la realización de dichos exprimentos se filmara con una cámara digital una pequeña zona de una de estas caras laterales (ver figura 4.1). Cada minuto se adquiría una imagen, de la cual se podía obtener la posición de las partículas que aparecían en ella.

En la figura 4.3 se muestran las trayectorias de cinco partículas durante un experimento de diez días de vibración a $300Hz$ y $10V$. La comparación de la componente vertical de estas trayectorias con la evolución de la posición de la superficie de la pila sugiere que la compactación de la pila es verticalmente homogénea, desde la base hasta la superficie de la pila (ver figura 4.4).

Un resultado muy interesante se obtiene al calcular la desviación cuadrática media de la posición como función del tiempo de separación τ (ecuación 4.5, figura 4.5). Para tiempos cortos, la dinámica del sistema es subdifusiva, volviéndose difusiva a tiempos mayores a un día aproximadamente. Este tipo de comportamiento fue observada anteriormente en medios granulados por Marty y Dauchot [14], y puede ser interpretado como consecuencia de una dinámica de 'caja', característica de sistemas vítreos [13]: para tiempos menores a $\tau^* \approx 22$ horas las partículas se encuentran atrapadas en una caja de dimensión $r^* \approx 0.026d$, en donde

d es el diámetro medio de las partículas, para después escapar de la caja y difundir hacia otras cajas (figura 4.5).

Las curvas presentadas en la figura 4.5 resultan del promedio sobre las cinco partículas analizadas. Si embargo, al observar la desviación cuadrática media de la posición $\langle \Delta x^2(\tau) \rangle$ o la distribución de tamaños de saltos Δx para cada partícula (figura 4.7) resulta que el comportamiento de cada partícula puede ser muy diferente al de las otras. Estas inhomogeneidades espaciales en la dinámica están también presentes en sistemas vítreos [36].

La evolución temporal de la dinámica de las partículas puede observarse en la figura 4.8, en donde la raíz cuadrada de la desviación cuadrática media de la componente horizontal de la posición, σ_x, está representada en función de la fracción de empaquetamiento. Sorprendentemente, contrario a lo que se habría podido esperar, a pesar de que el sistema está cada vez más compacto, la dinámica de las partículas parece no cambiar. En otras palabras, la compactación del sistema no parece estar asociada a la disminución de la agitación de partículas individuales, lo cual apoya las propuestas teóricas que atribuyen al aumento en la densidad a fenómenos colectivos del sistema [37].

Con el objetivo de estudiar el grado de homogeneidad temporal de manera más local, así como la homogeneidad espacial de manera más cuantitativa, calculamos una especie de 'actividad' de las partículas en intervalos de tiempo de tamaño τ a través de la función $W(t_w, \tau)$ definida en la ecuación 4.6. La función W reveló que únicamente entre las dos partículas más alejadas entre sí había una clara diferencia en la dinámica, lo cual podría estar relacionado con una distancia de correlación característica del orden de entre tres y cinco partículas. La función W también permitió investigar la posible naturaleza intermitente de la dinámica de las partículas en analogía con sistemas vítreos. Contrario a lo que esperábamos, no se encontró evidencia de dicha intermitencia.

A.6 Fuerza de arrastre

La fuerza de arrastre sobre una partícula intrusa moviéndose a velocidad constante a través del medio granualar fue estudiada en nuestro sistema con la ayuda de un montaje de tipo máquina de Attwood, como se muestra esquemáticamente en la figura 5.1. Un hilo metálico sostenido por dos poleas y tensado por dos masas en sus extremos, atraviesa al medio granular al pasar por dos delgadas rendijas que se encuentran en las paredes laterales del recipiente. La mayor de las masas que tensan al hilo descansa sobre un medidor de fuerza que a su vez se encuentra unido a una plataforma que se desplaza verticalmente a velocidad constante controlada por un motor. Además, un grano intruso puede unirse con pegamento al hilo. De este modo, al

moverse la plataforma, el hilo y el grano intruso son jalados a través del medio granular, el cual se resiste al movimiento con una fuerza que es detectada por el medidor de fuerza de la plataforma. Nótese que el experimento puede realizarse con el medio granular vibrado.

La figura 5.2 muestra mediciones típicas de la fuerza en función del desplazamiento para el hilo solo así como con un intruso de $6mm$ de diámetro y para distintas intensidades de vibración. Las cantidades que nos van a interesar estudiar a partir de cada una de estas señales de fuerza son la fuerza de arrastre media, F_∞, la fuerza de arrastre máxima, F_{peak} (ver figura 5.3), y las fluctuaciones de la fuerza, δF (ecuación 5.1). También nos va a interesar el coeficiente de fricción, μ, asociado a la fuerza de arrastre y definido en la ecuación 5.2, en donde S es la superficie del objeto arrastrado y P la presión de confinamiento. Todas estas cantidades las estudiamos de forma sistemática variando la velocidad de arrastre, v, el diámetro del intruso, D, y la intensidad de vibración, $\langle \epsilon_k \rangle$.

Lo primero que se hizo fue estudiar la fuerza de arrastre del hilo solo, es decir, sin tener un grano intruso pegado a él. La figura 5.4 muestra F_∞ como función de la velocidad de arrastre para el hilo solo y para los casos extremos de vibración máxima y nula. Para el caso sin vibración, la fuerza de arrastre no es constante, lo cual contrasta con los experimentos de otros grupos que han estudiado la fuerza de arrastre en materiales granulados no vibrados [21]. Cuando la intensidad de vibración es máxima, el comportamiento de la fuerza es aún más sorprendente. Para velocidades bajas la relación entre fuerza y velocidad es lineal, como si fuera un fluido Newtoniano, presentando después, al aumentar la velocidad, una transición hacia una relación no lineal. Resulta interesante que este tipo de reología la presentan también sistemas térmicos en estado vítreo [42]. Por lo tanto, a partir de estos resultados, podría pensarse que, de manera general, un sistema granular se comporta igual que dichos sistemas térmicos con la vibración jugando un papel totalmente equivalente al de la temperatura. Sin embargo, veremos más adelante que al hacer estas mismas mediciones con un grano intruso pegado al hilo, no se encuentran los mismos resultados, por lo que la reología mostrada por el hilo no refleja las propiedades reológicas generales del sistema granular.

Una vez caracterizada la fuerza de arrastre con el hilo solo, pasamos a hacer experimentos con un grano intruso pegado al hilo. Las figuras 5.8 y 5.9 muestran la fuerza de arrastre en función de la velocidad para diferentes intensidades de vibración y tamaños del intruso. Esta vez, la relación entre estas dos variables es logarítmica y, además, no está presente a bajas velocidades el comportamiento lineal encontrado con el hilo solo.

Aprovechando los experimentos realizados con el hilo solo, podemos encontrar la contribución del intruso a la fuerza de arrastre si restamos a la fuerza total la fuerza sobre el hilo solo bajo las mismas condiciones de arrastre y vibración. De este modo definimos la fuerza de arrastre sobre el intruso como $F_\infty^{(int)} \equiv F_\infty - F_\infty^{(thr)}$. El coeficiente de fricción asociado a esta

fuerza (definido en la ecuación 5.4), está graficado como función de la velocidad en la figura 5.10. Puede observarse que cuando no hay vibración, la fricción no depende de la velocidad de arrastre, lo cual coincide con los resultados de Albert et al. [21]. En contraste, cuando la vibración de los granos es máxima, la relación entre fricción y velocidad es logarítmica. Este tipo de comportamiento es característico de la fricción sólido - sólido. Este hecho resulta interesante ya que los modelos que describen correctamente la fricción en sólidos están basados en procesos microscópicos activados térmicamente [49, 50, 51]. Esto sugiere que en nuestro sistema los mismos mecanismos están presentes con la vibración jugando un papel análogo al de la temperatura.

Continuando con la analogía entre la reología de nuestro sistema granular y la frición sólido - sólido, estudiamos el comporamiento del parámetro de 'efecto directo', A, definido en la ecuación 5.5, como función de la intensidad de vibración. Los resultados obtenidos se muestran en la figura 5.13. Aunque es difícil concluir algo debido a la gran incertidumbre en las mediciones, nuestro parámetro A en función de la intensidad de vibración difiere cualitativa y cuantitativamente del obtenido en polímeros vítreos medido por Baumberger et al. [45] como función de la temperatura.

Bajo ciertas condiciones de vibración y arrastre, nuestro sistema granular puede comportarse como un fluido complejo en el sentido en que, al comienzo del movimiento del intruso, la fuerza de arrastre crece hasta un cierto valor máximo F_{peak}, para después relajar y alcanzar un valor estacionario F_∞ (ver figura 5.3). La figura 5.14 muestra el coeficiente de fricción máximo y estacionario como función de la intensidad de vibración para un intruso de diámetro $D = 4.25mm$. Resulta interesante la forma en que el máximo inicial va desapareciendo conforme aumenta la intensidad de vibración, de forma análoga al suavizamiento de un fluido complejo conforme se aumenta la temperatura [40].

El efecto del tamaño del intruso en la fuerza de arrastre el coeficiente de fricción se muestra en las gráficas de la figura 5.15. Cuando no hay vibración, la fuerza de arrastre escala de manera lineal con D, del mismo modo en que lo haría si se tratara de un fluido viscoso. Sin embargo, de acuerdo con la ley de Stokes, la fuerza de arrastre en un fluido crece también linealmente con la velocidad de arrastre, mientras que en el caso granular no vibrado, es independiente de la velocidad. Más aún, la relación lineal entre fuerza y diámetro del intruso se traduce en un coeficiente de fricción que decrece al aumentar el tamaño del intruso. Este resultado es coherente con los experimentos de Albert et al. [21] y puede entenderse como un efecto de talla finita cuando el intruso se vuelve comparable al tamaño de los granos del medio.

El caso con vibración en la figura 5.15 presenta algunas diferencias importantes con respecto al caso sin vibración. Por un lado, la relación entre la fuerza y el diámetro del intruso

no es lineal, aunque el coeficiente de fricción se comporta cualitativalmente igual al caso sin vibración. Por otro lado, con vibración la fuerza sí depende de la velocidad de arrastre. Esta dependencia de la velocidad también la encontraron en sus experimentos Geng y Behringer [22]. Estos autores explican la dependencia en la velocidad como consecuencia de la poca rigidez del material de sus partículas (usaron un polímero fotoelástico). Geng y Behringer argumentan que la deformación elástica de las partículas introduce en el proceso de arrastre un tiempo característico de relajación que explica la relación entre la fuerza y la velacidad. En nuestro caso, las partículas son rígidas, pero sería la vibración la que introduciría un tiempo característico de relajación.

Las fluctuaciones de las señales de fuerza como función de la distancia de arrastre fueron estudiadas a partir de la desviación cuadrática media de la fuerza, $\delta F_f = \sqrt{(1/N)\sum_{i=1}^{N} F_f^2(x_i)}$, en donde $F_f(x) \equiv F(x) - F_\infty$, y también a partir del espectro de potencia de las señales, $S(k)$, definido en la ecuación 5.6.

Los espectros de potencia de la fuerza de arrastre estacionaria de los intrusos fueron todos Lorencianos con una longitud característica que coincide con el diámetro medio de las partículas del medio granular (ver figura 5.18). Estos resultados coinciden con los de Geng y Behringer [22]. Por otro lado, las fluctuaciones de la fuerza resultaron ser independientes del tamaño del intruso (figura 5.17). En la sección 5.3.6 se presenta un modelo de tipo Ornstein-Uhlenbeck (figura 5.21; ecuación 5.10) que recupera la fenomenología de la parte fluctuante de la fuerza de arrastre.

A.7 Conclusiones y perspectivas

La posibilidad de una descripción universal y unificada de todos los sistemas que presentan atoramiento, aún si se trata de sistemas tan distintos como líquidos, espumas o materia granular, fue la motivación que nos llevó a diseñar un dispositivo experimental que permitió estudiar la física de un sistema granular ideal cerca del atoramiento.

Implementamos una nueva forma de agitar los granos, logrando hacerlo de forma más desordenada en comparación con experimentos previos de vibración granular. Más aún, evitamos por completo la convección, un punto esencial cuando se trata de estudiar los fenómenos de compactación granular.

Las características del dispositivo experimental hicieron posible la realización de muy variadas y a la vez complementarias mediciones que permitieron una caracterización muy completa de las propiedades mecánicas de nuestro medio granular.

Observamos en nuestro sistema fenómenos que habían sido observados previamente en otros experimentos en medios granulares, como fue el caso de la compactación logarítmica, el efecto Kovacs y la dinámica de 'jaula', la invarianza de la fuerza de arrastre con la velocidad en un sistema sin vibración o el espectro Lorenciano de las fluctuaciones de la fuerza de arrastre. El hecho de haber reproducido en nuestro sistema, con todas sus peculiaridades, todos estos fenómenos, apoya la idea de que se trata de fenómenos robustos y generales de los matriales granulados.

También obtuvimos resultados novedosos. Por ejemplo, la relación entre la energía cinética media y la velocidad de compactación. El comportamiento de la fuerza de arrastre en el sistema granular vibrado análogo al de la fuerza de fricción en sistemas sólido - sólido es un resultado interesante que apoya la idea de aplicar modelos de procesos activados térmicamente para describir sistemas granulares vibrados, en donde la vibración jugaría el papel de la temperatura.

Un resultado central de este trabajo fue la constatación de que, con vibración, la dinámica microscópica de partículas individuales no evolucionaba en el tiempo mientras que la densidad global del sistema seguía aumentando. Este sorprendente resultado apoya la idea de que la compactación granular es resultado de fenómenos colectivos del sistema que no necesariamente se reflejan al nivel de partículas individuales [37].

En cuanto a las perspectivas del trabajo, sería importante estudiar de forma sistemática los procesos de relajación de la densidad ante cambios de intensidad de vibración. También sería interesante estudiar los modos colectivos que intervienen en el proceso de compactación con la técnica de seguimiento de partículas pero siguiendo de manera simultánea partículas que se encontraran en distintas zonas de la pared lateral del sistema. Un experimento análogo al de Makse et al. [16] podría hacerse colocando junto a la pared lateral granos intrusos de distinta densidad al de los granos del medio.

En los experimentos de fuerza de arrastre convendría hacer variar la presión de confinamiento. Sería interesante conocer el efecto de la presión en el régimen lineal observado para el hilo solo con vibración.

Valdría la pena también continuar con los experimentos de difusión de luz e intentar complementarlos con los de compactación.

Con el estado actual del dispositivo, estamos limitados en la máxima intensidad de agitación, con lo que siempre trabajamos en la fase bloqueada del sistema. Sería interesante ser capaces de agitar los granos con mayor intensidad y estudiar la transición entre una fase fluida y la fase bloqueada.

A modo de comentario final, en relación a la aplicación de conceptos de física estadística para describir medios granulares, el presente trabajo muestra con evidencia experimental el

hecho de que en efecto existen analogías sorprendentes entre los sistemas que se atoran, aún si se trata de sistemas tan disímiles como medios granulados, espumas y vidrios. Sin embargo, tales analogías deben hacerse con cuidado. Por ejemplo, a partir de la relación lineal que encontramos entre la fuerza de arrastre y la velocidad en nuestros experimentos con el hilo solo, habríamos podido pensar que el sistema granular tenía propiedades de fluido Newtoniano, lo cual fue desmentido más adelante por los experimentos de arrastre de granos intrusos.

Bibliography

[1] J. Duran, *Sables poudres et grains*. Paris: Eyrolles, 1997.

[2] L. Vanel, D. Howell, D. Clark, R. P. Behringer, and E. Clément, "Memories in sand: Experimental test of construction history on stress distributions under sandpiles," *Phys. Rev. E*, vol. 60, p. R5040, 1999.

[3] M. E. Cates, J. P. Wittmer, J. P. Bouchaud, and P. Claudin, "Jamming, force chains, and fragile matter," *Phys. Rev. L*, vol. 81, p. 1841, 1998.

[4] A. J. Liu and S. R. Nagel, "Jamming is not just cool anymore," *Nature*, vol. 396, p. 21, 1998.

[5] S. F. Edwards and R. B. S. Oakeshott, "Theory of powders," *Physica A*, vol. 157, p. 1091, 1989.

[6] H. A. Makse and J. Kurchan, "Testing the thermodynamic approach to granular matter with a numerical model of a decisive experiment," *Nature*, vol. 415, p. 614, 2002.

[7] M. D. Ediger, C. A. Angell, and S. R. Nagel, "Supercooled liquids ans glasses," *J. Phys. Chem.*, vol. 100, p. 13200, 1996.

[8] J. B. Knight, C. G. Fandrich, C. N. Lau, H. M. Jaeger, and S. Nagel, "Density relaxation in a vibrated granular material," *Phys. Rev. E*, vol. 51, p. 3957, 1995.

[9] E. R. Nowak, J. B. Knight, E. Ben-Naim, H. M. Jaeger, and S. Nagel, "Density fluctuations in vibrated granular materials," *Phys. Rev. E*, vol. 57, p. 1971, 1998.

[10] O. Carvente and J. C. Ruiz-Suárez, "Crystalization of confined non-brownian spheres by vibrational annealing," *Phys. Rev. Lett*, vol. 95, p. 018001, 2005.

[11] C. Josserand, A. V. Tkachenko, D. M. Mueth, and H. M. Jaeger, "Memory effects in granular materials," *Phys. Rev. Lett.*, vol. 85, p. 3632, 2000.

[12] A. J. Kovacs *Adv. Polym. Sci*, vol. 3, p. 394, 1963.

[13] E. R. Weeks, J. C. Crocker, A. C. Levitt, A. Schofield, and D. A. Weitz, "Three dimensional direct imaging of structural relaxation near the colloidal glass transition.," *Science*, vol. 287, p. 627, 2000.

[14] G. Marty and O. Dauchot, "Subdiffusion and cage effect in a sheared granular material," *Phys. Rev. Lett.*, vol. 94, p. 015701, 2005.

[15] O. Pouliquen, M. Belzons, and M. Nicolas, "Fluctuating particle motion during induced granular compaction," *Phys. Rev. Lett.*, vol. 91, p. 014301, 2003.

[16] C. Song, P. Wang, F. Portiguar, and H. A. Makse, "Experimental and computational studies of jamming," *cond-mat/0503079*, 2005.

[17] GDRMidi, "On dense granular flows," *Eur. Phys. J. E*, vol. 14, p. 341, 2004.

[18] K. Wieghardt, "Experiments in granular flow," *Annu. Rev. Fluid Mechanics*, vol. 7, p. 89, 1975.

[19] O. Zik, J. Stavans, and Y. Rabin, "Mobility of a sphere in vibrated granular media," *Europhys. Lett.*, vol. 17, p. 315, 1992.

[20] D. Chehata, R. Zenit, and C. R. Wassgren, "Dense granular flow around an immersed cylinder," *Physics of Fluids*, vol. 15, p. 1622, 2003.

[21] R. Albert, M. A. Pfeifer, A. L. Barbasi, and P. Schiffer, "Slow drag in a granular medium," *Phys. Rev. Lett.*, vol. 82, p. 205, 1999.

[22] J. Geng and R. P. Behringer, "Slow drag in two-dimensional granular media," *Phys. Rev. E.*, vol. 71, p. 011302, 2005.

[23] P. Philippe and D. Bideau, "Granular medium under vertical tapping: Change of compaction and convection dynamics around the liftoff threshold," *Phys. Rev. Lett.*, vol. 91, p. 104302, 2003.

[24] A. Kabla and G. Debregeas, "Contact dynamics in a gently vibrated granular pile," *Phys. Rev. Lett.*, vol. 92, p. 035501, 2004.

[25] P. Marchal and L. Choplin, "Elements de physique statistique appliques a la rheologie des milieux granulaires non-cohesifs: le modele du chateau de sables mouvants," *Rheologie*, vol. 5, pp. 10–20, 2004.

[26] D. A. Weitz and D. J. Pine, *Dynamic light scattering: The method and some applications*, vol. 49 of *Monographs on the physics and chemistry of material*, ch. Diffusing-wave spectroscopy, pp. 652–720. Oxford University Press, Oxford, 1993.

[27] G. D'Anna, P. Mayor, A. Barrat, V. Loreto, and F. Nori, "Observing brownian motion in vibration-fluidized granular matter," *Nature*, vol. 424, p. 909, 2003.

[28] E. Vincent, J. Hammann, and M. Ocio, *Recent Progress in Random Magnets*. World Scientific, Singapore, 1992.

[29] J. P. Bouchaud, L. F. Cugliandolo, J. Kurchan, and M. Mézard, *Spin Glasses and Random Field*. World Scientific, Singapore, 1997.

[30] M. Nicodemi, "Dynamical response functions in models of vibrated granular media," *Phys. Rev. Lett.*, vol. 82, p. 3734, 1999.

[31] A. Barrat and V. Loreto, "Response properties in a model for granular matter," *J. Phys. A*, vol. 33, p. 4401, 2000.

[32] P. L. Krapivsky and E. Ben-Naim, "Collective properties of adsorption-desorption processes," *J. Chem. Phys.*, vol. 100, p. 6778, 1994.

[33] A. J. Kolan, E. R. Nowak, and A. V. Tkachenko, "Glassy behavior of the parking lot model," *Phys. Rev. E*, vol. 59, p. 3094, 1999.

[34] J. Talbot, G. Tarjus, and P. Viot, "Adsorption-desorption model and its application to vibrated granular materials," *Phys. Rev. E*, vol. 61, p. 5429, 2000.

[35] J. J. Arenzon, Y. Levin, and M. Sellito, "Slow dynamics under gravity: a nonlinear diffusion model," *Physica A*, vol. 325, p. 371, 2003.

[36] M. T. Valentine, P. D. Kaplan, D. Thota, J. C. Crocker, T. Gisler, R. K. Prud'homme, M. Beck, and D. Weitz, "Investigating the microenvironments of inhomogeneous soft materials with multiple particle tracking," *Phys. Rev. E*, vol. 64, p. 61506, 2001.

[37] M. Wyart, S. R. Nagel, and T. A. Witten, "Geometric origin of excess low-frequency vibrational modes in weakly connected amorphous solids," *Europhys. Lett.*, vol. 72, p. 486, 2005.

[38] F. Heslot, T. Baumberger, B. Perrin, B. Caroli, and C. Caroli, "Creep, stick-slip, and dry-friction dynamics: Experiments and a heuristic model," *Phys. Rev. E*, vol. 49, p. 4973, 1994.

[39] P. Coussot, Q. D. Nguyen, H. T. Huynh, and D. Bonn, "Avalanche behavior in yield stress fluids," *Phys. Rev. Lett.*, vol. 88, p. 175501, 2002.

[40] F. Varnik, L. Bocquet, and J. L. Barrat, "A study of the static yield stress in a binary lennard-jones glass," *Journal of Chemical Physics*, vol. 120, p. 2788, 2004.

[41] R. M. Nedderman, *Statics and kinematics of granular materials*. Cambridge: Cambridge University Press, 1992.

[42] P. Sollich, F. Lequeux, P. Hebraud, and M. Cates, "Rheology of soft glassy materials," *Phys. Rev. Lett.*, vol. 78, p. 2020, 1997.

[43] P. Sollich, "Rheological constitutive equations for a model of soft glassy materials," *Phys. Rev. E*, vol. 58, p. 738, 1998.

[44] J. H. Dieterich and D. Kilgore *Pure Appl. Geophys.*, vol. 43, p. 283, 1984.

[45] T. Baumberger, P. Berthoud, and C. Caroli, "Physical analysis of the state- and rate-dependent friction law. ii. dynamic friction.," *Phys. Rev. B*, vol. 60, p. 3928, 1999.

[46] Y. Sang, M. Dube, and M. Grant *Phys. Rev. Lett.*, vol. 87, p. 174301, 2001.

[47] O. K. Dudko, A. E. Filippov, J. Klafter, and M. Urbakh *Chem. Phys. Lett.*, vol. 352, p. 499, 2002.

[48] E. Riedo, E. Gnecco, R. Bennewitz, E. Meyer, and H. Brune, "Interaction potential and hopping dynamics governing sliding friction," *Phys. Rev. Lett.*, vol. 91, p. 084502, 2003.

[49] J. R. Rice and A. L. Ruina, "Stability of steady frictional slipping," *J. Appl Mech.*, vol. 50, p. 343, 1983.

[50] L. Prandtl and Z. S. F. Angew *Math. U. Mech.*, vol. 8, p. 85, 1928.

[51] G. A. Tomlinson *Philos. Mag. Series*, vol. 7, p. 905, 1929.

[52] G. Caballero, J. Lanuza, and E. Clement., "Compaction and mobility in randomly agitated granular assemblies," in *Powders and Grains 2005* (Garcia-Rojo, Herrmann, and McNamara, eds.), (London), p. 339, Taylor and Francis Group, 2005.

[53] B. Miller, C. O'Hern, and R. P. Behringer, "Stress fluctuations for continuously sheared granular materials," *Phys. Rev. Lett.*, vol. 77, p. 3110, 1996.

[54] A. Baldassarri, F. Dalton, A. Petri, S. Zapperi, G. Pontuale, and L. Pietronero., "Crackling response of a granular medium under shear," *cond-mat/0507533*, 2005.

[55] J. P. Bouchaud. Personal communication.